



Cite this: *Energy Environ. Sci.*,
2016, 9, 323

Organometal halide perovskite solar cells: degradation and stability

Taame Abraha Berhe,^a Wei-Nien Su,*^a Ching-Hsiang Chen,^a Chun-Jern Pan,^b Ju-Hsiang Cheng,^b Hung-Ming Chen,^b Meng-Che Tsai,^b Liang-Yih Chen,^b Amare Aregahegn Dubale^b and Bing-Joe Hwang*^{bc}

Organometal halide perovskite solar cells have evolved in an exponential manner in the two key areas of efficiency and stability. The power conversion efficiency (PCE) reached 20.1% late last year. The key disquiet was stability, which has been limiting practical application, but now the state of the art is promising, being measured in thousands of hours. These improvements have been achieved through the application of different materials, interfaces and device architecture optimizations, especially after the investigation of hole conductor free mesoporous devices incorporating carbon electrodes, which promise stable, low cost and easy device fabrication methods. However, this work is still far from complete. There are various issues associated with the degradation of Omh-perovskite, and the interface and device instability which must be addressed to achieve good reproducibility and long lifetimes for Omh-PSCs with high conversion efficiencies. A comprehensive understanding of these issues is required to achieve breakthroughs in stability and practical outdoor applications of Omh-PSCs. For successful small and large scale applications, besides the improvement of the PCE, the stability of Omh-PSCs has to be improved. The causes of failure and associated mechanisms of device degradation, followed by the origins of degradation, approaches to improve stability, and methods and protocols are discussed in detail and form the main focus of this review article.

Received 4th September 2015,
Accepted 20th October 2015

DOI: 10.1039/c5ee02733k

www.rsc.org/ees

Broader context

Low cost, stable and efficient light harvesting crystalline materials have great promise for future cost-effective clean energy and for the environment. Solar cell devices made of organometal halide perovskite materials are now revolutionizing the area of photovoltaics with energy conversion efficiencies of 20.1%, which represents a fivefold jump in cell efficiency within three years. The major obstacle of bringing organometal halide perovskite solar cells to the commercial market is the poor long term device stability, which has not been able to exceed a few thousands of hours until now. This review article presents an in-depth and updated discussion on the progress in stability, addressing the mechanisms and origins behind degradation, approaches to improve stability, protocols and related analytical methods to study the existing and other unknown limitations on the stability of organometal halide perovskite solar cells. Furthermore, the review is also meant to give an overview to readers who are new to this topic.

1. Background

To become economically feasible, organometal halide perovskite solar cells (Omh-PSCs) should remain free from degradation under normal operating conditions over several years, preferably tens of years. Their stability is vital for practical application,

but the evaluation and prediction of the device lifetime are not easy as the stability is related to the fading process of individual solar cells.¹ Because different varieties of solar devices have various degradation mechanisms, the accelerated stress tests appropriate for one type of solar cell may not be useful in studying the degradation of other types. Organometal halide (Omh) perovskites are a class of materials in the perovskite family with alternating layered structures of organic and inorganic constituents. Omh-perovskites are noted for their cheap production, and methylammonium lead iodide ($\text{CH}_3\text{NH}_3\text{PbI}_3$) is one of the most representative materials. Solar cells made of this kind of material have grown so fast within a few years and have reached a certified efficiency over 20%. Its theoretical maximum is greater

^a NanoElectrochemistry Laboratory, Graduate Institute of Applied Science and Technology, National Taiwan University of Science and Technology, Taipei 106, Taiwan. E-mail: wsu@mail.ntust.edu.tw

^b NanoElectrochemistry Laboratory, Department of Chemical Engineering, National Taiwan University of Science and Technology, Taipei 106, Taiwan. E-mail: bjh@mail.ntust.edu.tw

^c National Synchrotron Radiation Research Center, Hsin-Chu, 30076, Taiwan

than 30% and this could beat the efficiency of silicon, the theoretical maximum of which is limited to 27%, and economically and practically limited to ~25%.²

However, the long term stability of this kind of solar cell is far from practical. *Ex situ* long-term stability tests for $\text{CH}_3\text{NH}_3\text{PbI}_3$ solid-state solar cells stored in air at room temperature without encapsulation were carried out for over 500 h under one sun illumination³ and 1000 h under full sunlight.⁴ This revealed that light soaking alone is not a major reason for this poor stability. Furthermore, long-term stability of Omh-PSCs for 500 h at 45 °C, under constant illumination⁵ at approximately 100 mW cm⁻² and 1000 h at 40 °C, with continuous exposure and operation under full spectrum simulated sunlight⁶ has also been achieved. The light-soaking tests become more challenging as the temperature increases; in fact, a light soaking test Omh-PSCs has not yet been reported for 1000 h at 80 °C. The device stability of mesoporous $\text{TiO}_2/\text{CH}_3\text{NH}_3\text{PbI}_3/\text{C}$ heterojunction (HJ) solar cells

without encapsulation is 2000 h at room temperature, in air and in the dark.⁷ The high temperature (80 °C) dark test may be too demanding for these solar cells as it has not yet been demonstrated. It is obvious that at high temperatures, *i.e.* above 60 °C, either certain fading mechanisms are accelerated or new degradation reactions occur, causing rapid absorber material and/or device degradation. The major causes responsible for this kind of degradation may be related to various possible external factors, such as moisture, oxygen, temperature, UV light, *etc.*, as well as internal intrinsic factors such as ion migration, electro-migrations and interfacial reactions. Thus, setting standard stability testing protocols requires an understanding of how and why the device degrades. Such an understanding should facilitate the future production of better materials for the cells.

In order to establish typical stability testing protocols for Omh-PSCs, stability definitions should be well understood. For example, what range of drop or raise in the performance



Taame Abraha Berhe

*Sciences till 2014. Currently, he is conducting his PhD under Prof. Bing-Joe Hwang and Prof. Wei-Nien Su, focusing on the synthesis and stability of organometal halide perovskite solar cells, structural changes and defect studies using *in situ* techniques.*

Taame Abraha is a PhD student in the Graduate Institute of Applied Science and Technology at National Taiwan University of Science and Technology, Taiwan. He received his Bachelor in Chemistry from Wollo University in 2009 and master's degree in Chemistry (Physical) from Bahir Dar University, Ethiopia in 2011. Then, he joined Adigrat University and worked as head of chemistry and Dean, College of Natural and Computational



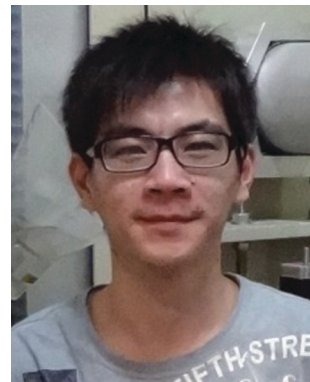
Wei-Nien Su

research programs. He received his PhD from the Wolfson School, Loughborough University (UK) and his Diplom-Ing. in Chemical Engineering from Universität Stuttgart (Germany).



Ching-Hsiang Chen

Ching-Hsiang Chen received his PhD in Chemical Engineering from National Taiwan University of Science and Technology (NTUST). He is currently the global business director in Uni-nanotech Co., Ltd. and he is also an adjunct assistant professor in the Sustainable Energy Development Center in NTUST. His research interests include surface enhanced spectroscopy and ultra fast spectroscopy in energy and biomedical science.



Chun-Jern Pan

*Chun-Jern Pan received his PhD degree from NTUST in 2012. He is currently a post-doctoral researcher in Prof. Bing-Joe Hwang's laboratory at the Department of Chemical Engineering, NTUST. Dr Chun-Jern Pan's research field is mainly in characterizing energy materials using *in situ* X-ray absorption spectroscopy and X-ray diffraction. These techniques have been adopted to investigate the structure of energy related materials, such as solar cell materials, catalysts and electrode materials for batteries.*

Wei-Nien Su is currently an assistant professor of the Graduate Institute of Applied Science and Technology at National Taiwan University of Science and Technology (NTUST), Taiwan. His research interests are rooted in materials synthesis and characterization of nanocatalysts for various electrochemical devices and energy applications. Prof. Su is currently involved in various international and national

of Omh-PSCs can be accepted for the device to be taken as a stable device? Secondly, is efficiency the only criterion in assessing the performance? As a final point, the ultimate application should also be taken into account. Even though standard protocols are not well-outlined, various frequently utilized protocols such as temperature (60 °C and 80 °C dark tests), light soaking tests at 1 Sun at 60 °C or 80 °C, heat-cycle durability tests, ultraviolet (UV) tests, and humidity tests can be used to assess stability, which commonly run for 1000 h. Hence, the aim of this article is to comprehensively review the causes of failure and associated possible mechanisms of degradation, the origins of degradations followed by approaches to improve the stability as well as the methods and protocols used to study degradation. Its objectives are also to shed light on possible approaches directed towards a more systematic study of degradation phenomena in Omh-PSCs. Therefore, the scope of this article is to critically assess stability and degradation information to aid the commercial enterprises and research institutes that work with these technologies.

The organization of this review originates from its background followed by overview information focusing on the need for Omh-PSCs and its associated mechanistic processes, as well as major contributions to the current status of performance improvement in order to provide an overview of basic principles and progressive improvements in efficiency and stability. Only promising steps have been achieved mainly in the area of device stability from minutes to thousands of hours. Thus, the various causes of failure and associated mechanisms of degradation have been comprehensively reviewed. Furthermore, the origins of device degradation in different device components that are capable of prohibiting the devices outside of an inert atmosphere are discussed in-depth. These components have been subdivided into Omh-perovskites, mixed Omh-perovskites, hole transport layers, and counter electrodes, each contributing their own degradation mechanisms. The device architecture is also



Meng-Che Tsai

Meng-Che Tsai received his PhD degree in Chemical Engineering from National Taiwan University of Science and Technology (NTUST) in Taiwan in 2013, and his advisor is Professor Bing-Joe Hwang. He is currently a postdoctoral fellow at NTUST. His research interests include the design and synthesis of advanced energy materials by using a computational approach containing energy conversion and storage.

another important issue which has an impact on the device stability. The main device architectures: planar (regular TiO₂), inverted and mesoporous TiO₂ are reviewed in line with their stability issues. The sequence of the different layers in the three architectures results in different interfacial reactions which can further affect the stability. The discussion of this interface is subdivided into ion migration into the interface and reactivity in the interface. Finally, we wrap up our discussion with possible ways toward stability improvements as a function of material, device architecture, and interface aspects, as well as protective means during operation. Tests, evaluation methods and protocols for stability studies are also suggested for future material and device development. This review manuscript is finalized with a comprehensive conclusion and prospects.

2. Overview of Omh-PSC devices

2.1 The need for Omh-PSCs

Studies focusing on Omh-PSCs are growing in number and attracting scientists from other subject areas: (1) physicists, constructing devices from new materials, typifying and optimizing performance, and realizing the basic photo-physical mechanisms; (2) chemists, developing and manufacturing suitable Omh-perovskite absorbers and dealing with structure-property relationships and (3) engineers, building novel device designs. The interplay among these subjects could lead to a great contribution towards potential improvements of Omh-PSCs in the future.

Solar cells with effective PCEs require materials to absorb in a wide spectral range, from visible to near infrared, to harvest most of the solar photons, and to efficiently convert the photon into free charges. In order to reduce the energy costs related to electron/hole separation and charge extraction, highly crystalline materials possessing good carrier mobility are required.



Bing-Joe Hwang

Bing-Joe Hwang studied Chemical Engineering and received his PhD in 1987 at the National Cheng Kung University, Taiwan. Since 2006, he has served as chair professor at National Taiwan University of Science and Technology. His research work has spanned a wide range of subjects from electrochemistry to spectroscopy, interfacial phenomena, materials science and theoretical chemistry. He has established both experimental and computational strategies for the development of new nanoscale materials. His theoretical work has led to a better understanding of reaction mechanisms on nanoparticles and to an improved ability to predict the properties of potential new materials for ion batteries, fuel cells and solar cells.



Fig. 1 Power conversion efficiency comparison of third generation solar cells: a-Si, DSSC, OPV and Omh-PSCs.

However, these are hampered by unreasonable costs, due to production procedures that use vacuum based or high-temperature processing, thereby limiting commercial application. On the other hand, third generation photovoltaic devices, *e.g.* amorphous silicon (a-Si), dye sensitized solar cells (DSCs) and organic photovoltaic (OPVs) can be made using simple low cost manufacturing processes.^{8,9} These technologies utilize a combination of amorphous and disordered materials. Hence, the energy costs associated with the extraction of free charges impose a fundamental limitation upon high efficiency systems. As shown in Fig. 1, the new Omh-perovskite structure-based materials are revolutionizing the photovoltaic field, with the efficiencies of Omh-PSCs, a-Si, DSCs and OPVs being 20.1%,¹⁰ 13.44%,¹¹ 13%¹² and 12%¹³ respectively. Recent research shows that there is a tradeoff between a wide spectral absorption range, highly crystalline structures that induce effective charge extraction, and low-cost fabrication techniques.

The material's organic-inorganic hybrid nature is what makes Omh-PSCs so efficient. Firstly, the organic constituent offers good solubility to the Omh-perovskite and facilitates self-assembly together with its precipitation and/or deposition from solution. Secondly, the inorganic part provides a comprehensive network by covalent and/or ionic interactions, instead of weaker forces such as Van der Waals or $\pi-\pi$ interactions. Such strong interactions account for the accurate crystalline structure in the deposited films. Thirdly, powerful optical absorption is a means to attain an excellent performance and literature reports confirmed that Omh-perovskites of interest are direct-bandgap semiconductors.⁹

2.2 Mechanistic processes in Omh-PSCs

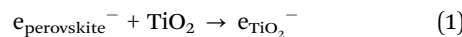
The basic energy diagram and elements of the mechanistic process of Omh-PSCs are represented in Fig. 2. The key idea

behind efficient solar energy conversion is the combination of 'carrier generation' by light absorption and 'charge separation'. In the absorber perovskite (see Fig. 2(a)), electrons undergo excitation. Fig. 2(b) shows the electron transport layer (ETL) and hole transport layer (HTL), both in contact with the Omh-perovskite. These electrons and holes are separated by an ETL that is conductive to electrons and rejects holes, and by a HTL that allows transport of the holes with no impedance, while blocking electrons, respectively. Such arrangements permit the Fermi level in the metal contacts to equilibrate with the separate Fermi levels of the electrons and holes, generating an external voltage, and to extract the carriers, giving a photocurrent in the external circuit.

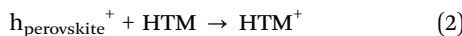
The mechanistic processes in devices using mesoporous TiO_2 are still under debate,¹⁴ as Omh-perovskite materials combine both the functions of light absorption and n-type or p-type conduction. The present mechanistic representation is explained as follows: the Omh-perovskite absorbs light and an excited state (electron-hole pair) is produced. Charge separation can take place at the interface through two processes: injection of a photogenerated electron into a TiO_2 nanoparticle (eqn (1)), or hole injection into a HTL (eqn (2)).

Charge separation reactions are in kinetic competition with other reactions, such as exciton annihilation, and lead to photoluminescence (eqn (3)), recombination in the perovskite (eqn (4)), as well as recombination of the charge carriers at the different interfaces (eqn (5) and (6)).¹⁴

Electron injection:



Hole injection:



Luminescence:



Recombination in perovskite:

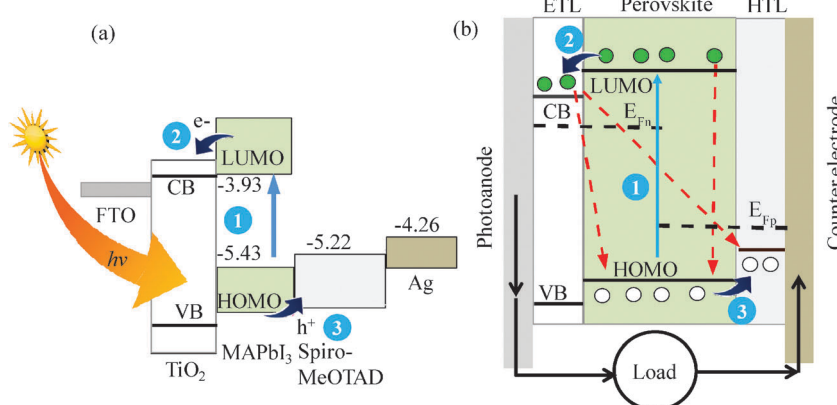
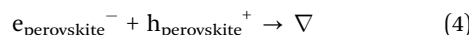
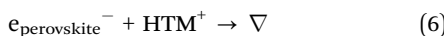
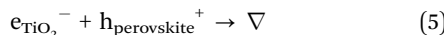


Fig. 2 (a) Schematic representation of the energy diagram in an Omh-perovskite (1) generating electrons and hole carriers that rapidly relax (2) to the conduction band (EC) of the ETL (TiO_2) and (3) to the HOMO of the HTL, respectively. (b) The scheme of the main process in Omh-PSCs, formed by the Omh-perovskite absorber material, supplemented by two selective contacts, the ETL and HTL.

Recombination at interface:



In a Omh-PSC, the incoming light is absorbed by the Omh-perovskite, which is anchored to the surface of TiO_2 nanocrystals. Theoretically, for efficient Omh-PSCs, the Omh-perovskite absorber regeneration by HTM must happen more rapidly than electron recombination.

2.3 Current status of performance in Omh-PSCs

As an area of focus in Omh-PSC devices, the PCE is an important consideration when making comparisons with the more mature silicon technology. Besides the PCE and fabrication processes, there are at least two other factors that have an impact on the success of Omh-PSCs. These factors, which have been given relatively little consideration, are stability and cost.^{8,9,15,16} Inorganic silicon-based solar cells may last approximately 25 years; so in this respect, Omh-PSC devices must be improved to become technologically attractive, economically feasible and commercially practicable.

2.3.1 Efficiency. Omh-perovskite materials were pioneered and studied, at first by Mitzi and co-workers,^{16–20} as active layers in light-emitting diodes and field-effect transistors. Different structures, *i.e.* 2D and 3D spatial distributions, of the Omh-perovskite

materials were fabricated and their optoelectronic proprieties were exploited in the fabrication of transistor and light emitting diodes.²⁰ The Omh-PSC evolution efficiency is shown in Fig. 3 and Table 1. In 2009, Miyasaka and coworkers²¹ demonstrated the potential of a $\text{CH}_3\text{NH}_3\text{PbI}_3$ absorber in solar cell devices based on TiO_2 mesostructure photoanodes with a power conversion efficiency of 3.81%. The authors were attracted by its self-organizing potential in the nanoporous TiO_2 layer of the solar cell. Later, Etgar and coworkers²² demonstrated that $\text{CH}_3\text{NH}_3\text{PbI}_3$ can act both as a light harvester and as an HTM in a $\text{CH}_3\text{NH}_3\text{PbI}_3/\text{TiO}_2$ heterojunction device. A HTM-free solid state mesoscopic $\text{CH}_3\text{NH}_3\text{PbI}_3/\text{TiO}_2$ heterojunction solar cell was demonstrated with a PCE of 5.5% under standard AM 1.5 solar light of 1000 W m^{-2} intensity and a PCE of 7.3% at a lower light intensity of 100 W m^{-2} .²² The advent of such straightforward solution-processed mesoscopic heterojunction solar cells shows the way to low-cost, high-efficiency solar cells.

Among the Omh-perovskite-structure based semiconductors, $\text{CH}_3\text{NH}_3\text{PbI}_3$ is the most common one, and these perovskites have a tendency to possess a high charge carrier mobility.^{18,20,21,23,24} For an Omh-PSC device, adequate mobility and high charge carrier lifetimes are important. Both Xing²⁵ and Stranks²⁶ confirmed that $\text{CH}_3\text{NH}_3\text{PbI}_3$ has relatively large diffusion lengths *i.e.* about 100–130 nm for both electrons and holes, which are higher values compared to other solution based processed semiconductors at low temperatures.

Omh-perovskite absorbers have been used as light absorbers in liquid electrolyte-based photoelectrochemical cells with PCEs from 3.81²¹ to 6.5%.²⁷ However, they will dissolve in the electrolyte, resulting in a fast performance decline. This degradation led to the replacement of the liquid electrolyte with a solid hole transporter material (HTM) in 2012.^{15,28} The HTM of spiro-MeOTAD was originally produced for organic light emitting diodes (LEDs)²⁹ but was also found to be useful for solid state dye sensitized solar cells (ssDSSCs)³⁰ and boosted the reported efficiency (9.7%) for Omh-PSCs.¹⁵ In the middle of 2012, other successes were reported using ref. 28. Firstly, mixed-halide $\text{CH}_3\text{NH}_3\text{PbI}_{3-x}\text{Cl}_x$, which displayed better stability and carrier transport than its pure iodide equivalent, was successfully used.^{28,31} Secondly, nanoporous TiO_2 surfaces were coated with a thin Omh-perovskite layer thereby forming extremely thin absorber solar cells. Thirdly, the conducting nanoporous TiO_2 was replaced by a similar but non-conducting Al_2O_3 insulator. This increased V_{oc} , raising the

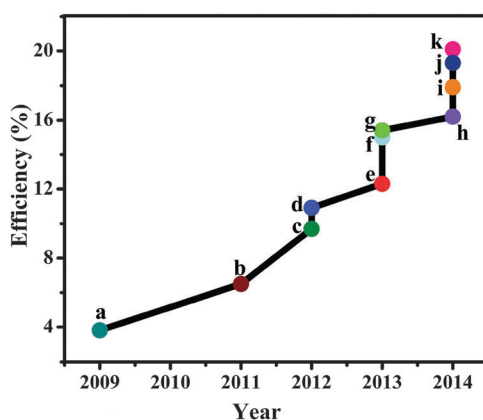


Fig. 3 Efficiency roadmap for Omh-PSC devices: efficiency values taken from publications and NREL's latest chart on record cell efficiencies.

Table 1 Summary of device structure and corresponding efficiencies for Omh-PSCs roadmap in Fig. 3

Symbol	Device structure	Efficiency (%)	Ref.
a	Liquid electrolyte/ $\text{CH}_3\text{NH}_3\text{PbI}_3/\text{TiO}_2$	3.81	21
b	Liquid electrolyte/ $\text{CH}_3\text{NH}_3\text{PbI}_3$ QD/ TiO_2	6.5	27
c	Spiro-MeOTAD/ $\text{CH}_3\text{NH}_3\text{PbI}_3$ /mesoporous TiO_2	9.7	15
d	Spiro-MeOTAD/ $\text{CH}_3\text{NH}_3\text{PbI}_2\text{Cl}$ /mesoporous Al_2O_3	10.9	28
e	PTAA/ $\text{CH}_3\text{NH}_3\text{PbI}_{3-x}\text{Br}_x$ /mp- TiO_2	12.3	33
f	Spiro-MeOTAD/ $\text{CH}_3\text{NH}_3\text{PbI}_{3-x}\text{Cl}_x$ / TiO_2 , 2-step solution deposition	15.0	5
g	Spiro-MeOTAD/ $\text{CH}_3\text{NH}_3\text{PbI}_{3-x}\text{Cl}_x/\text{TiO}_2$, evaporated thin film p-i-n architecture	15.4	34
h	PTAA/ $\text{CH}_3\text{NH}_3\text{PbI}_{3-x}\text{Br}_x$ /mesoporous TiO_2	16.2	35
i	PTAA/ $\text{CH}_3\text{NH}_3\text{PbI}_{3-x}\text{Br}_x$ /mesoporous TiO_2	17.9	35
j	Spiro-MeOTAD/perovskite/tritium-doped TiO_2	19.3	36
k	PTAA/(FAPbI ₃) _{1-x} (MAPbBr ₃) _x /mesoporous- TiO_2	20.1	10 and 37

cell efficiency to 10.9%. Omh-perovskites have a broader potential due to their ambipolar properties. The fourth reported success was the ability to form a simple planar device with the scaffolding totally removed.³¹

The cooperative work of Seok, Grätzel and colleagues led to a reported efficiency of 12.0%, using both optional layers, including a solid Omh-perovskite capping layer overlying the scaffolding (nanoporous TiO_2 infiltrated by Omh-perovskite).³² Different HTMs were investigated, including spiro-MeOTAD, with poly-triarylamine proving to be the best. Seok and coworkers further reported another efficiency improvement of 12.3% with the same structures and $\text{CH}_3\text{NH}_3\text{PbI}_{3-x}\text{Br}_x$.³³ Less than 10% of bromine gave the best initial efficiency, because of its smaller band gap, but a greater proportion of Br than 20% offered moisture stability. This is caused by the structural transition from tetragonal to pseudo-cubic due to the smaller ionic radius of Br.¹⁸ A PCE of 15.0% was reported from the Grätzel research group using a nanoporous $\text{TiO}_2/\text{CH}_3\text{NH}_3\text{PbI}_3/\text{spiro-MeOTAD}/\text{Au}$ device architecture.⁵ They used TiO_2 as scaffolding and a two-step method for perovskite absorber deposition, which improved the morphology.

Snaith and coworkers³⁴ illustrated a high PCE of 15.4% with an open-circuit voltage (V_{oc}) of 1.07 V and a short-circuit current density (J_{sc}) of 21.5 mA cm^{-2} using the mixed halide $\text{CH}_3\text{NH}_3\text{PbI}_{3-x}\text{Cl}_x$ deposited as a light absorber thin layer material with spiro-MeOTAD as the hole transporter. Furthermore, Seok and coworkers realized a cell efficiency of 16.2% using $\text{CH}_3\text{NH}_3\text{PbI}_{3-x}\text{Br}_x$ (10–15% Br) and a poly-triarylamine HTM.³⁵ The thickness ratio of the perovskite-infiltrated TiO_2 scaffolding relative to the continuous perovskite layer was the key to the improved efficiency. This was increased to a PCE of 17.9% in early 2014.³⁵ An efficiency of 19.3% in a planar geometry without an antireflective coating was demonstrated by Yang and coworkers.³⁶ To improve the electron transport properties, Y-doped TiO_2 has been successfully used as the mesoporous scaffold in perovskite solar cells. Recently, Seok and colleagues have developed a solar cell with an efficiency of 20.1%^{10,37} by combining MA and FA (formamidinium), as confirmed in November 2014, by the U.S. National Renewable Energy Laboratory. Similar to MA, FA is a small, positively charged molecule made of carbon, hydrogen, and nitrogen. But FAPbI₃ absorbs light further into the near infra-red, thereby potentially boosting the cells efficiency.³⁸ Despite accommodating a wide variety of cell designs and producing excellent PCEs, Omh-PSCs must first overcome a number of technical issues before widespread commercialization is possible. These include the scale-up of the cell area, the elimination of lead toxicity and the lack of long-term device stability.³⁹ Efforts to address these shortcomings have begun to show promise, with a *ca.* 1 cm^2 Omh-perovskite device producing an efficiency value as high as 8.3%⁴⁰ and lead-free Omh-PSCs being now reported.^{41,42}

2.3.2 Stability. The current highest PCE reached by Omh-PSCs is 20.1% and, while the stability is low, it is by no means a barrier to application in many situations. The major obstacle is the relatively short lifetime achieved with current technology. To bring Omh-PSCs onto the market, in addition to higher efficiencies and cost-effective processing, a long device lifetime

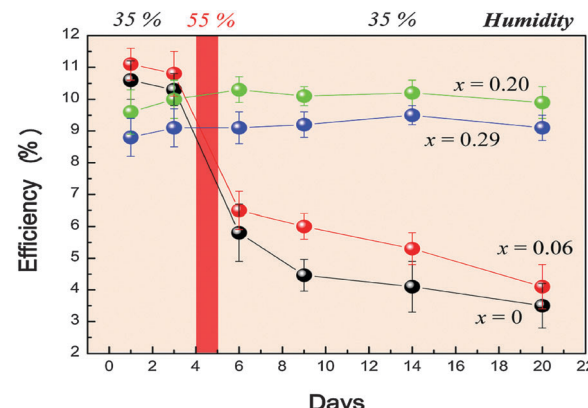


Fig. 4 Moisture effect on the stability of heterojunction solar cells based on $\text{MAPb}(\text{I}_{1-x}\text{Br}_x)_3$. Reprinted with permission.³³ Copyright 2013 American Chemical Society.

will be necessary. In 2011, the devices were only stable for 10 minutes before degradation (about 80% degradation)²⁷ because $\text{CH}_3\text{NH}_3\text{PbI}_3$ QDs tend to dissolve gradually into the redox electrolyte (unstable in iodide-containing liquid electrolyte, due to rapid dissolution). In 2012, the stability was remarkably improved from minutes to over 500 h by using a spiro-MeOTAD based solid-state Omh-PSC device.¹⁵ This improvement is attributed to the discovery of the solid hole conductor.³³ Fig. 4 shows the effect of moisture on the stability of heterojunction like Omh-PSCs solar cells made of $\text{MAPb}(\text{I}_{1-x}\text{Br}_x)_3$. The device was maintained at 35% humidity, stored in air at room temperature and intentionally exposed to a humidity of 55% for one day on the fourth day. This device showed enhanced stability at low humidity (<50%). On the other hand, the device stability began to reduce at relatively high humidity ($\geq 55\%$). This might be due to degradation of the $\text{MAPb}(\text{I}_{1-x}\text{Br}_x)_3$ material.³³ The performance of this device is more stable after 20 days at values of $x = 0.2$ and $x = 0.29$ compared to the values of $x = 0$ and $x = 0.06$. Thus, an appropriate atomic ratio of the halide anions is an important implication for improvement of the stability.³³

Since $\text{CH}_3\text{NH}_3\text{PbI}_3$ films are not stable in a humid atmosphere, controlling environmental conditions to a moisture level of less than 1% is recommended for device preparation.⁵ Moreover, a sealed device subjected to long-term light soaking at a light intensity of 100 mW cm^{-2} and a temperature of 45°C showed promising stability and maintained more than 80% of its initial PCE after a period of 500 h.⁵ The device was prepared under an argon filled glovebox and maintained at the optimal electric power output during the ageing process using maximum power-point tracking.

It is obvious that mesoporous TiO_2 free solar cells are significantly more flexible to UV irradiation compared to TiO_2 based solar cells. The performance of TiO_2 based devices is limited to only 5 h stability due to the fast decay in photocurrent and the small decay in photovoltage when tested in ambient conditions.⁶ Opposing the behavior of TiO_2 -based solar cells, the photocurrent become stable nearly at 15 mA cm^{-2} for over 1000 h in a Al_2O_3 -based Omh-perovskite solar cell.⁶ Fig. 5 shows the

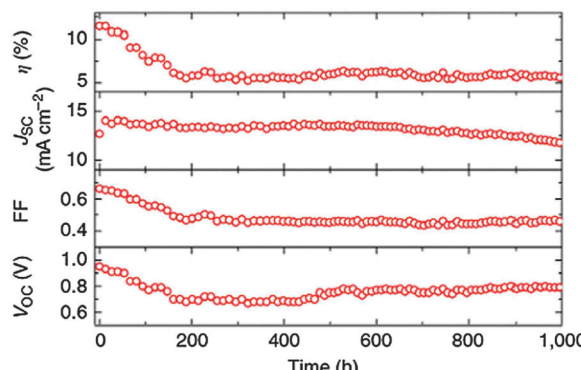


Fig. 5 Stability test of a mesoporous TiO_2 -free solar cell device. Reprinted with permission.⁶

stability test of a meso-super structured Al_2O_3 -based Omh-perovskite solar cell (MSSC) exposed to continuous simulated AM 1.5 76.5 mW cm^{-2} illumination at 40 °C. The FF and V_{oc} started to drop in the first 200 h experienced and this initial decline may be because of different factors such as oxygen desorption at vacancy sites on the compact TiO_2 layer, partial de-doping of the spiro-MeOTAD,⁴³ modifications at the spiro-MeOTAD/Au interface, or slight modifications within the Omh-perovskite.

Kwon and co-workers⁴⁴ reported the *ex situ* long-term stability of Omh-PSCs using three HTMs: spiro-MeOTAD, P3HT and poly[2,5-bis(2-decyl dodecyl) pyrrolo[3,4-*c*]pyrrole-1,4(2H,5H)-dione-(*E*)-1,2-di(2,20-bithiophen 5-yl)ethene] (PDPPDBTE), under a 20% humidity atmosphere for over 1000 h. The PCE of the spiro-MeOTAD based device slowly reduced when the ageing period was extended. The device showed a 28% decrease in the PCE in relation to the early PCE. Furthermore, the stability of the PDPPDBTE cells improved remarkably, and the initial performance was retained at a PCE of 8.4% after 1000 h. The improved stability may be due to its hydrophobic behaviour, which avoided water flow into the Omh-perovskites. Moreover, the solar cell stability of mixed halide perovskites, $\text{MAPb}(\text{Br}_{x}\text{I}_{1-x})_{3-y}\text{Cl}_y$, grown on nanostructured- TiO_2 and in a thin film configuration, was monitored to study cell stability as a function of the halide composition.⁴⁵ Hence, the stability of Omh-PSC devices has been limited, mainly due to ambient moisture because alkylammonium salts are, in general, highly hygroscopic. Interestingly, the insertion of bromine into the Omh-PSC structure benefits the cell stability.³⁴ Those cells without bromine show an efficiency drop of 20%, 30 days after preparation, which is ascribed mainly to a decrease in the FF. However, the equimolar Br/I devices showed a significant enhancement of 37% PCE.⁴⁵

This improvement could be a consequence of the rearrangement of the Omh-PSCs 3D configuration over time. In particular, the efficiency improvement may be attributed to the insertion of the smaller bromine anions, leading to a more compact Omh-PSC structure in which the degradation of the MA cation is prevented.⁴⁵ Therefore, a deeper analysis including microstructural and crystallographic studies must be performed to elucidate the origin of this observation. Recently, it has been pointed out that the presence of nano-structured TiO_2 changes the

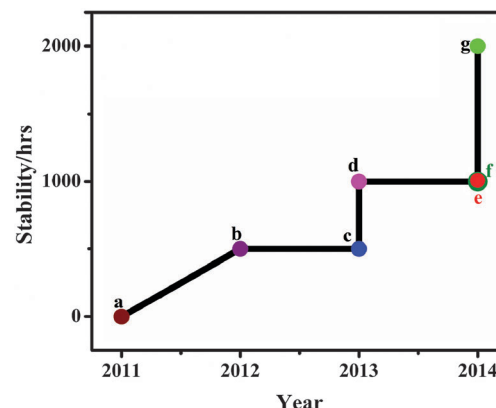


Fig. 6 Roadmap in stability for Omh-PSCs made from Omh-perovskite absorbers.

crystalline properties of synthesized Omh-PSCs, affecting the photoluminescence behavior.^{46–48} In addition, recombination effects should also be expected, but further research is needed to correlate the observed changes in recombination with the crystalline properties of Omh-perovskite samples.

Han and co-workers⁴ applied a solution drop-casting method to fabricate a novel device where its scaffolding was made of a double layer of TiO_2 and ZrO_2 enclosed in a porous carbon film. The resulting mixed cation Omh-perovskite showed higher electrical charge efficiency than conventional (planar) Omh-perovskite cells. The triple layer also resulted in a better surface contact, leading to a considerably higher stability of 1008 h in direct sun exposure. It was also shown that devices with mesoporous $\text{TiO}_2/\text{CH}_3\text{NH}_3\text{PbI}_3/\text{C}$ architectures, without encapsulation, had stabilities of over 2000 h in air in the dark.⁷ The stability evolution for Omh-PSCs is shown in Fig. 6 and Table 2.

The ability to process carbon electrodes at low temperatures on top of the $\text{CH}_3\text{NH}_3\text{PbI}_3$ layer without destroying its structure not only reduces costs and simplifies the fabrication procedures, but also improves device stability.

Although some improvements have been made to the stability of Omh-PSCs, stability issues have not yet been well-addressed. The major issue pertaining to the commercialization of an Omh-PSC device is mainly its stability. Not only issues of ambient stabilities with respect to moisture, temperature, light and oxygen, but also issues concerning intrinsic stabilities at the interface, together with questions related to the device's architecture, remain as major obstacles to practical application. All of these stability issues and obstacles are the main focus of this review article and will be discussed separately in the following sections.

3. Causes of failure and associated mechanisms of degradation

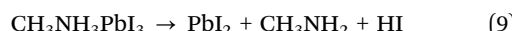
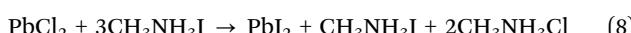
The formation of Omh-perovskite materials depends on the chemical composition of the precursor and the reaction controlling parameters, such as the temperature and pressure of the system. Dualeh and co-workers proposed that at lower temperature,

Table 2 Summary of device architecture and its stability for Omh-PSCs based on the roadmap in Fig. 6

Symbol	Device structure	Stability/h	Conditions				Ref.
			Temp.	Atmosphere	H		
a	TiO ₂ /CH ₃ NH ₃ PbI ₃ QD/liquid electrolyte/Pt ^k	0.17	RT	Air	—	27	
b	TiO ₂ /CH ₃ NH ₃ PbI ₃ /spiro-MeOTAD/Au ^k	500	RT	Air	—	15	
c	TiO ₂ /CH ₃ NH ₃ PbI ₃ /spiro-MeOTAD/Au ^m	500	45 °C	Ar gas	<1%	5	
d	Al ₂ O ₃ /CH ₃ NH ₃ PbI _{3-x} Cl _x /spiro-MeOTAD/Au ^m	1000	40 °C	N ₂ atmosphere	—	6	
e	TiO ₂ /CH ₃ NH ₃ PbI ₃ /PDPPBTE/Au ^k	1000	RT	Air	20%	44	
f	TiO ₂ /ZrO ₂ /(5-AVA) _x (MA) _{1-x} PbI ₃ /C ^k	1008	RT	Air	—	4	
g	M-TiO ₂ /CH ₃ NH ₃ PbI ₃ /C ^k	2000	RT	Air	—	10 and 37	

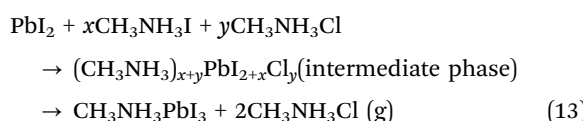
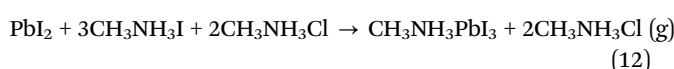
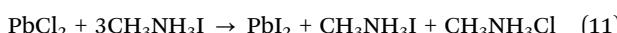
^m Encapsulated, ^k non encapsulated device, Temp. = temperature, H = humidity, RT = room temperature.

the conversion to the Omh-perovskite dominates following eqn (7)–(9) however, at a higher annealing temperature, there is the additional formation of PbI₂ (eqn (8)).⁵⁰



It has been confirmed that the CH₃NH₃PbI₃ crystal lattice does not decompose up to 300 °C, after which the organic constituent rots, governed by eqn (9).^{24,32} However, recent studies show that CH₃NH₃PbI₃ begins to transform to PbI₂ at lower temperatures up to 140 °C.⁵⁰ The excess organic CH₃NH₃Cl formed in this reaction, is believed to sublime, leaving only the CH₃NH₃PbI₃ on the mesoporous TiO₂ film, as observed from XRD measurements.⁵¹ The rate of sublimation of the organic species CH₃NH₃Cl increases with temperature, as does the precursor CH₃NH₃I, thus driving eqn (7) and (8). From these measurements it is evident that the formation of the Omh-perovskite films is a multistage process, comprising solvent vaporization, perovskite crystallization and the sublimation of excess organic CH₃NH₃Cl. These processes occur simultaneously and their relative rates determine the composition and morphology of the final film.

The release of chlorine-containing compound(s) clearly suggests the formation of crystalline MAPbX₃ films. Thus, it is vital to realize the potential chemical reaction mechanisms for the formation process of MAPbX₃. Dualeh and co-workers anticipated that eqn (10) dominates the annealing process.⁵¹ However, Zhao noted that the initial CH₃NH₃I and PbCl₂ are white and the solution mixture appears to be a light yellow color, indicating that a chemical reaction should take place forming a new phase.⁴⁹ Hence, eqn (10) possibly will engage numerous intermediate steps.



Firstly, since the molar amount of CH₃NH₃I is 3 times that of PbCl₂, eqn (11) is proposed, where part of CH₃NH₃I reacts with PbCl₂ to form PbI₂. As a result of eqn (11), the spun film contains mixed phases of PbI₂ (appears light yellow), CH₃NH₃I, CH₃NH₃Cl, and possibly some unreacted PbCl₂. During annealing, two reaction processes may occur: (1) in eqn (12), CH₃NH₃I reacts with PbI₂ to form dark brown CH₃NH₃PbI₃; meanwhile, the excess CH₃NH₃Cl breaks away from the film. The question of how excess CH₃NH₃Cl escapes from the film remains unclear, but different literatures report it as either sublimation or decomposition.⁵² (2) During the early stages of annealing or during spin coating, an intermediate phase may appear as indicated in eqn (13). In this case, during the decomposition of this intermediate phase, the CH₃NH₃PbI₃ crystal network can grow, during which the driving force can be the release of gaseous CH₃NH₃Cl (or other organic chlorides).⁴⁹

Despite the understanding of the formation of Omh-perovskite materials for solar cell use, the full advantage of these materials and their devices is still not realized due to the presence of unsolved problems. One typical example is a lack of clear understanding on the mechanism of the active material and device degradations which controls essential processes like the device life time and the mechanical stability of Omh-PSC panels. For the successful development of Omh-PSCs, it is essential to understand the degradation behaviour of Omh-perovskites and devices in general. The study of Omh-perovskite degradation behaviour is a pre-requisite for Omh-PSC applications. Such degradations can be linked to extrinsic (oxygen, light, moisture and temperature) induced and intrinsic (thermal and electric field) induced degradations. Fig. 7 shows a general scheme representing the recombination process at mesoporous TiO₂, moisture dissolution of the Omh-perovskite and photooxidation processes that take place at the interface between HTM and the counter electrode. The diffusion of O₂ is gradually sped up by UV light in the presence of TiO₂. The produced oxygen free radicals can then react with the HTM and/or active Omh-perovskite materials. H₂O is also readily activated by oxygen and light in the presence of organic molecules. Moreover, molecular oxygen and moisture may flow through the tiny pinholes present in the counter electrodes as represented in Fig. 7. Omh-perovskite materials such as CH₃NH₃PbI₃ and CH₃NH₃PbBr₃ are prone to chemical attack, thus devices typically degrade in a matter of minutes to hours under 1000 W m⁻² illumination in the ambient atmosphere. However, the impacts of these parameters that

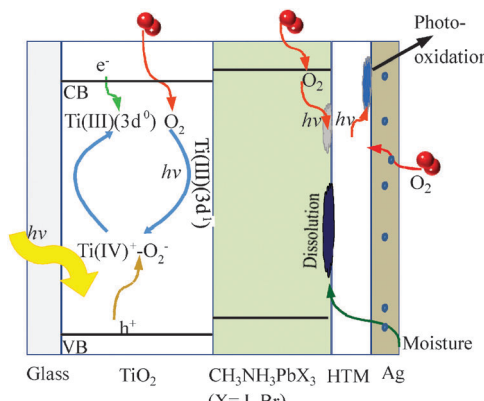


Fig. 7 General schematic representation of hole–electron pair recombination, moisture dissolution of Omh-perovskite and photooxidation processes at the interface between the HTM and counter electrode.

decrease or increase the degradation rate are not exactly clear. The objective of this section is to draw the extrinsic and intrinsic degradation phenomena and associated degradation mechanisms of Omh-perovskite materials and Omh-PSC devices when built-in in photovoltaic systems and to review the various factors influencing the stability of Omh-perovskite materials and Omh-PSCs.

3.1 Oxygen induced degradation

An important factor in the operation of any device is for it to be stable in air without the use of any type of encapsulation. The rationale behind this is that every group of materials in a device that realizes ambient stability will address an input to future improvement. Yang and co-workers compared devices stored in dry air and under nitrogen atmospheres and showed that degradation of the Omh-perovskite materials occurred in ambient air – thereby, highlighting the need for protection.³⁶ The diffusion of molecular oxygen can be activated by UV illumination in the

presence of organic molecules,^{53–55} which promote the formation of peroxide or superoxide compounds that attack and degrade the active layers.⁵⁶

The defect chemistry of the n-type semiconducting oxide gives rise to the curious behavior of fast device decline, which is primarily introduced by oxygen vacancies and interstitial defects, resulting in a non-stoichiometric composition (TiO_{2-x}). Two under-coordinated Ti(III) and one oxygen vacancy are generated when bridging oxygen atoms become eliminated. The elimination of bridging oxygen atoms from the lattice frequently results from thermal annealing. Because of their unsaturated co-ordination the generated under-coordinated Ti(III) and oxygen vacancy are reactive and adsorb O₂ molecules to form a Ti(IV)⁺–O₂^{·-} complex.⁵⁷ Among the various types of adsorbed oxygen (O⁺, O₂^{·-}, O⁻), the superoxide radical, (O₂^{·-}) is thermodynamically stable and an electron is transported to the adsorbed oxygen from the TiO_{2-x} surface.⁵⁸ Likewise, formation of O₂^{·-} can take place through a different reaction if electrons are available in excess in sub-bandgap states or the CB,⁵⁷ i.e. Ti(IV) + e_{CB} + O₂ → Ti(IV)⁺O₂^{·-}(α). Fig. 8 represents the formation of deep trap states and a depletion area as a result of oxygen adsorption and desorption processes at the mesoporous TiO₂. In Omh-PSCs, the formation of a Ti(III) (3d¹) trap state is due to the transfer of one electron to the Ti(IV) (3d⁰) of TiO₂ from the perovskite. Thus, the electron easily transfers in to Ti(IV) from Ti(III) because of the smaller bandgap between Ti(III) and Ti(IV). Those under-coordinated Ti(III) generated due to oxygen vacancies reside in sub-band gap states and work as deep trap sites. Furthermore, they attract molecular oxygen in ambient conditions, resulting in the formation of α (Ti(IV)⁺O₂^{·-}(ads)).^{57,59,60} Likewise, electrons in sub-band gap states may create β (Ti(IV)⁺O₂^{·-}(ads)). These modified states do not interfere with the device's performance when illuminated. The formation of the depletion layer can be as a result of the positive potential at the TiO₂ surface, caused by the presence of O₂^{·-}.^{6,61} Devices continuously illuminated at

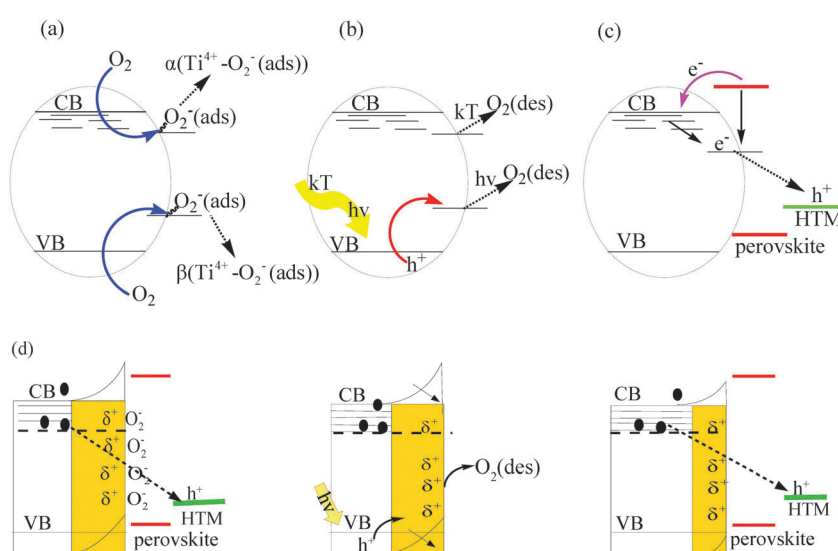


Fig. 8 Oxygen induced formation of deep trap states and depletion area at mesoporous TiO₂ surface and interface: (a)–(c) the patterning of superoxide, α and β (Ti(IV)⁺–O₂^{·-}). (d) Desorption of negatively charged superoxide molecules and their impact on the depth of the depletion zone (orange shaded area).

high temperatures deteriorate. Changing of the α superoxide complex to a Ti(III) and liberating O₂ may take place when photo-excitation of the mesoporous TiO₂ results in the formation of electron-hole pairs, through which holes in the VB are trapped with O₂⁻ in the Ti(IV)⁺O₂⁻, as shown in Fig. 8(b). The corresponding free electron in the conduction band (CB) is then trapped at the regenerating deep trap site and will ultimately recombine with an excess hole in the spiro-MeOTAD, as shown in Fig. 8(c). An adsorbed negative charge may result in an increase in the depletion area, thereby creating an upward bend in the CB that diminishes interfacial charge carrier recombination. In addition, O₂ desorption upon illumination diminishes this upward band bending and hence results in the disappearance of the Schottky barrier, a flattening of the CB-edge and a lowering of the Fermi level^{62,63}, as shown in Fig. 8(d). Oxygen-induced defects in TiO₂ are the major reasons that cause device degradation during operation.^{64,65}

3.2 Light induced degradation

UV illumination can diminish the performance of Omh-PSCs upon exposure during long-term operation due to the generation of many possible fading processes. Electron recombination thereby creates localized trapping sites and diminishes the depletion layer and TiO₂ band excitation. This may lead to the oxidation of halogen atoms in the Omh-perovskite or HTM occurring, due to UV illumination. Of course, it should be recognized that there are other sources of degradation besides UV light, e.g. oxidation, heat and ordinary visible light. UV illumination is in many cases the major cause of degradation and thus is of great concern, meaning it is necessary to use stable and broadly absorbing UV materials in order to protect both the light absorber and the substrate by either initiating a decomposition that proceeds by another mechanism such as oxidation, or by directly absorbing UV energy.

UV-induced degradation mechanisms can be explained by considering the surface chemistry of TiO₂. Mesoporous TiO₂ incorporates surface trapping states or defects (Ti³⁺), functioning as efficient deep electron-releasing states;^{66,67} the electrons in these localized trapping states,⁶⁸ bind with O₂ molecules from the environment, adsorbing the trapping states,^{69–72} and generating a complex of O₂⁻-Ti⁴⁺.^{71–73} Hence, the adsorption process is responsible for the photocurrent degradation caused by the adsorption of oxygen on TiO₂ surfaces.^{66,67,69–73} Upon bandgap excitation of TiO₂, a hole in the VB recombines with the electron at the oxygen adsorption site. This creates an electron-hole pair and desorbs oxygen.^{61,72} The excess of holes in the HTM will gradually rebind with the unbound electron remaining from the E_g excitation of the titania.^{53,74,75} The holes in spiro-MeOTAD recombine the trapped electrons.^{76–78} At a steady-state, the partial pressure of oxygen within deep trap sites governs the quantity of unfilled oxygen vacancy states. This is because of the sluggish and reversible desorption rate of oxygen.^{72,73}

In Omh-PSCs, the inorganic Pb²⁺-X⁻ creates a well ordered inorganic matrix which successfully absorbs and re-emits light. Thus, UV illumination of the local environment of the Pb-X bond could generate halogen free radicals and break down the

perovskite into dihalogens (I₂, Br₂, and Cl₂). Therefore, oxidation induced halogen elimination may be one possible reason for degradation of Omh-PSCs. Likewise, light exposure of MAPbI₃ leads to an irreversible breakdown into PbI₂.^{51,79,80}

3.3 Moisture induced degradation

Moisture is one of the main reasons of degradation that diminishes the PCE of unencapsulated Omh-PSC devices. Seok and co-workers³³ suggested that moisture degrades the PCE of unencapsulated Omh-PSC devices causing device fading and recommended that the fabrication of Omh-PSCs should be carried out in a controlled atmosphere with a humidity level of <1%.⁵ Besides, a proper humidity level (30 ± 5% relative humidity) is essential for high quality films, enhanced optoelectronic properties, and improved mass transport processes.³⁶ For instance, a CH₃NH₃PbI_{3-x}Cl_x film grown at 30% relative humidity in air had improved optoelectronic properties compared with a film grown in dry conditions. Moreover, You and coworkers⁸¹ reported a significant improvement in film morphology when Omh-perovskite precursor films were annealed in ambient air (humidity of 35% ± 5%) compared to films annealed in a nitrogen filled glovebox with the O₂ and H₂O level lower than 5 ppm. The latter annealing process results in a pristine film with a grain size of 100–300 nm, and apparent pin holes and grain boundaries.⁸¹

These pin holes and grain boundaries introduce ‘energetic disorder’ that impedes charge transport, induces recombination, and lowers photovoltaic performance.⁸² Omh-perovskite films annealed in ambient air, however, give larger individual crystal and grain sizes (beyond 500 nm), as well as reduced pin-holes and grain boundaries.^{81,82} This indicates that moisture-assisted crystal growth induces grain boundary creep as a result of the absorption of moisture within the grain boundaries and then the merging of adjacent grains together. Consequently, this effectively increases the grain size, avoids pinhole formation and finally improves the carrier lifetime.^{81,82} Additionally, adsorbed water molecules could undergo auto-ionization at the surface into hydroxyl and proton ions. As a result, surface OH⁻ sites may be formed between which protons may migrate and act as charge carriers. Thus, it would be interesting to investigate the contribution of these ions into the mass transport processes and optoelectronic properties. Furthermore, You and co-workers⁸¹ systematically studied the effect of the moisture level (20–80% humidity) on Omh-perovskite film formation. Omh-perovskite films annealed in conditions above 80% humidity showed a small amount of PbI₂ phase present in the crystals, indicating Omh-perovskite film decomposition to PbI₂ at higher humidity levels. While moisture is beneficial for high quality Omh-perovskite film growth, its relative amount should be carefully controlled.⁸¹

Moisture degradation of Omh-perovskites may be correlated with the transformation of MAPbI₃ to its MAI salt and metal halides, and hence metal halide removal may also cause Omh-PSC device degradation. Wang and co-workers⁸³ reported that during the process of assembling and testing, moisture in the atmosphere can directly degrade these materials, as indicated

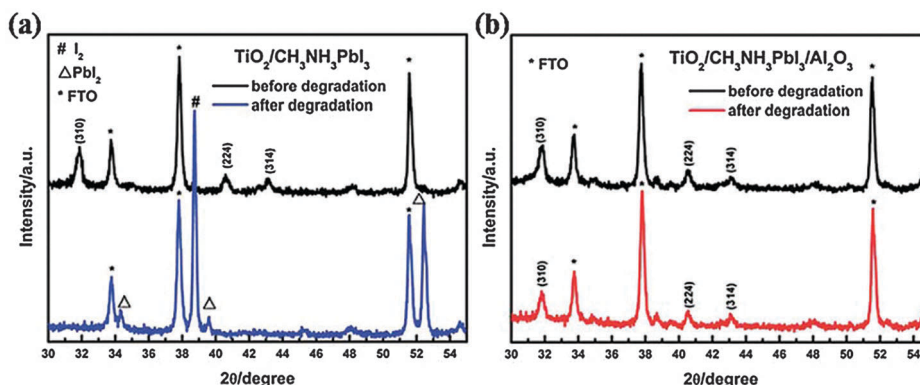
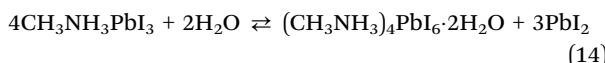


Fig. 9 XRD patterns of films of (a) $\text{TiO}_2/\text{CH}_3\text{NH}_3\text{PbI}_3$ before and after degradation, and (b) $\text{TiO}_2/\text{CH}_3\text{NH}_3\text{PbI}_3/\text{Al}_2\text{O}_3$ before and after degradation. Reproduced from ref. 83 with permission from The Royal Society of Chemistry.

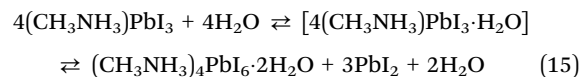
by the XRD pattern for films of $\text{TiO}_2/\text{CH}_3\text{NH}_3\text{PbI}_3$ and $\text{TiO}_2/\text{CH}_3\text{NH}_3\text{PbI}_3/\text{Al}_2\text{O}_3$ in Fig. 9. They proposed that the first step in Omh-perovskite decomposition is the reversible deprotonation of the MA cation by water, forming methylamine, hydrated HI, and PbI_2 . If this hypothesis is correct, one would expect that the volatile CH_3NH_2 would be rapidly flushed from the headspace of the *in situ* sample holder, meaning that the process would be unlikely to be reversible. Given the apparent reversibility in the bulk powder, thin films would also display a similar reversible conversion to the hydrate phase. Furthermore, the exposure of $\text{CH}_3\text{NH}_3\text{PbI}_3$ to moisture produces a hydrate product rather than simply resulting in PbI_2 .⁸⁴

In the past, Vincent and coworkers were able to study $(\text{CH}_3\text{NH}_3)_4\text{PbI}_6 \cdot 2\text{H}_2\text{O}$, which forms readily by the addition of aqueous $\text{Pb}(\text{NO}_3)_2$ to an aqueous solution of $\text{CH}_3\text{NH}_3\text{I}$.⁸⁵ In contrast to the perovskite crystal structure of $\text{CH}_3\text{NH}_3\text{PbI}_3$, the crystal structure of $(\text{CH}_3\text{NH}_3)_4\text{PbI}_6 \cdot 2\text{H}_2\text{O}$ consists of an assembly of PbI_6^{4-} octahedra and $(\text{CH}_3\text{NH}_3 \cdots \text{H}_2\text{O} \cdots \text{H}_3\text{NH}_3)_2^{4+}$ dimers arranged on a distorted NaCl-type lattice.⁸⁵ This unique structure creates a zero-dimensional network of isolated PbI_6 octahedra, as opposed to the extended three-dimensional network observed in $\text{CH}_3\text{NH}_3\text{PbI}_3$. Similarly, $(\text{CH}_3\text{NH}_3)_4\text{PbI}_6 \cdot 2\text{H}_2\text{O}$ is a pale yellow crystalline solid, and it has been suggested that the conversion from $\text{CH}_3\text{NH}_3\text{PbI}_3$ to $(\text{CH}_3\text{NH}_3)_4\text{PbI}_6 \cdot 2\text{H}_2\text{O}$ can occur in humid air.⁷⁹ Similarly, Kelly and co-workers reported further evidence for this intermediate product using a more systematic investigation of Omh-perovskite degradation processes, except that they found PbI_2 as the ultimate product.⁸⁶ The formation of a hydrated intermediate containing isolated PbI_6^{4-} octahedra as the first step of the degradation mechanism strongly suggests that the initial step of the Omh-perovskite decomposition process is not an acid-base reaction of the MA cation, but rather hydration of the Omh-perovskite film (as illustrated in eqn (14) with $(\text{CH}_3\text{NH}_3)_4\text{PbI}_6 \cdot 2\text{H}_2\text{O}$, although other hydrate compositions may be possible):⁸⁶



Since eqn (14) does not produce any volatile byproducts, it would be expected to be at least partially reversible; however,

given the propensity of PbI_2 to crystallize and give rise to phase separation, the process is unlikely to be fully reversible. The formation of hydrated intermediates containing isolated PbI_6^{4-} octahedra as the first step in the decomposition process at $98 \pm 2\%$ RH and further decomposition of $\text{CH}_3\text{NH}_3\text{I}$ to CH_3NH_2 and HI would ultimately leave PbI_2 as the only byproduct of the reaction.⁸⁶ Similarly, density functional theory analysis confirms that moisture degrades the Omh-perovskite structure because it weakens the hydrogen bonding between the PbI_6 octahedra and methyl ammonium cation.⁸⁷ While previous studies proposed $(\text{MA})_4\text{PbI}_6 \cdot 2\text{H}_2\text{O}$ as the first moisture degradation product,^{84,86} Leguy and co-workers recently confirmed that the first hydrate produced is monohydrate, $\text{MAPbI}_3 \cdot \text{H}_2\text{O}$ rather than the dihydrate $((\text{MA})_4\text{PbI}_6 \cdot 2\text{H}_2\text{O})$. $(\text{MA})_4\text{PbI}_6 \cdot 2\text{H}_2\text{O}$ can be produced upon additional hydration of $\text{MAPbI}_3 \cdot \text{H}_2\text{O}$, as described in (eqn (15)).⁸⁸



The formation of $\text{MAPbI}_3 \cdot \text{H}_2\text{O}$ can be a reversible process and form crystalline MAPbI_3 when it is dehydrated. Primary confirmation recommends that even photovoltaic performance could be restored using dehydration techniques.⁸⁸ In contrast, exposure to excess water consequences in an irreversible change into PbI_2 and ultimately leads to the complete dissolution of the MAPbI_3 layer.⁸⁹ These results help elucidate the fundamental decomposition pathways in Omh-perovskite films, which should lead to more stable materials and more commercially viable devices. It is, therefore, important to figure out the thermodynamic and kinetic merits of these degradation mechanisms. Moreover, the chemistry of moisture degradation still requires further more detailed computational and experimental evidences in order to rationalize and establish clear moisture degradation mechanisms.

3.4 Temperature induced degradation

Increasing the annealing temperature, from 40°C to 100°C for 30 min, improved the performance of a perovskite QD-sensitized TiO_2 film.²¹ However, a further increase in the

annealing temperature from 100 °C to 160 °C diminished the efficiency from 4.73% to 3.71%, due mainly to the decay in the photocurrent density. External quantum efficiency (EQE) spectra showed that the decreased photocurrent density with high temperature treatment (160 °C) is attributed to a significant loss in EQE in the long wavelength region (above 500 nm). Both the annealing temperatures and the storage temperature are important parameters that may cause Omh-PSC device degradation, as can be seen from Table 2. Though there is no literature report, it is clear that Omh-PSC devices need to pass tests such as thermal stress tests at 80 °C run for 1000 h, for the purposes of practical application. It is obvious that the operating temperature will increase to even higher than 80 °C and heat the sample film during operation due to continuous illumination from a solar simulator (e.g., 0.1 W cm⁻² sun light).⁹⁰ In addition to light, moisture and oxygen induced degradations, Omh-perovskites undergo thermal degradation. This fact will, therefore, lead to additional primary problems in the course of Omh-perovskite degradation processes. This degradation may produce PbI₂ and organic salt forms. The thermal stability of CH₃NH₃PbI₃ was confirmed to be even higher than 300 °C.^{24,32,91} However, latest literatures confirmed that the organic decomposition temperatures could be lowered up to 140 °C.^{51,52,83} The temperature induced decomposition of methylammonium iodide may lead to the formation of HI and CH₃NH₂. CH₃NH₂ could stay within the network of the perovskite, and then disturb the photovoltaic processes.⁵² Furthermore, the presence of metal halides, for example, PbI₂, as a degradation product of Omh-perovskite, is another issue. Due to their poor optical behaviour and poor light absorption ability as well as their higher bandgap, lead halides cause device deterioration. Additionally, the mechanism of expansion and compression in the dimensional changes of the perovskite structure at low and high temperatures is not yet clear. Moreover, high temperatures can cause the diffusion of interlayer, diffusion of the metal counter electrode, ohmic contact degradation and device architecture degradation, and thus the mechanisms for these phenomena should be reported carefully. For this reason, new Omh-perovskites which possess enhanced intrinsic resistance towards temperature are better candidates for future development in areas of Omh-PSC based photovoltaic technologies.^{79,92} For instance, FAPbI₃ is more temperature resistant than MAPbI₃.⁹²

3.5 Thermal and electric field induced intrinsic degradation

The interface is the main origin of degradation in Omh-PSCs. The question of how the interface can cause degradation is related to the intrinsic deprivation of Omh-PSCs. The origin of this degradation is: (1) the temperature induced flow of components due to thermal evaporation during deposition and light illumination during operations. This thermal induced migration of component materials at the interface results in inter-diffusion, phase segregation and separation, presenting an inherent strain. (2) Electric field induced ion migration which leads to electro-migration and hysteretic effects. In the electro-migration process, an electric current flowing in a conductor may move metal ions. Electro-migration pushes anions to the anode and builds up a compressive stress there. The vacancy concentration in the anode becomes less than the equilibrium vacancy concentration according to the Nabarro Herring model of point-defect formation in a stressed solid.⁹³ In the hysteresis process, ion migration is particularly sensitive to the concentration of mobile vacancies (or interstitials) depending on the mechanism. Thus, the size of crystalline domains, degree of crystallinity and stoichiometry can affect the transient behavior of Omh-PSC devices.⁹⁴ This transient behavior is different from device to device. For instance, the larger transient difference between mesoporous and planar devices is most probably due to variations in the composition stoichiometry or morphology. Therefore, minimizing ion migration is an essential mechanism in extending the stability of devices.

Moreover, TiO₂ has a strong ability to extract electrons from organic materials as photocatalysts and from iodide (I⁻) as electrodes in DSSCs. Hence, the driving force of the decomposition mechanism may be due to the effect of electron extraction by TiO₂ from an iodide anion accelerated by light illumination during operation. The possible decomposition pathway at the TiO₂ surface may be as shown in eqn (16)–(18):⁹⁵



Decomposition of a CH₃NH₃PbI₃ crystal under UV light illumination is shown in Fig. 10. Since CH₃NH₃PbI₃ is a combination of CH₃NH₃⁺, Pb²⁺, and I⁻ ions, TiO₂ can extract electrons from I⁻,

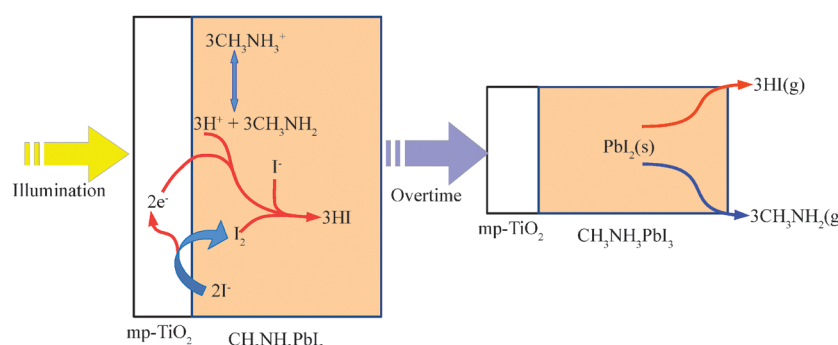


Fig. 10 Degradation scheme of CH₃NH₃PbI₃ on mesoporous TiO₂ (mp-TiO₂) during UV light exposure tests. Redrawn based on ref. 95.

producing I_2 at the interface between TiO_2 and $CH_3NH_3PbI_2$ as shown in eqn (16). This will lead to breakdown of the perovskite crystal. Eqn (17) is in equilibrium. The electron taken by TiO_2 can go back to the TiO_2 surface, and eqn (18) can take place while releasing HI (Fig. 10). As H^+ is consumed by eqn (18), the equilibrium of eqn (17) can favor the right hand side, with the release of CH_3NH_2 due to its low boiling point ($17\text{ }^\circ C$).⁹⁶ It is, therefore, crucial to realize three of the possible major consequences of iodide ion migration that could occur in $MAPbI_3$ based Omh-PSCs: (i) iodide may diffuse out into the TiO_2 layer, (ii) its distribution may be influenced by the electric field in the Omh-perovskite materials or by any modification of it, which is because iodide moves as a negative ion, and (iii) iodide migration may appear to be involved in some of the observed electrical metastability of the device. These all are pertinent to the interface stability. The stability of the Omh-perovskite layer under light exposure drastically vanishes, and shortens the lifetime of the Omh-perovskite. The origin of degradation for $CH_3NH_3PbI_3$ layer is the interface between TiO_2 and $CH_3NH_3PbI_3$. This degradation is as a result of the variable positioning of the $CH_3NH_3^+$ cation in the $CH_3NH_3PbI_3$ crystal.^{97–99}

Moreover, recent computational reports^{100–104} overview the defect formation energy for various defects together with the cations (MA_{Pb} and Pb_{MA}) and antisites (MA_I , Pb_I , I_{MA} , and I_{Pb}) exchange, interstitials (MA_i , Pb_i , and I_i) and vacancies (V_{MA} , V_{Pb} , and V_I). The kinetically and energetically unstable antisites impulsively break up into the respective vacancies and interstitials.¹⁰⁴ Because of their low formation energy, interstitials and vacancies are the most likely defects. Interestingly, Angelis and coworkers¹⁰⁵ developed a diffusion path to model vacancies and defect migration along the perovskite crystal for all of the four explored defects, as shown in Fig. 11. Vacancies and interstitial defects are referred to with dashed circles and red atoms, respectively. While dashed lines show the trajectory of the vacancies, solid lines represent migration of the ions. Fig. 11a shows the formation of a vacancy, V_I , in an equatorial position and its migration towards an axial site. V_I in equatorial or axial sites have almost the same energy ($<0.01\text{ eV}$). However, the axial site is preferred by 0.07 eV over the equatorial site for V_{Br} , as shown in the supplementary information of ref. 105. The inorganic scaffold is responsible for the hopping of V_{MA} between its nearby cavities that lie in the ab plane, as shown in Fig. 11b. Moreover, V_{MA} diffuses across the framework of the Pb_4I_4 structure. Similarly, Fig. 11c indicates an in-plane migration of V_{Pb} where V_{Pb} travels beside the square created by four I and four Pb atoms. Similar to V_I , the pathway in the direction of the c axis from Fig. 11d refers to iodine interstitials (I_i). In the initial and/or last configurations, the interstitial iodine atom places in between a couple of equatorial and/or axial I atoms, with almost the same lengths (3.96 and 3.87 \AA), respectively.^{105,106}

This migration of defects/ion such as iodine vacancies across the interface can induce interface degradation, affect device operational mechanisms and finally cause device failure during operation.¹⁰⁵ The formation of metal oxides, metal halides and molecular halogens can take place due to oxidation and reduction processes in the presence of oxygen and light.

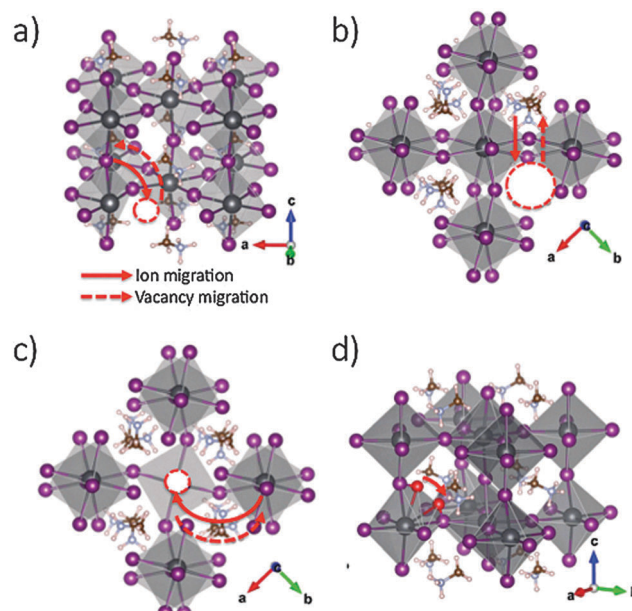


Fig. 11 Pathway for migration of vacancies and defects: iodine (a), methylammonium (b), lead (c) and iodine defects (d). The colours of black, purple, white, blue and brown represent Pb, I, H, N and C atoms, respectively. Reproduced from ref. 105 with permission from The Royal Society of Chemistry.

The chemistry of such ion/defect migration induced interfacial reactions, as well as its impact on the device stability, needs further detailed computational and experimental study. Above all, in order to investigate the ion-migration mechanisms of $MAPbI_3$, studies on ion occupations are of great importance.

4. Origins of Omh-PSCs degradation

In addition to identifying the main causes of degradation, it is critical to isolate the key origin of degradation. Thus, more detailed discussion on device components and architecture and interface, including the buffer, is essential, all of which are the focus of this section.

4.1 Effects of device components

Omh-PSCs are multilayered devices which are a combination of an active Omh-perovskite material, n-type and p-type electron and hole selective layers, as well as the counter electrode. In addition, different interlayers for different functions can be inserted. These multilayered devices are prone to component degradation. The origin of this degradation can be from components such as light harvesting active materials, electron and hole selective layers, anode and cathode materials, as well as the interlayer or buffer layer materials, which are the main focus of this subsection.

4.1.1 Omh-perovskites. Omh-perovskite semiconductor materials include $CH_3NH_3PbI_3$, $CH_3NH_3PbBr_3$, and mixed Omh-perovskites including mixed metal cations, organic cations and mixed halide anions. Omh-perovskite structures have become innovative alternatives for the next-generation of high performance

solar cells, because they combine the advantages of both systems (organic and inorganic cages).

4.1.1.1 Triiodide anions. A critical issue for Omh-perovskite materials is their stability. The highest reported stability of Omh-PSCs with light absorbing MAPbI₃ is 2000 h.⁷ Compared to Si solar cells, this stability is quite poor due to the ambient sensitivity of the CH₃NH₃PbI₃ semiconductor. This instability has been a major obstacle since Omh-perovskite-type materials contain hygroscopic amine salts. CH₃NH₃PbI₃ undergoes a rapid change to hydrated CH₃NH₃PbI₃ and then to PbI₂ in the presence of moisture at room temperature,^{84,86} resulting in a significant decline in the device performance.¹⁰⁷ Furthermore, the formation of stress and microstrain, and the origin of degradation in the CH₃NH₃PbI₃ perovskite structure under severe conditions are still open questions. CH₃NH₃PbI₃ structural changes during operation is also another challenge. For instance, this can cause poor thermal and photoconductivity, and hysteresis in the device during operation.^{108,109} Furthermore, when the operating temperature increases to a higher temperature (~58 °C) the structure of MAPbI₃ changes from the ordered tetragonal into the disordered cubic structure. Conversely, when the operation/processing temperature decreases to room temperature, its structure returns back to its ordered tetragonal shape.^{110,111} Thus, how this ordered-disordered structure of the MAPbI₃ material could affect both the performance and long term stability is also another issue.

Moreover, the poor resistance of CH₃NH₃PbI₃ and a device based on this material towards the combined effect of all these operating conditions can be even more problematic. This may restrict the use of these compounds for many practical applications and commercialization. Interestingly, the beneficial or detrimental behavior of grain boundaries in CH₃NH₃PbI₃ film still remains under debate. Previous reports on perovskites have demonstrated that grain boundaries are less harmful than in other semiconductors,^{112,113} and are rather beneficial for the collection of perovskite carrier efficiency.¹¹⁴ On the other hand, it is reported that single-crystal perovskites demonstrated a rather higher performance^{115–117} illustrating a progress in carrier lifetime.^{118,119} Conversely, current reports suggested that grain boundaries are connected with PL quenching, demonstrating that they are not as kind as have been recommended in the past. Instead of this, they destruct the carrier lifetime.¹²⁰ These interesting debates on the role of grain boundaries for carrier lifetime and performance in perovskite materials are future interesting topics of study. Despite their impact on carrier lifetime and performance, the contributions of these grain boundaries towards operational and long term stabilities of Omh-PSCs are not yet known.

4.1.1.2 Tribromide anions. MAPbI₃ reverts to its precursors due to its hydroscopic nature.³³ However, the bromide-based perovskites have been proved to be less moisture-sensitive.¹²¹ A higher stability or resistance to photobleaching and decomposition was reported after exposing MAPbBr₃ films to conditions of stress (*i.e.* light intensity, and temperature).¹²² The better

stability of MAPbBr₃ films, compared with their iodide counterpart, may be related to differences in the bond strengths and the crystalline forms of the two Omh-perovskites. Thus, further investigation is still required on how bromine inclusion provides better stability in both material and device aspects. Despite the better photochemical stability of MAPbBr₃ films, its larger optical band gap ($E_g \approx 2.3$ vs. 1.58 eV for MAPbI₃) would reduce the PV performance of MAPbBr₃ single junction devices.²² Katz proposed that MAPbBr₃ could be efficiently used as a top sub cell in future tandem Omh-perovskite-based PV architectures.¹²² A mixed halide Omh-perovskite, MAPb_{1-x}Br_x, with a larger band gap than MAPbBr₃, may therefore have applications in Omh-perovskite based solar cells that combine high efficiency and stability.

4.1.2 Mixed Omh-perovskites. As discussed in Section 4.1.1.1, CH₃NH₃PbI₃ suffers from long-term ambient stability due to its sensitivity towards moisture.^{84,86} In addition, Weber and co-workers reported the temperature-dependent structure of CH₃NH₃PbX₃ (X = Cl, Br, I).⁹⁹ The structure of CH₃NH₃PbX₃ changes from orthorhombic to cubic structures as a function of temperature. The order of the methylammonium cation is also different in different crystal structures. It is also worth noting that at room temperature, CH₃NH₃PbI₃ forms a tetragonal structure below 327.4 K, whereas CH₃NH₃PbBr₃ and CH₃NH₃PbCl₃ form cubic structures at 236.9K or above. This order-disorder behavior of the perovskite structure caused by thermal cycles could give a variance in microstructure and stability. Moreover, Swainson and co-workers found a phase transition of CH₃NH₃PbBr₃ just below 1 GPa and amorphization around 2.8 GPa, without the process undergoing a long-range orientation ordering of cations.¹²³ The volume reduction under compression was attributed to the tilting of the PbBr₆ octahedra. Suga and co-workers also gave the pressure-temperature phase relations of CH₃NH₃PbX₃ crystals in the range between 0.1 Pa and 200 MPa in detail.¹²⁴ The crystalline phase of the Omh-perovskite can change due to environmental conditions, such as temperature and pressure, which directly affects the stability of Omh-PSCs. In order to improve the stability of Omh-PSCs, emphasis should be given on gaining a comprehensive understanding of the crystal structure of Omh-perovskite under different conditions such as moisture and temperature, as well as the relationship between the crystal structure and pressure. In general, the poor structural stability of Omh-perovskites could be improved by modifying the Goldschmidt tolerance factor (t_f) using appropriate substitutions, which can be defined by the following mathematical expression in eqn (20),^{125,126}

$$t_f = \frac{r_A + r_X}{\sqrt{2}(r_B + r_X)} \quad (19)$$

where r_A , r_B , and r_X are the radii of cation A, cation B, and halogen, respectively, in the ABX₃ structure. That equation is applied at room temperature to the empirical ionic radii. In order to stabilize the cubic structure, the t_f of Omh-perovskites should be closer to unity.¹²⁷ To form a stable Omh-perovskite structure, the size of the ionic radius is restrained by the tolerance factor. The ionic radius is the most important ionic parameter that dominates the crystal structure of ionic compounds.

The ideal cubic structure may be seen as a network of BX_6 octahedra, where all the octahedra are corner sharing. The 'A' ions occupy the cubo-octahedral holes in between the octahedra. Many derivatives of the ideal structure are found and the distortion of the structure from cubic is often considered to be determined by the relative sizes of the different ions of the compound.

4.1.2.1 Metal (B) cation. The organic cation CH_3NH_3^+ in ABX_3 is responsible for the structural stability of the Omh-perovskite materials, while the electronic properties are largely determined by the inorganic matrix (metal-halide hybridized orbital).^{102,128,129} The main problem associated with MAPbI_3 is its poor ambient stability under different environmental conditions.^{24,33} In order to avoid this limitation for both indoor and outdoor application, any modifications that can be made to strengthen the material stability would be beneficial. One successful technique is to combine PbI_2 with SnI_2 to form $\text{CH}_3\text{NH}_3\text{Sn}_x\text{Pb}_{1-x}\text{I}_3$, which has an E_g value of 1.1 eV. The edge of the incident-photon-to-current efficiency (IPCE) curve extended to 1060 nm.^{25,82,130} Nevertheless, Sn^{2+} easily changes to Sn^{4+} in the atmosphere. Consequently, this leads to device deterioration. Other Omh-perovskites incorporating divalent metal cations such as Be^{2+} , Mg^{2+} , Ca^{2+} , Sr^{2+} , Ba^{2+} , Zn^{2+} , Ge^{2+} , Fe^{2+} , Co^{2+} and Ni^{2+} do not yet report on this application. Another tactic is to replace the organic cations, as it has been established that enlargement of the octahedral network significantly influences the bandgap of the Omh-perovskite.

4.1.2.2 Organic 'A' cation. The organic cation in ABX_3 is a key part of the Omh-perovskite that determines its structure and dimensionality, and has a direct influence on the stability and opto-electronic properties of the material. The cubo-octahedral cavity, defined by the four edge-sharing BX_6 octahedra, only permits the incorporation of small cations into the 3D perovskite structure. The phenomenological derivation of t_f allows an estimation of the stability based on the size of its constituents.¹³¹ To obtain a cubic phase, t_f should be unity; however, for most of the cubic structures the value of t_f ranges from 0.78–1.05, due to a slight expansion in distorted structures.¹³² In fact, by changing r_A , t_f can be varied but only in a restricted range of values around unity ($t_f = 1$ corresponds to a perfectly packed Omh-perovskite structure) to have a stable and evenly distorted 3D Omh-perovskite structure.¹³³ The dynamic position conduction band of $\text{CH}_3\text{NH}_3\text{PbI}_3$ films, due to the disordered organic cation, plays a major role in extending the lifetime.¹³⁴

So far, the most investigated organic cation counterpart for the substitution of MA (CH_3NH_3^+) has been FA ($\text{HC}(\text{NH}_2)_2^+$), which gives rise to a t_f of 0.99, higher than $t_f = 0.91$ for $\text{CH}_3\text{NH}_3\text{PbI}_3$ (ion size: FA – 2.53 Å, MA – 2.17 Å, Pb^{2+} – 1.19 Å and I^- – 2.20 Å). In a recent report, the FA cation, which is slightly larger than methylammonium, was confirmed to form a 3D Omh-perovskite with a lower bandgap of about 1.47 eV. Omh-perovskites are described as any compound which crystallizes in the ABX_3 structure, containing corner-sharing BX_6 octahedra with the cationic component neutralizing the total charge.

MAPbI_3 exhibits a tetragonal shape at room temperature as a result of the distortion of the cubic crystal.¹³⁵ The organic cation was considered as it does not take part in determining the band structure, and works to fulfill charge neutrality within the lattice.¹³⁶ However, its size is quite vital. The size of the organic cation can cause the entire network to enlarge or be compressed.

FAPbI_3 is not sensitive, even at high temperature, compared to MAPbI_3 . While MAPbI_3 discolors in 30 minutes, FAPbI_3 does not discolor even at 150 °C under ambient conditions. Subjecting the material to a moist atmosphere resulted in fading of the FAPbI_3 , the same as for MAPbI_3 .¹³⁷ However, recent work on the long-term stability of Omh-PSCs suggests that with sufficient encapsulation, FAPbI_3 functions continuously under illumination for thousands of hours, and this is not likely to act as a serious limitation to commercialization.^{5,6} Furthermore, superior temperature stability is exceptionally promising towards long term thermal durability, and this would be an additional topic that needs to be studied. Stable Omh-PSCs with a cationic alloy structure have recently been fabricated in the laboratory.⁴ A 5-aminovaleric acid (5-AVA) cation replaced some of the MA cations in the cuboctahedral site of MAPbI_3 , forming the new mixed cation Omh-perovskite, $(5\text{-AVA})_x(\text{MA})_{1-x}\text{PbI}_3$. A more stable new Omh-perovskite, $(\text{PEA})_2(\text{MA})_2[\text{Pb}_3\text{I}_{10}]$ ($\text{PEA} = \text{C}_6\text{H}_5(\text{CH}_2)_2\text{NH}_3^+$, $\text{MA} = \text{CH}_3\text{NH}_3^+$) has also been reported.¹³⁸ Films of these materials are more moisture resistant than films of MAPbI_3 and devices can be fabricated under ambient humidity levels. This moisture resistance ability may be due to the more hydrophobic tail 'R' group, which may mask the hydrophilic nature of the materials. However, the fundamental reason for alloy stabilization of the structures requires further study.

4.1.2.3 Mixed anion halides

$\text{MAPb(I}_{1-x}\text{Br}_x\text{)}_3$. The stability of MAPbI_3 can be significantly improved with a small fraction of Br or Cl.^{33,139} Although the MAPbI_3 hybrid solar cell does not show significant PCE degradation at low humidity (<50%), the MAPbI_3 began to decompose at relatively high humidity ($\geq 55\%$), displaying a color change from dark brown to yellow.³³ Hence, the solar cells were intentionally exposed to a relatively high humidity (55%) for one day while keeping the humidity to 35% on the other days. Interestingly, the $\text{MAPb(I}_{1-x}\text{Br}_x\text{)}_3$ ($x = 0, 0.06$) hybrid solar cells exhibited serious PCE degradation after exposure to 55% humidity, whereas the other $\text{MAPb(I}_{1-x}\text{Br}_x\text{)}_3$ ($x = 0.2, 0.29$) cells maintained their PCE. A low sensitivity to humidity of the cells based on $\text{MAPb(I}_{1-x}\text{Br}_x\text{)}_3$ ($x \geq 0.2$) might be associated with their compact and stable structure, because the substitution of larger I atoms with smaller Br atoms in $\text{MAPb(I}_{1-x}\text{Br}_x\text{)}_3$ leads to a reduction to the lattice constant and a transition to a cubic phase. As a result of introducing Br⁻ ions into the perovskite structure, the lattice parameter changes from 5.921 for the $\text{CH}_3\text{NH}_3\text{PbBr}_3$, 6.144 for the MABr/MAI 2 : 1, and 6.223 for the MABr/MAI 1 : 2. The change in the lattice parameter is due to the difference in the ionic radii of Br⁻ (1.96 Å) and I⁻ (2.2 Å).¹⁴⁰ The smaller ionic radius of Br⁻ is the main reason for the formation of the cubic structure when Br is introduced into the perovskite structure.¹⁴¹ Thus, the role of bromine inclusion

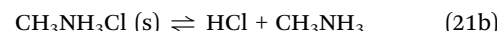
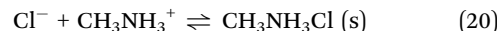
in thermal, light and ambient stabilities should be identified. Such a comparative study could help towards better stability improvements.

MAPbI_{3-x}Cl_x In contrast to CH₃NH₃PbI₃, this iodide–chloride mixed-halide Omh-perovskite was remarkably stable to processing in air. The absorption spectra demonstrated good light-harvesting capabilities over the visible to near-IR spectrum and were also stable to prolonged light exposure, as demonstrated by 1000 h of constant illumination under simulated full sunlight.^{6,139} The improved stability can be associated with its compact and stable structure, due to the substitution of larger I atoms with smaller Cl atoms in MAPbI_{3-x}Cl_x. This leads to a reduction of the lattice constant and a transition to a cubic phase, which is similar to the substitution of iodide using bromide.¹²² This compact structure would decrease the sensitivity of the MAPbI_{3-x}Cl_x material to moisture, light and temperature due to its higher binding constant compared to the MAPbI₃ materials. But these need to be investigated. Overall, there is no clear evidence of the role of chlorine insertion to enhance stability. Both MAPbI₃ and MAPbI_{3-x}Cl_x have similar light absorption ranges, while MAPbI_{3-x}Cl_x has a longer recombination lifetime than MAPbI₃, followed by a longer electron diffusion length. In this regard, MAPbI_{3-x}Cl_x does not require a mesoporous electron transport layer (*e.g.* TiO₂) unlike MAPbI₃.^{26,112} The long electron diffusion length enables MAPbI_{3-x}Cl_x to work perfectly on insulating scaffolds and in bulk films.^{34,142}

MAPbBr_{3-x}Cl_x Among the family of Omh-perovskites, MAPbBr_{3-x}Cl_x has a larger band gap than iodine based Omh-perovskites such as MAPb(I_{1-x}Br_x)₃ and MAPbI_{3-x}Cl_x. MAPbBr_{3-x}Cl_x has enormous capability for high energy photons in photovoltaic applications such as tandem cells, or in other devices which possess photon spectral splitting.^{143,144} But the Omh-perovskite materials suffered from a moisture-related decomposition because of the hygroscopic amine salts.^{33,145} In a stability test, MAPbBr_{3-x}Cl_x was found to be less moisture-sensitive.¹²¹ The as prepared MAPbBr_{3-x}Cl_x films were left in the dark at room temperature with exposure to ambient air for 30 days. The materials did not show any apparent changes in the XRD patterns observed after this time, indicating the good stability of MAPbBr_{3-x}Cl_x. This significantly improved stability may be due to a small fraction of Br or Cl substitution.^{33,139} It is not clear which atom contributes more to the structural stability. Similarly, the thermal and radiation stability of MAPbBr_{3-x}Cl_x is not yet resolved. Hence, detailed evidence for the contributions of bromine and chlorine to thermal and radiation stability of the perovskite structure and to the thermal and photoconductivity are required.

4.1.2.4 Chloride inclusion. The issue of chloride loss has recently been raised.^{49,51,146} Currently considered loss pathways center around MACl^{49,51,147} sublimation, or the degradation of MACl into volatile hydrochloric acid (HCl) and methylamine species, facilitated by residual water.⁸³ The loss mechanism suggests that chloride must diffuse into the film's surface to ultimately escape the system, meaning that bulk sensitive

composition measurements, *e.g.* XRD, EDS may miss the residual chloride remaining at the Omh-perovskite's surface.¹⁴⁸



Sublimation of CH₃NH₃Cl (eqn (21a)), or its decomposition into HCl and CH₃NH₂ (eqn (21b)) may be responsible for the loss of chloride during film growth. Thus, the inclusion of Cl⁻, from either metal chloride (*e.g.*, PbCl₂) or organochloride such as CH₃NH₃-Cl, has become the most commonly applied strategy.

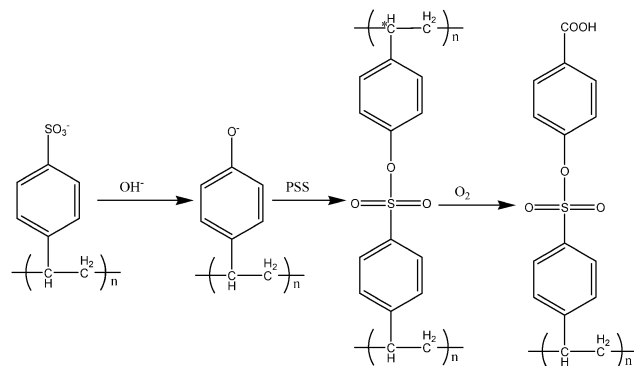
In terms of how Cl additives such as CH₃NH₃Cl contribute to improve stability and/or reduce degradation, several reasons are considered. (1) Cl inclusion could increase the binding constant, which may reduce the rapid dissolution or degradation of CH₃NH₃PbI₃ in moisture. This fact might be related to the stable structure of CH₃NH₃Cl, owing to a more compact Omh-perovskite cubic structure in which the degradation of the methylammonium cation is prohibited.^{122,149} (2) It facilitates the removal of excess CH₃NH₃⁺ ions.⁴⁹ Excess CH₃NH₃⁺ ions may act as defects or impurities at surface or interface sites, which may lead to the blocking of interfacial processes. (3) Cl-rich nucleation sites lead to better crystal coalescence¹⁴⁶ or high quality film crystallinity,⁴⁹ and also provide a stable morphology as well as a better coverage in Omh-PSCs fabricated by one-step solution processes (because poor morphology stability and poor coverage could lead to device deterioration). (4) It enhances the lifetime of the photoexcited species (the presence of chlorine may creep grain boundaries¹²⁰ and ultimately controls perovskite grain structures¹⁵⁰). All of these factors contribute to higher stability. Despite this helpful information, there is no clear evidence on the chlorine inclusion/stability relationship. In general, mixing halides in Omh-perovskites has shown beneficial effects in terms of enhancing stability. CH₃NH₃Pb(I_{1-x}Cl_x)₃ is remarkably stable during processing in air compared to CH₃NH₃PbI₃. The atomic ratio of Cl in CH₃NH₃Pb(I_{1-x}Cl_x)₃ was proposed to be up to one third, as it is in precursors.^{97,139} However, recent experiments^{142,151} showed that its atomic ratio is less than 4% and that most of the precursor Cl may be lost. Therefore, the ratio of Cl into iodine should be seriously controlled. For real practical applications, the miscibility between Cl and iodine mixed halides, and the fundamental contributions of Cl to stability need to be addressed. Similarly, different devices incorporating CH₃NH₃Pb(I_{1-x}Cl_x)₃ material showed different performances – one has inferior performance but the other improved performance.¹⁵⁰ Thus, how the chlorine inclusion mechanisms during fabrication processes affect device stability is not yet well understood. Whether bromide sources could act in a similar manner to chloride sources as additives in Omh-PSC fabrication is also another important open question for the community.

4.1.3 Hole transport layer. Hole transporting layers such as spiro-MeOTAD, PEDOT:PSS and other polymers, and inorganic materials are significantly more stable than liquid electrolytes, but devices based on these materials are also susceptible to

chemical degradation, during which photooxidation processes and hole–electron pair recombination may occur. In this section, we mainly focus on the most commonly used HTMs, spiro-MeOTAD and PEDOT:PSS.

4.1.3.1 Spiro-MeOTAD. Spiro-MeOTAD is a material widely used in Omh-PSCs for hole transporting purposes. Spiro-MeOTAD is coated beneath the counter electrode and can easily be exposed to the atmosphere. As a result, degradation can take place due to air exposure, continuous light irradiation, elevated temperature and dust. Qi and colleagues investigated the causes of degradation of Omh-PSCs which use spiro-MeOTAD as the hole selective material.^{152,153} Due to its amorphous properties, spiro-MeOTAD is a crucial HTM; on the other hand, small molecular species from the air could simply spread, and pass freely through minuscule pinholes in the amorphous material. Unfortunately, these pinholes are too small to be seen with an optical microscope.^{152,153} Moreover, the decline in J_{sc} and FF is possibly caused by Omh-perovskite layer degradation, which can be caused by (1) air molecules (O_2 , H_2O , etc.) migrating and interacting with Omh-perovskite *via* the pinholes and/or (2) out-diffusion of mobile ions in the Omh-perovskite film *via* the pinholes in the spin coated spiro-MeOTAD.¹⁵⁴ The pinholes may create pathways for foreign molecules such as water and other gas molecules in air to diffuse through the thin film, as shown in Fig. 12. These air molecules would then become impurities in the solar cells, leading to degradation and resulting in a drop in solar cell efficiency.

It is now clear that the presence of oxidized spiro-MeOTAD is required for Omh-PSCs. However, oxygen reduction reactions might also occur. The generation of O_2^- would change the oxidized spiro-MeOTAD concentration and device characteristics during the operation. For the future development of devices with long-term stability, it will be important to exclude oxygen reduction. Further work is needed to determine if this can be achieved by sealing the devices after preparation under ambient atmosphere, or whether the devices should be fabricated and sealed to exclude oxygen and moisture.



Scheme 1 Proposed oxido-de-sulfonato substitution of PSS in PEDOT:PSS layers. Reprinted from ref. 159. Copyright 2008, with permission from Elsevier.

4.1.3.2 PEDOT:PSS. Poly(ethylenedioxythiophene):poly(styrene sulfonic acid) (PEDOT:PSS) is generally used in the form of a water solution/suspension for solar cells as the HTM,¹⁵⁵ and has recently been used in inverted Omh-PSCs as a hole selective material.^{156–158} This hygroscopic property of PEDOT:PSS destabilizes the interface and will result in device deterioration. Moreover, compared to PEDOT, the amount of PSS usually dominates in the polymer mixture and the diffusion of PSS into other layers can occur and possibly result in degradation. For instance, the PSS may undergo a oxido-de-sulfonato-substitution forming the phenolate which can then react with PSS, forming two PSS chains linked together *via* a sulfonic ester group, as shown in Scheme 1.¹⁵⁹ The asterisk in Scheme 1 indicates oxidation of the carbon. Additionally, corrosion will be enhanced not only in connection with low work function metals such as Al or Ca used as a counter electrode, but also in connection with an ITO electrode.^{56,160}

Dauskardt and coworkers¹⁶¹ verified how the hygroscopic properties and poor adhesion of PEDOT:PSS onto the active layer causes a general loss of device performance in a roll-to-roll processed normal geometry organic photovoltaic devices. The objective was to show that the thermomechanical stress in a real life device would suffer.

4.1.4 Metal counter electrode. Gold, silver and aluminum metals are commonly used as counter electrode materials in mesoporous, planar and inverted Omh-PSCs.¹⁵⁷ The drawbacks of silver may be its corrosion in contact with the halide ions from the Omh-perovskite light absorber, forming silver halides such as AgCl in humid environments, and short circuits or shunting paths with the mesoporous TiO_2 , leading to device degradation.⁶ The high cost of a Au electrode also requires a high-vacuum evaporation technique, thereby limiting its future application. Low-cost carbon may be an ideal material to substitute Au as a back contact with Omh-perovskite heterojunction (HJ) solar cells at low temperature, because its function is similar to that of Au.⁷

4.2 Effect of device architecture

Both the device stability and efficiency of Omh-PSCs depend on their architecture, which will in turn influence the choice of materials and deposition methods. Three main device architectures

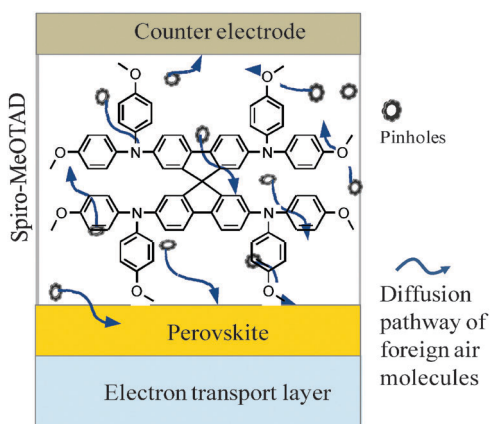


Fig. 12 Diffusion of foreign air molecules into the device through spiro-MeOTAD.

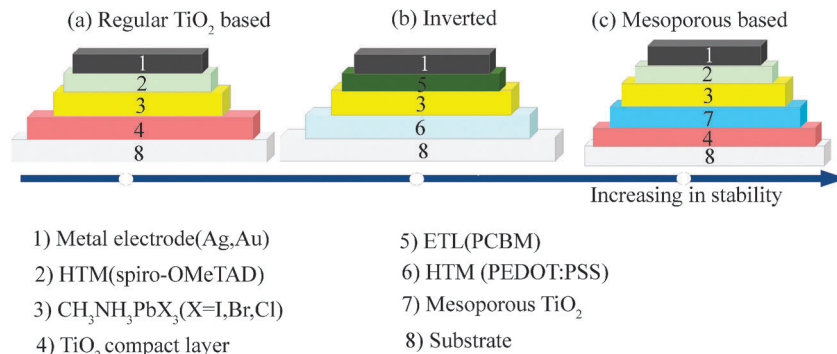


Fig. 13 Stability comparison of three Omh-PSC device architectures.

present in Omh-PSCs: the planar (regular TiO_2 based), inverted (PEDOT:PSS based) and mesoporous structures, are schematically represented in Fig. 13. Since the initial evolution of Omh-PSCs, many research groups have been focusing on efficiency and fabrication processes; hence, several review papers are available.^{96,162–165} In this section we will only focus our discussion on the device architecture stability. Investigation of device architecture, which remains unclear in terms of its effects on the device stability, should also be included in long-term stability tests.

4.2.1 Planar (regular) TiO_2 . The planar (or alternatively regular) architecture inherits features of the most commonly utilized mesoscopic Omh-PSC device architecture (FTO/cl- TiO_2 /perovskite/spiro-MeOTAD/Au). Primarily, any excellent electron transporting layer can be deposited on fluorine doped tin oxide or other substrate, and then after the Omh-perovskite layer, the HTM and finally, the counter electrode, are coated in chronological order. The application of a single compact n-type metal oxide layer makes the regular type different from the mesoporous devices which consist of both compact and meso-structured scaffolds. The regular configurations have been observed to boast high efficiencies, similar to their mesoscopic counterparts. Their stability, however, is still in minutes⁹⁴ compared to their mesoscopic counterparts. This may be due to: (1) faster charge collection at the interface, due to ion migration resulting from an applied bias or field, creating transport barriers in the planar architecture and (2) a strong hysteresis effect in planar devices: undesirable shifts in electrical conductivity that occur when applying increasing or decreasing amounts of voltage to a cell.¹⁶⁶ Thus, in detailed studies on the stability of the compact TiO_2 -perovskite and Omh-perovskite-HTM interface stability, pore filling properties, sensitivity towards light and moisture, formation of a shunting path with the HTMs and/or metal electrodes and carrier accumulation due to excess ions, and the formation of trap states and defects at the Omh-perovskite and compact TiO_2 surfaces, the effects of the presence of excess ions in the Omh-perovskite on the device architecture will be critical.

4.2.2 Inverted (PEDOT:PSS based). Chen and coworkers pioneered an inverted based device architecture made of PEDOT:PSS coated directly on the transparent conductive substrate and C_{60} derivatives such as [6,6]-phenyl C_{61} -butyric acid methylester (PCBM) and indene- C_{60} bisadduct (ICBA), coated next

to the Omh-perovskite, as electron selective layers, respectively.¹⁶⁷ The ambipolar properties, especially the superior p-type character of $\text{CH}_3\text{NH}_3\text{PbI}_3$ which is greatly biased by the p-n heterojunction idea in organic solar cells, was the motivation for the authors' initial material choice.¹⁶⁸ The planar heterojunction architecture with an inverted design achieved a higher PCE in a very short time, from 3.9% to over 16%.¹⁵⁷ PEDOT:PSS has high conductivity and is extensively employed as an electrode in organic electronic devices such as organic light-emitting diodes, organic photovoltaics and organic field-effect transistors.^{169–171} However, PEDOT:PSS is extremely hygroscopic, and thus dispersing it in water may limit the long-term stability of inverted Omh-PSC devices. A direct coating of PEDOT:PSS aqueous solution would degrade the $\text{CH}_3\text{NH}_3\text{PbI}_3$ film.

Therefore, it can be proposed that inverted based Omh-PSC devices may face challenges such as: (1) electrochemical reactions occurring at the ITO and aluminum electrodes, (2) the inclusion of moisture and impurities within the organic–metal interface enhancing ionic conduction and hence accelerating corrosion, (3) accelerated degradation due to illumination of the device, (4) the very high electron affinity of PCBM (and other fullerenes), which would seem more prone to reaction with the metal electrode, and finally (5) the $\text{CH}_3\text{NH}_3\text{PbI}_3$ film is destroyed by the hygroscopic PEDOT:PSS aqueous solution. Aluminum is not a passive metal and it may react with organic compounds producing organo-aluminum compounds or alternatively anion radicals. These compounds are highly reactive species that will react with any proton donors present (e.g. a trace of water or with oxygen). None of these challenges are confirmed, thus they should be investigated to obtain a detailed understanding of the stability of inverted Omh-PSCs. A 10–20 nm ultrathin layer of poly(*N,N'*-bis(4-butylphenyl)-*N,N'*-bis(phenyl) benzidine)(polyTPD) was introduced between PEDOT:PSS and $\text{CH}_3\text{NH}_3\text{PbI}_3$ layers using a meniscus-coating process.^{40,172} A 10–20 nm ultrathin hybrid interfacial layer of a NiO compact layer and an insulating Al_2O_3 (meso- Al_2O_3) scaffold, which leads to little hysteresis and more stable power output under working conditions has been confirmed for an inverted device.¹⁵⁶ Furthermore, in comparison to PEDOT:PSS based inverted Omh-PSCs with the best efficiencies (~15%),^{173,174} the meso- Al_2O_3 device showed an improved stability. This shows that the potential of the NiO/meso- Al_2O_3 interfacial layer should be superior to that of PEDOT:PSS.

4.2.3 Mesoporous TiO₂. The stability of Omh-PSCs in liquid electrolyte is approximately 10 min because CH₃NH₃PbI₃ tends to dissolve gradually in the redox electrolyte (I⁻/I₃⁻). In order to solve this problem, Grätzel, Park and coworkers investigated a new mesoporous solar cell based on a CH₃NH₃PbI₃ semiconductor and spiro-MeOTAD as a solid HTM, and sub-micron thick films of mesoporous titanium dioxide, showing excellent long term stability of 500 h under AM 1.5 G illumination. The mesoporous device structure incorporates active and passive scaffolds such as mesoporous TiO₂ and mesoporous Al₂O₃ scaffolds, respectively. The highest stability reported with mesoporous TiO₂ is 1000 h with a 28% reduction relative to its initial PCE.⁴⁴ There may be many factors causing degradation relating to mesoporous TiO₂. Some of them are:^{175–177} (1) the sensitivity to UV exposure, and (2) the presence of surface defects (oxygen vacancies) in TiO₂. The interaction of these defects or vacancies with both water and oxygen, creating electronic defect states, can result in device degradation. Oxygen binds to the Ti³⁺ sites and modifies these trap sites.⁷² Furthermore, lead iodide can be produced upon the breakdown of Omh-perovskites at the interface.⁵¹ Because of its wide bandgap ($E_g = 2.3$ eV) and poor optical properties, the formation of PbI₂ is unnecessary. For reasons that are not yet completely known, the formation of a PbI₂ phase is more well-known in a mesoporous scaffold than on a planar substrate.¹⁷⁸ Thus, mesoporous based solar cell devices prepared with PbI₂ have confirmed poor performance, attributable to its appreciably inferior transport properties (smaller diffusion coefficient) compared with CH₃NH₃PbI₃-based devices.¹⁷⁹ Moreover, the presence of PbI₂ might result in energy misalignment at the TiO₂ interface and the trapping of free charges created in the Omh-perovskite phase, resulting in an inferior device performance. It may also give more stringent requirements for the processing of these thin films.¹⁸⁰

The two devices for mesoscopic architecture Omh-PSCs are HTM based, and HTM-free structured solar devices. In the former, the breakthrough for better stability of the mesoporous architecture was 500 h using spiro-MeOTAD, which is now widely used as an HTM with excellent PCEs. However, due to the limited choice of materials, the progress in stability of inorganic HTMs has been sluggish compared to their organic counterparts. Although CuSCN (PCE = 12.4%),¹⁸¹ NiO (PCE = 11.6%)¹⁸² and CuI (PCE = 6%),¹⁸³ have been listed as excellent, low cost and stable inorganic HTMs, they still have low efficiency when compared to organic HTMs. On the other hand, polymer HTMs, in addition to the most commonly used spiro-MeOTAD, including poly(triarylamine) (PTAA) and poly(3-hexylthiophene-2,5-diyl) (P3HT), have been tested, because of their better hole mobility and good film-forming properties. Among all, PTAA was confirmed to have the highest efficiency of up to 12%, in contrast to 6.7% for P3HT.³² This efficiency was seriously decayed in 55% relative humidity over one day. This was the first most important breakthrough in the development of polymer HTMs, which undergo pore-filling limitations, and this may lead to a diminishing of the performance, an inferior stability, and could even harm the device.¹⁸⁴

The majority of HTMs use hygroscopic additives such as Li salts, tetrabutylpyridine (TBP) or a cobalt complex to enhance

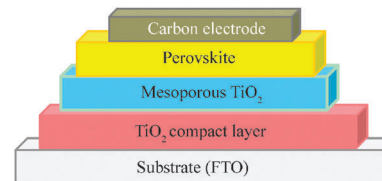


Fig. 14 Typical architecture for Mesoporous TiO₂ based HTM free Omh-PSCs.

their conductivity. Several groups have reported Omh-PSCs without additives in the HTM, which simplifies the cost and fabrication procedures. Liu and co-workers described a tetraphiafulvalene derivative as a HTM (TTF-1).¹⁸⁵ Moreover, iodine can react with the TBP leading to an iodopyridinate complex, as in dye sensitized solar cells,¹⁸⁶ resulting in iodine depletion from the absorber materials. Han and coworkers introduced a TTF-1 derivative into Omh-PSCs without the use of p-type dopants.¹⁸⁵ The improved stability was attributed to the avoidance of the use of deliquescent and hygroscopic additives. This dopant free approach is responsible for the improved lifetime of the device compared to the approach incorporating p-type HTM dopant additives. Moreover, these additives may act as a source of moisture that could degrade the organic HTM materials and shorten the device lifetime. Similarly, these HTMs are not only expensive, but can also limit the long term device stability. Although various novel HTMs have shown promising results, the HTM-free Omh-PSC device schematically illustrated in Fig. 14 has many advantages, such as lacking a need for air-sensitive HTMs, its simplicity, cheap cost of production and excellent stability. Meng and coworkers demonstrated HTM free Omh-PSC devices with 10.5% PCE.¹⁸⁷ The excellent carrier lifetime and ambipolar nature^{25,26} enabled the pioneering of the HTM free architecture. Interestingly, HTM-free structured mesoscopic solar cells have now been made with PCEs over 10% and stabilities of over 2000 h.⁷ Etgar and co-workers showed an initial study using TiO₂ nanosheets as the mesoporous layer.²²

4.3 Effect of interface

Although studies have revealed that device degradation is mainly attributable to moisture ingress, high temperatures, and UV light, significant degradation of Omh-PSC devices is still observed even when they are well-encapsulated or characterized in an inert environment.⁶ These observations imply that the environmental effects are not the only critical factors determining device stability, but that there are also intrinsic factors within the devices that contribute to degradation. One example is the unstable electronic structure of the organic/cathode interface, due to the gradual diffusion of metal into organic films. Similar phenomena are observed in ITO anode/organic interfaces, where reactive oxygen species, generated by UV treatment of the indium-tin oxide (ITO) substrate, slowly degrade the organic layer. Other degradations may be related to the organic/electrode interface, and time-dependent chemical reactions at the donor/acceptor interface can also cause device deterioration. Other causes may be attributed to the spatial isolation of

organic films from electrodes and the reduction of the energetic transport barrier.

4.3.1 Ion migration. The rate of electromigration increases with temperature, electric field and illumination, and has four prerequisites – mobile ions, a voltage gradient, a continuous flow of moisture, and soluble ions. Silver is the metal most susceptible to migration, since a low activation energy is required to initiate the migration process.¹⁸⁸ The severity of electromigration may increase with the applied potential gradient and the time to reach active materials. When Ag is under an applied electric field, or thermal evaporation, it may leave its initial location in an ionic form and redeposit at another location. Silver migration causes short circuits and device failure, especially in high humidity environments. Moreover, it is well known that the cations at the A-sites and B-sites of Pb-based complex ABX_3 perovskite minerals such as PbBO_3 can be replaced by many other cations. Substitution is mainly determined by the differences in valence and ionic radius.¹⁸⁸ The size of Ag^+ is almost the same as Pb^{2+} (about 0.149 nm), and much larger than B-site cations such as Nb^{5+} (0.064 nm) and Zn^{2+} (0.074 nm).¹⁸⁹ Thus, it can be proposed that Ag^+ enters into the Pb-site of MAPbX_3 Omh-perovskite materials, substituting for Pb^{2+} , though this has not yet been reported. The nonequivalent replacement of Ag^+ for Pb^{2+} may also be responsible for undesirable MAPbX_3 layer structural distortion during device operation. The intrinsic low melting point of silver may account for the structural change and abnormal grain growth of the Omh-perovskites near the interface and this has to be investigated.

The role of ion migration initiated by photo-excitation in slower processes occurring during pre-conditioning of the devices has been proposed as a cause for hysteresis.⁹⁴ Hysteresis commonly takes place in metal halides such as PbI_2 , in which photo-excitation generates halide vacancies, facilitating halide ion migration.¹⁹⁰ Furthermore, anions such as I^- ions move towards the electron selective layer, *i.e.* TiO_2 , and cations such as MA^+ and Li^+ migrate into the HTM contact when a reverse bias is applied during illumination.⁹⁴ This causes an injection barrier for both electrons and holes at their respective interfaces, resulting in hysteresis.

4.3.2 Reactivity. Chemical reactions and inter diffusion at the interface can greatly affect the overall device stability. Indeed, of all types of instabilities in the cell, the interface instability is the one where its chemistry is almost not yet investigated in Omh-PSC devices. It is, therefore, important to consider detrimental interfacial reactions in detail to find out the intrinsic instabilities. The possible origins of degradation that could take place at the interface of Omh-PSC devices, leading to interface instability, are: (i) corrosion of silver forming silver halides at the interface; (ii) silver connections forming shunting paths with the mesoporous TiO_2 in the absence of oxygen; (iii) photo-oxidation of the HTM organic materials degrading the electron/hole transport properties and thus the photovoltaic stability; (iv) Omh-perovskite decomposition at the $\text{TiO}_2/\text{CH}_3\text{NH}_3\text{PbI}_3$ interface through light exposure, since TiO_2 has a strong ability to extract electrons from iodide (I^-); and (v) formation of metal oxides which finally leads to device deterioration. Docampo and

Snaith^{6,191} demonstrated that silver contacts often form shunting paths with mesoporous TiO_2 in the absence of oxygen. As a result, a Schottky barrier can be formed. Similarly, Snaith and coworkers¹⁹² confirmed that metal migrating through the HTM layer is partially responsible for the quick device degradation. They showed that depositing the HTM within an insulating mesoporous “buffer layer” comprised of Al_2O_3 prevents the migration, while also facilitating control of the HTM thickness. This prevents the device from degradation, even after 350 h of operation.

5. Suggested approaches to improve stability of Omh-PSCs

Not only efficiency, but also stability is a critical requirement for the practical application of Omh-PSCs. It is, therefore, necessary to improve stability to an extent that will make Omh-PSC technology attractive from a commercial standpoint. Based on current information, device instability is the sum of all the device component materials, device architecture and interfaces. Stability improvement therefore can be expected to result mainly from Omh-perovskite materials, device architectures and interfaces. Researchers must focus on two major issues regarding the stability and longevity of Omh-PSCs: firstly, strategies to provide extrinsic stability through the use of proper encapsulation to prevent degradation caused by ambient oxygen and water, and secondly, research to improve the understanding of the intrinsic stability of different thin film perovskite materials, array of the device, and interfaces. The most suitable approaches that should be considered include chemical engineering modifications to active materials, design and optimization of device architecture, and systematic interface engineering. These approaches should provide a means to improve both the operation and long term stabilities of Omh-PSC devices.

5.1 Omh-perovskite material aspects

The stability of Omh-perovskite materials is an issue in Omh-PSCs. Both chemical composition and structural engineering techniques could be considered for issues related to material stability. Appropriate chemical composition engineering is an essential approach to stabilize Omh-perovskite materials by the chemical modification of the X site anions and of the organic ‘A’ site cation.¹⁹³ The size of the A cation is critical for the formation of stable close-packed Omh-perovskite structures. As aforementioned, the relative ionic radii of A, B and X in the ABX_3 Omh-perovskite structures have been widely used in a method of establishing the distortion of the MX_6 octahedron; in particular, a relatively smaller ionic radius for X favors the formation of cubic structures.²⁴ In particular, the A cation must fit into the space composed of four adjacent corner sharing MX_6 octahedra. The structural and opto-electrical differences of MAPbI_3 and FAPbI_3 are likely to originate from the difference in the ionic radius of the MA (1.8 Å) and FA ions (1.9–2.2 Å). Such structural instability of Omh-perovskites can be improved by regulating the Goldschmidt tolerance factor (t_f) using

appropriate substitutions, which is a useful indicator of the stability and distortion of crystal structures. Another technique is structural engineering of the Omh-perovskite absorbers, to produce moisture resistant 3D structured analogous materials. The recently reported new layered (2D) structure Omh-perovskite absorbers ($\text{PEA}_2(\text{MA})_2[\text{Pb}_3\text{I}_{10}]$ ($\text{PEA} = \text{C}_6\text{H}_5(\text{CH}_2)_2\text{NH}_3^+$, $\text{MA} = \text{CH}_3\text{NH}_3^+$) may offer greater tunability at the molecular level for material optimization and are more moisture resistant than films of commonly used $(\text{MA})[\text{PbI}_3]$ materials.⁸⁰ Devices containing these layered materials are stable even in moist environments. As a result of the tunability behavior of the layered structure, these materials may be capable of better stability for future development. Understanding the multifaceted and interplaying chemistry of Omh-PSCs, and developing new materials based on such knowledge will indisputably open up astonishing stability breakthroughs and revolutions for this type of solar cell.

5.2 Device architecture aspects

While the absorber material and interface stability are essential requirements for long term stability, they are by no means sufficient, because the end user is ultimately interested in the device stability for a given application. Thus, the engineering of suitable device architectures is required. Among the three Omh-PSC device architectures – mesoporous, regular and inverted, the mesoporous one incorporating a carbon top electrode without hole conductor is stable, low cost, simple and promising for practical applications.

So far, for Omh-perovskite-based solar cells, PCE values ranging from 3.81% to more than 20% have been obtained by optimizing the technology and array of device structure, making it competitive for future commercialization. Zhou and coworkers³⁶ reported an 80% drop in the PCE over a 24 h period when the device with planar geometry was stored under ambient conditions, and a 95% drop in the PCE after 6 days. While this loss in performance is highly problematic, even more concerning is that the decomposition product (PbI_2) is sparingly soluble in water (1.6 mM at 25 °C);¹⁹⁴ this would present an enormous ecotoxicological problem if a module becomes damaged in the field.

With these issues in mind, a substantial effort has gone into improving the long-term stability of Omh-PSCs.^{79,83,195} Protective Al_2O_3 layers⁸³ and hydrophobic oligothiophene HTMs¹⁹⁵ have both been employed as a means of protecting the underlying Omh-perovskite film, while alternative Omh-perovskite compositions^{33,80} have also been explored as a way of improving the stability of the Omh-perovskite itself. Moreover, Snaith and coworkers have prepared Omh-perovskite-based MSSCs, within which the mesoporous n-type TiO_2 is entirely replaced with an insulating mesoporous Al_2O_3 scaffold.^{28,142} An Al_2O_3 scaffold, which acts as a scaffold or supporting material, showed improved device stability with an almost stable photocurrent of 15 mA cm⁻² over a 1000 h exposure period.⁶ However, some of the most promising results have come from the use of carbon-based electrodes.^{4,79,196} Wei and co-workers¹⁹⁷ used inkjet printing to produce $\text{CH}_3\text{NH}_3\text{PbI}_3/\text{C}$ bilayer devices which retained *ca.* 90% of their initial PCE after storage in 30% relative humidity (RH) for 12 days. Similarly, Zhang and co-workers¹⁹⁶ and Zhou

and co-workers⁷ replaced the typical Ag or Au back-contact with carbon paste deposited by a doctor-blade. Most dramatically, through the use of functionalized carbon nanotubes embedded in an insulating polymer matrix, Habisreutinger and co-workers⁷⁹ were able to protect Omh-perovskite devices from a steady stream of running water for a short time. Although these simple Omh-PSCs are promising photovoltaic devices, several HTM and metal counter electrode-related drawbacks hinder their practical application.

Moreover, to accomplish the necessities for commercial applications, two of the most important issues in Omh-PSCs should be addressed.^{15,142,198} Firstly, devices incorporating HTMs require an undesired cost due to the more expensive price of HTMs such as spiro-MeOTAD and the most conserving issue of poor device stability. The second issue is the counter electrode made of Ag or Au, which have issues relating to: (1) silver corrosion and the attack of perovskites forming silver halides, (2) noble metals such as Au or Ag are not applicable for large-scale production due to the deposition technique, *i.e.* thermal evaporation, which initiates hot metal to diffuse in to different layers and is highly energy consuming and complicated, and (3) the high cost of the Au electrode also requires a high-vacuum evaporation technique, thereby limiting its future commercialization. Therefore, the current goal focuses on the removal of the HTMs and substitution of these metal electrodes to improve stability, simplify the cost of device fabrication and recognize large-scale fabrication. Carbon-based electrodes have been extensively investigated, due to its high earth abundance, low cost, low-temperature processing (100 °C), large-scale printing processing^{34,113,199} appropriate work function of -5.0 eV (-5.1 eV for Au),^{7,200} and promising long-term stability.^{4,7} This remarkable stability can be attributed to the thick carbon cathode layer, which can work as a water-retaining layer to protect the perovskite material from being destroyed.²⁰¹ This result indicates the underlying potential of commercial carbon paste as a promising candidate for stable and highly efficient Omh-perovskite solar cells.²⁰¹ Furthermore, many literatures have clearly established that Omh-PSCs can act as a p-i-n device and thus HTMs are not the first priority for operation.^{112,202} Besides, Omh-perovskite has been considered as both a light harvester and a hole transporting material.^{34,142,167} The electron-hole diffusion length of $\text{CH}_3\text{NH}_3\text{PbI}_3$ can even exceed 100 nm.^{25,26} All of this evidence indicates that complicated HTMs are not necessary in the fabrication of Omh-perovskite-based photovoltaic devices. HTM free Omh-PSC devices employing an impermeable counter electrode have the potential to overcome these drawbacks and extend long term device stability. This new device concept has greatest potential for practical application and further improvements, both in efficiency and stability, can be expected.

5.3 Interface aspect

The nanoscale interface properties including interface defect structure relaxation, grain boundary phase transformations, and grain boundary size present in different layers determine the eventual stability of the device. Thus, understanding these interface properties, and charge separation and transfer across

the nanoscale interface is critical. It has been shown that the instability of Omh-PSCs is primarily a result of charge accumulation at the interfaces due to ion migration, resulting in a change in the built-in electric field of the devices and hysteretic effects.^{102,112,128,145} The long-term stability of Omh-PSCs can be improved by a proper choice of interlayer and appropriate engineering of barrier layers to protect the Omh-perovskite film beneath and avoid an unnecessary barrier in different interface layers. The thermal and moisture-sensitive nature of the Omh-perovskite interface is an important concern. In order to overcome such challenges, a protecting polymer matrix and single-walled carbon nanotubes have been pioneered.⁷⁹

It is obvious that the mesoporous TiO_2 is sensitive to UV illumination and acts as a source of interface instability which causes device performance loss. Moreover, this performance loss is not only observed for the unsealed device but also for the sealed devices. This loss in performance of the sealed device could not be attributed to the degradation of Omh-perovskite and/or HTM. Instead, it could rather result from the mesoporous electrode during device illumination. Therefore, the changes in optical and electrical behavior of the sealed electrode (TiO_2) need to be studied in more detail. Fast decay of the excited state and the appearance of a low resistance shunting path could lead to the loss in J_{sc} and V_{oc} for the sealed devices.^{59,203} There are two approaches to overcome the interface destabilization due to mesoporous TiO_2 : first, mesoporous TiO_2 can be replaced by other mesoporous scaffolds such as aluminum-oxide. The use of insulating materials such as SnO_2 with a thin layer of MgO ,²⁰⁴ Al_2O_3 ⁷² and other alternative metal oxides to replace TiO_2 showed an improved resistance to UV light. Secondly, an insulating metal oxide is introduced to passivate the photoinduced trap states in TiO_2 that are formed during illumination. Different techniques have been used to coat the TiO_2 by a variety of metal oxides.^{205,206} The purpose of these metal oxides is to create energy barriers, change the CB potential, or diminish surface traps, and finally to retard recombination. Semiconductors such as Al_2O_3 ^{207–210} have been employed to produce protecting barriers at the TiO_2/HTM interface, raising the physical separation of injected electrons from the oxidized Omh-perovskite/HTM. Fig. 15 shows schematic representations of a device with

an ultra-thin layer of coating before and after perovskite coatings. Fig. 15a represents a coating option before the Omh-perovskite coating that is responsible for diminishing localized TiO_2 surface traps and recombination from the TiO_2 conduction band to the HOMO of the perovskite and the HTM. Another problem for Omh-PSCs is that the Omh-perovskite cannot totally cover the surface of the TiO_2 photoanode completely.^{27,211} Wang and co-workers⁸³ found a similar phenomenon, *i.e.* there are uncovered sites on TiO_2 forming indirect contacts with the HTMs. These uncovered sites act as a potential cause of recombination for electrons from the CB of TiO_2 to the HTMs.

The electrode/electrolyte ($\text{TiO}_2/\text{electrolyte}$) interface is the main problem causing recombination of charge in liquid and quasi-solid DSSCs due to its susceptibility to different reactions. Any modification of this interface will have a great role in improving its stability. In the field of liquid DSSCs and quasi-solid DSSCs,^{212–214} post-modification is one of the key techniques. For instance, the use of 4-*tert*-butylpyridine is an important interface modification means to retard recombination.²¹² Insulating metal oxides such as Al_2O_3 ,^{215,216} ZnS ^{217,218} and TBAI ²¹⁹ have also proved to be effective in retarding electron recombination. Post-modification by Al_2O_3 has two roles. One is to protect $\text{CH}_3\text{NH}_3\text{PbI}_3$ and the sensitized film degradation due to moisture and sunlight. Another is that Al_2O_3 serves as an insulation barrier between TiO_2 and HTM to retard the electron recombination process. Though some activity has been directed at investigating the TiO_2/HTM interface, little effort has been directed at the Omh-perovskite/HTM interface through post-modification. Recently, post-modification using aluminum oxide⁸³ and Y_2O_3 ²²⁰ in Omh-perovskite solar cells has been reported. This type of modification protects the active material from moisture degradation, as shown in Fig. 15b. However, the thickness of the layer has to be controlled. Thicker over-layers between the TiO_2 and Omh-perovskite block the injection efficiency, but enhance recombination or decay of the excited state. Therefore, post modification of the Omh-perovskite/HTM interface is a promising approach for shielding the perovskite, protecting it from external factors such as moisture and improving the lifetime of electrons by retarding recombination.

Similarly, the interface between the counter electrode and p or n-type layers ((metal/HTM or p-type layer) and metal/ETL or n-type layer interface) could be sensitive to a chemical reaction which can deform the interface properties. Deposition processes, for instance, thermal evaporation techniques, can cause the diffusion of hot reactive metals across the interface and this normally changes the behavior of the interface.^{221,222} The formation of a new aluminum–carbon bond is supposed to be the main cause of interface instability for devices based on an aluminum counter electrode.^{223,224} In order to overcome such problems, it is better to consider: (1) the use of other techniques like a spray-deposition technique,^{225,226} (2) replacing reactive metals such as silver by other alternatives such as carbon and (3) applying small work function metals like Ba, Ca and Mg for application in inverted architecture devices. More interestingly, a blade-coating technique has been demonstrated to improve the ambient stability of the Omh-perovskite, acting as air-protection

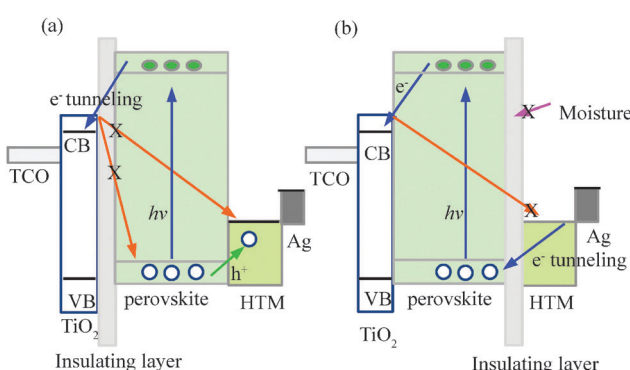


Fig. 15 Schematic representation of a device with an ultra-thin layer of coating or insulating material before (a) or after (b) Omh-perovskite sensitization on the mesoporous TiO_2 surface.

patches to block oxygen/moisture infiltration by encouraging the development of self-assembled crystalline domains at the Omh-perovskite surface.²²⁷ All of these findings indicate the fundamental role of interfacial engineering in improving the interface stability of Omh-PSCs.

5.4 Device operation aspect

5.4.1 UV filters. The exposure of Omh-PSCs to UV light can retard their performance during long-term operation. For instance, UV light can result in TiO_2 direct band excitation which may lead to oxidation of the perovskite and HTMs. In order to prevent direct band gap excitation of TiO_2 , the easiest solution would be to apply a UV cut-off filter, and in fact there are reports where UV cut-off filters have been used in stability testing.^{76,228–233,241} UV cutoff filters are usually used during long-term stability measurements.^{234–238} Interestingly, the use of a UV-filter has been stated as beneficial for the stability of Omh-PSCs based on $\text{CH}_3\text{NH}_3\text{PbI}_3$ and TiO_2 nanoparticles.⁶ It is then clear that the perfect way to keep products from UV deprivation is to have some way of removing all the UV light before it

strikes the material which it will degrade. Unfortunately, it is not always feasible to attain this in practice.

5.4.2 Device encapsulation. Encapsulation enables scientists to eliminate the most damaging components of an Omh-PSC from UV radiation or environmental molecules, as shown in Fig. 16, which is an important approach to protect the device, and increase its stability.²³⁹ An encapsulation method which retains device flexibility is essential from the viewpoint of industrial engineering.²⁴⁰ The most extreme illustration is perhaps a device sealed completely in glass.²⁴¹ These techniques result in inflexible solar cells free from oxygen and water diffusion. Another more advanced encapsulation approach is to use a thermosetting epoxy glue device sealing approach.²²⁸ Moisture and oxygen cannot penetrate this type of encapsulation and this extends the long term stability of the device. Yang's group reported primary stability investigations on Omh-PSCs stored in different environments including nitrogen, dry air, and ambient atmosphere.³⁶ The Omh-PSC devices showed a rigorous decay in ambient air compared with the devices stored in dry air and nitrogen atmospheres, indicating that the decomposition/dissolving of the Omh-perovskite materials is induced by moisture or air. This indicates that better stability can be achieved with more advanced encapsulation methods.³⁶

More interestingly (and as yet still unexplained), higher performance loss is observed for the sealed (encapsulated) device compared to the unsealed (unencapsulated) one, as shown in Fig. 17. This could be due to (1) the progressive occurrence of shunting during operation and (2) the formation of deep trap sites in the mesoporous electrode. However, there are alternative approaches to overcome such performance loss during operation. In the first approach, the combination of encapsulation with a UV filter would be better for improving the stability of the device compared to a device without a UV filter, as indicated in Fig. 17. The second approach uses both doping and encapsulation assisted reduction of trap states; Fig. 18 shows the parameter

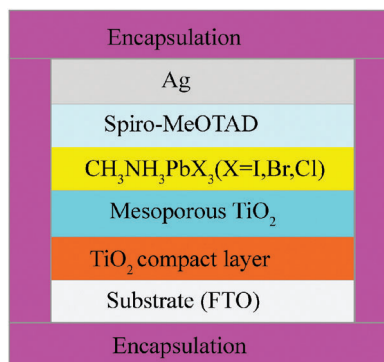


Fig. 16 Schematic representation of Omh-PSC encapsulation.

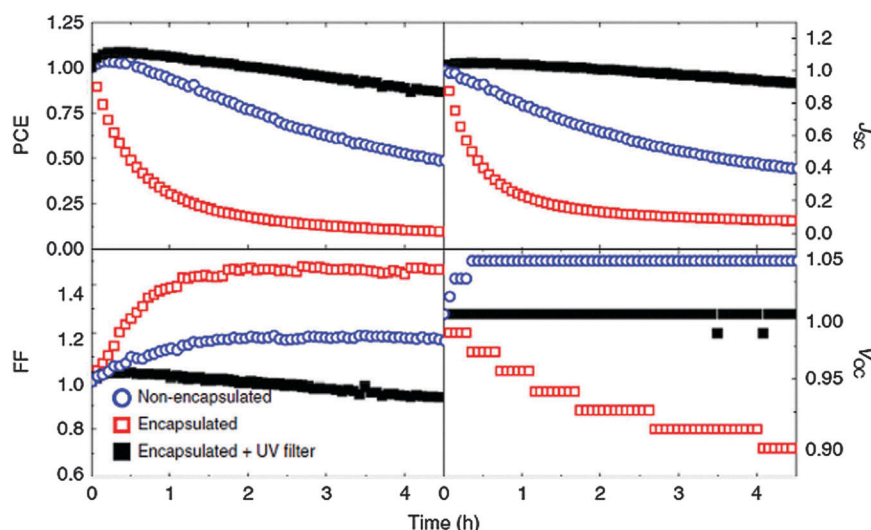


Fig. 17 Non-encapsulated (blue open circles) and encapsulated (filled black squares) with and without a <435 nm cutoff filter (open red squares) aged Omh-perovskite solar cell device. Reprinted with permission.⁶

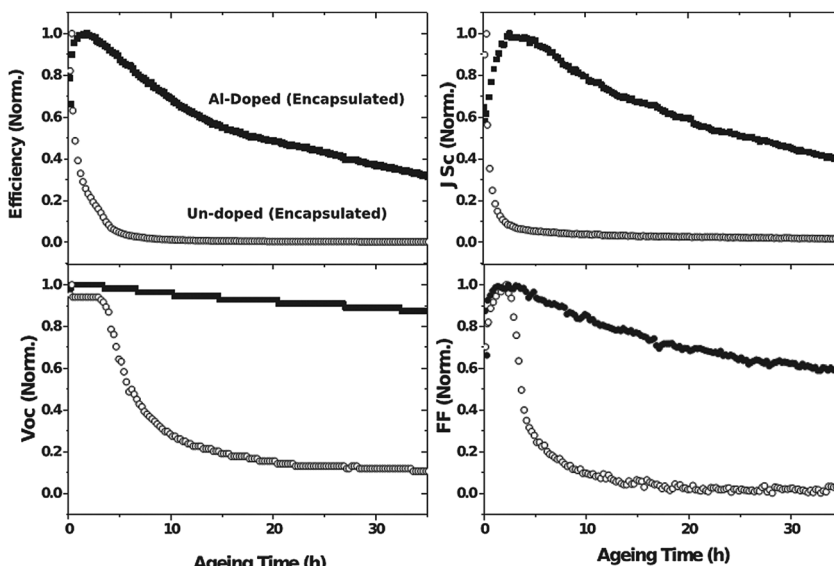


Fig. 18 Plot of performance parameters versus ageing time for a TiO_2 based ssDSSC device doped with aluminum followed by encapsulation. Reproduced with permission from ref. 64.

evolution for aged devices under inert atmosphere operation. The cell which is not doped decayed drastically in the first 30 min, but the Al doped device did not. This indicates that the decrease in the sub-band gap density of states arised from Al doping, assisting the reduction of short-term device deterioration. Thus, aluminum enduringly appeases these defects through the interstitial substitution of Ti adjacent to oxygen defect sites.

Moreover, three optional methods⁶ are proposed to minimize TiO_2 -based solar device power loss during operation: firstly, build up a means to efficiently and firmly appease the TiO_2 surface states, secondly, stop the UV light from reaching the mesoporous TiO_2 ,⁶⁴ and thirdly, use down-converting nanoparticles, efficiently absorb the UV light and re-emit visible light.^{242,243} Establishing routes to harvest all the shorter wavelength light ($<435\text{ nm}$) before it contacts the mesoporous TiO_2 should allow for improved stability without the cost of reduced photocurrents.^{238,243}

6. Protocols and methods for studying degradation mechanisms

After establishing all the causes and degradation processes, as well as the origins of degradations and approaches to improve stability, it is a prerequisite to be able to understand the underlying degradation mechanisms and the causes and origins for these degradations using appropriate physical and chemical, and theoretical (computational) techniques. There are also various protocols to study the fading mechanisms, such as the lifetime and the IV curve (the most detailed source of information), isotopic labeling, and accelerated testing conditions. There are some procedures which are important for lifetime testing protocols, e.g. dark, laboratory weathering, thermal cycling tests, as well as low light testing, which is commonly carried out under accelerated conditions of temperature, humidity and illumination. This will

help extract all the limitations and challenges for practical application. Establishing methods and protocols would be a critical and essential aspect in overcoming the differences or gaps among various research reports released from different groups.

6.1 Possible methods for studying degradation of Omh-PSCs

The degradation process includes a multifaceted sort of process which is not easy to illustrate. Some of these aspects are: flow of H_2O and O_2 induced device degradation, active material and interface degradation, electrode and interlayer migration, reaction of hot metal with the ETL and HTM, and macroscopic and morphology related modifications. It is thus a challenging task to identify degradation mechanisms and to quantify the degree of contribution from every mechanism towards the whole loss of device performance. Degradation processes can be studied in terms of different useful properties such as (1) the bulk and surface behaviour, (2) the interface properties and (3) the array of device architecture. This can be achieved using both computational or theoretical, and physical and chemical characterization techniques. Information can be obtained from specific study methods and/or from entire devices, which is averaged information. These methods should be considered as key ways to obtain accurate information, while possibly also suggesting new routes of investigation.

6.1.1 Characterization of Omh-perovskite material bulk and surface properties. Studies of material behavior (crystal structures, phase changes, and surface traps) are ways to identify problems that may compromise material stability. The bulk and surface properties of Omh-perovskite materials can be studied to characterize changes in the surface chemistry, structural and phase changes, carrier lifetime, mass loss, thermal behavior, and mechanical properties. All of these properties provide chemical and/or physical information about Omh-perovskite material stability and degradation. Furthermore, degradation information

can be obtained from both theoretical and experimental investigations. Although most of the literature reports are from experimental analysis, the contributions from theoretical or computational viewpoints using first principles, *ab initio* and DFT methods are also essential in investigating the structure, orientations, vibrational frequencies, interaction energy, charge distributions and other properties.

6.1.1.1 Chemistry of surface. The study of surface chemical processes plays a significant role in basic chemical research. At the molecular level, the surface atoms (compared to the bulk) experience a different chemical environment, which is due largely to the reduced number of neighbouring atoms. As a consequence, these surface atoms with changed atomic and electronic structures exhibit high chemical reactivity. This chemical reactivity can lead to corrosion or degradation when in contact with the environment; therefore, studying the surface changes in Omh-perovskite materials when exposed to different conditions such as, moisture, temperature, and air, is essential. At present, a vast number of experimental and theoretical surface chemistry techniques have been developed. The *in situ* techniques are specifically of great importance. X-ray photoelectron spectroscopy (XPS),^{244–246} Scanning Kelvin probe microscopy (SKPM),^{112,185} Rutherford backscattering (RBS),²⁴⁷ X-rays for reflectometry, Surface Enhanced Raman spectroscopy (SERS), and Ambient pressure X-ray photoelectron spectroscopy (AP-XPS) are some of the surface sensitive techniques.

6.1.1.2 Structural/phase and optical properties. Omh-perovskites are intrinsically complex materials, where the presence of various types of interactions and structural disorder may play an important role on the resulting material properties. *Ex situ* and *in situ* measurements, such as UV-vis, X-ray diffraction, vibrational spectroscopy (infrared^{248,249} and, DFT simulation assisted Raman²⁵⁰ and Raman^{251,252}), spectroscopic ellipsometry⁸⁸ and X-ray absorption spectroscopy (XAS) are essential techniques for studying optical properties, structure and phase transformations in materials. Light soaking has been identified to split XRD peaks in a $\text{CH}_3\text{NH}_3\text{PbI}_{3-x}\text{Br}_x$ film, indicating that crystalline phases segregate with Br as the main species and iodine as a minor species, with the latter able to act as a trap site.²⁵³ While the *in situ* absorbance measurements provide a convenient spectroscopic method to track film degradation kinetics, they provide no structural information on changes in crystallinity or phase that occur during degradation. *Ex situ* powder X-ray diffraction (pXRD) experiments could be carried out in order to identify both the initial Omh-perovskite phase and any crystalline degradation products. While pXRD could be set to study the crystallographic structure, crystallite size (grain size), and preferred orientation in polycrystalline or powdered solid samples, *in situ* grazing incidence X-ray diffraction (GIXRD) measurements are more useful to elucidate the reaction mechanism for the decomposition process upon accelerating conditions such as moisture and light.⁸⁶ Moreover, the combination of a fast 2D area detector with a high brightness synchrotron X-ray source allows the acquisition of 2D diffraction data in real time, providing important insight into the film decomposition process.

6.1.1.3 Carrier lifetime. The carrier lifetime of materials can be studied by monitoring time-resolved photoluminescence (TRPL) measurements. Snaith and co-workers reported TRPL measurements for Omh-PSCs and TRPL curve decay ($\tau_e = 273 \pm 7$ ns, where τ_e is the time taken for the PL to fall to 1/e of its initial intensity) was observed.²⁶ A PL lifetime as high as 200.1 ns was also demonstrated, and the long lifetime is tentatively ascribed to the Cl doping effect.²⁴⁵ In order to investigate the feasibility and impact of these Lewis base treatments, Noel and coworkers performed a spectroscopic, theoretical, and device based investigation.¹¹⁸ Nonradiative decay was inhibited significantly within the treated perovskite films, especially under low levels of photo-excitation. More research needs to be done to understand how this novel family of solar absorber materials gives rise to long charge carrier lifetimes. A comparison of hysteretic effects and transient behavior on mesoporous titania based perovskite devices to regular thin film devices was done using IV curves and slow transient external quantum efficiency measurements.⁹⁴ Currently, more advanced techniques, such as correlated scanning electron microscopy and confocal photoluminescence measurements, have been applied to explore the structure/function relationship in Omh-perovskite films. The results obtained indicated the presence of considerable local PL heterogeneity with average carrier lifetime of >1005 ns for $\text{CH}_3\text{NH}_3\text{PbI}_3(\text{Cl})$ films,¹²⁰ implying that substantial scope remains for minimizing non-radiative decay. Regardless of these wonderful advancements in studying and understanding from both experimental and the theoretical observations, until now, the cause for the prolonged carrier lifetime of Omh-perovskites remains unclear. Some theoretical observations imply that the dynamic position of the conduction band minimum could be the reason for this prolonged carrier lifetime in MAPbI_3 films.¹³⁴

6.1.1.4 Thermal properties. Since the formation of $\text{CH}_3\text{NH}_3\text{PbI}_3$ is influenced by the release of MAX, it is important to characterize the thermal properties of $\text{CH}_3\text{NH}_3\text{I}$ and $\text{CH}_3\text{NH}_3\text{Cl}$. As shown in Fig. 19a, the thermal gravimetric analysis (TGA) curves show nearly 100% weight loss between 250 °C and 360 °C for $\text{CH}_3\text{NH}_3\text{Cl}$ and between 290 °C and 370 °C for $\text{CH}_3\text{NH}_3\text{I}$, respectively. The lower onset of the weight loss temperature of $\text{CH}_3\text{NH}_3\text{Cl}$ suggests that it is easier to turn into the gaseous phase compared to $\text{CH}_3\text{NH}_3\text{I}$. Moreover, it is important to understand in what manner $\text{CH}_3\text{NH}_3\text{Cl}$ and $\text{CH}_3\text{NH}_3\text{I}$ could possibly escape from the precursor films during the annealing process. As shown in Fig. 19b, the endothermic peaks in the differential scanning calorimetry curves indicate that the escape of $\text{CH}_3\text{NH}_3\text{Cl}$ and $\text{CH}_3\text{NH}_3\text{I}$ is related to a sublimation process.⁴⁹

Both the TGA and DSC results confirm that the release of $\text{CH}_3\text{NH}_3\text{I}$ occurs at a higher temperature compared to $\text{CH}_3\text{NH}_3\text{Cl}$. This confirms that a higher annealing temperature is required for the $\text{CH}_3\text{NH}_3\text{I}/\text{PbI}_2$ precursor mixtures.

6.1.1.5 Mechanical properties. The mechanical properties²⁵⁴ of Omh-perovskite materials and the mechanical failure mechanisms of devices can play critical roles in the operational stability of Omh-PSCs for portable and outdoor applications. This section

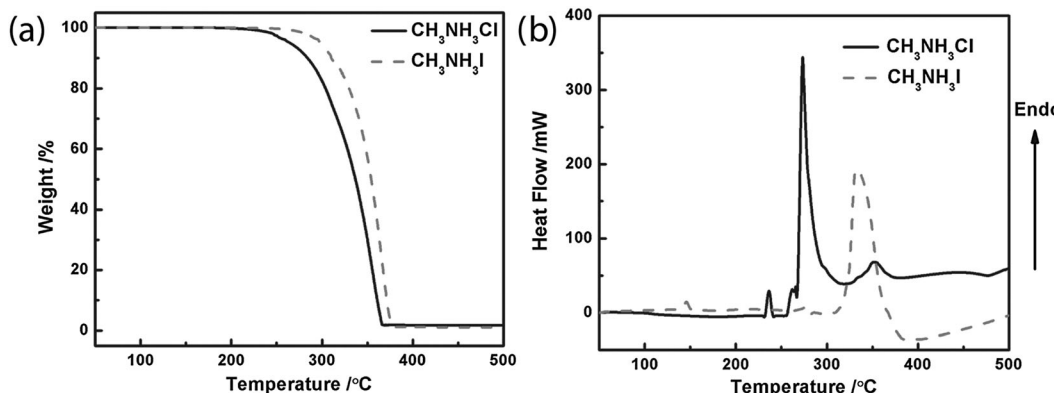


Fig. 19 (a) TGA and (b) DSC curves for $\text{CH}_3\text{NH}_3\text{I}$ and $\text{CH}_3\text{NH}_3\text{Cl}$ powders. Reproduced with permission from ref. 49.

highlights mechanical properties—principally the stiffness and brittleness of pure films of these semiconductors and component layers *e.g.* fullerenes. The ubiquitous acceptor PCBM has many deleterious effects on the mechanical stability of OPV devices. Pure PCBM phases have low cohesive energy,²⁵⁵ high tensile and low crack onset strains,²⁵⁶ and weak interfaces with other device layers.¹⁶¹ Several potential determinants of mechanical properties, including molecular structures, polymorphisms, microstructures and textures have not yet been critically reported.

6.1.2 Device architecture. The most in depth source of information is the measurement of *IV*-curves as a function of time. From the evolution of the *IV*-curves, information on J_{sc} , V_{oc} , FF, PCE, R_{sh} and R_s can be extracted and the broad-spectrum of the curve can be applied to follow the decay of the device's performance. The principles of an equivalent circuit play an important role in modelling the characteristics of a diode for the extraction of extra device parameters, such as parallel and series resistances. The *IV* curve for Omh-PSCs can, however, change dramatically as it decays. Recently, Grätzel and coworkers demonstrated that an *IV*-curve of the device measurement at different light intensities of the light source using an array of white LEDs could be ascribed to a decrease in the shunt resistance.³⁵ Measuring all diode parameters at a standard interval is therefore helpful, rather than just measuring a single diode characteristic.

Different analytical techniques can be used in addition to the *IV* curve, such as intensity-modulated photocurrent/photo-voltage spectroscopies (IMPS/IMVS),^{257,258} impedance,²⁵⁹ time-of-flight,²⁶⁰ and open-circuit voltage decay.²⁶¹ The different layers in both mesoporous TiO_2 and compact TiO_2 device structures affect the separation, transport, and recombination kinetics of the photoinduced charge carriers. According to Wang and co-workers, a mesoporous electron conductor is necessary to optimize $\text{CH}_3\text{NH}_3\text{PbI}_3$ -based solar cell devices with a high PCE.¹⁷⁸ This mesoporous TiO_2 is more likely to induce the formation of PbI_2 than compact TiO_2 .¹⁷⁸ Femtosecond time-resolved transient absorption spectroscopy probed in the visible spectrum, when coupled with XRD, is a useful tool for this purpose.¹⁷⁸

6.1.3 Interface characterization. Identifying issues related to interfaces are quite complex, including concerns over transport barriers, charge separation, band bending, and charge transfer. Analytical techniques/methods such as *IV* characterizations,

angle-resolved XPS (AR-XPS),²⁶² Fourier transform photocurrent spectroscopy (FTPS) and transient absorption spectroscopy (TAS) measurements, charge extractions by linearly increasing voltage (CELIV), first-principles DFT modeling,²⁶² transient absorption spectroscopy (TAS), energy dispersive X-ray spectroscopy (EDX) and electron energy loss spectroscopy (EELS) and surface-sensitive XPS measurements,^{49,112,263} spectroscopic ellipsometry or X-ray reflectivity,²⁶⁴ and energy dispersive X-ray reflectometry,¹⁵⁹ are helpful in studying interfacial issues. Miscellaneous processes can be integrated while interfaces/surfaces are exposed to water and oxygen, and finally, can cause segregation on the surface. The best option to investigate the interior of Omh-PSCs with respect to their chemistry is to systematically get rid of each layer in the device and examine the exposed interfaces 2–6, as shown in Fig. 20.

For chemical degradation, oxygen or water-induced degradation, chemical characterization is preferred such as TOF-SIMS, together with isotopic labeling using H_2^{18}O and $^{18}\text{O}_2$ to acquire in-depth information on where, and to what degree of the capture takes place. ^{18}O has a natural abundance of 0.2%, *i.e.* simply remunerated through the measurements of the intensity of the ^{16}O signal. In order to obtain a semi-quantitative measure of ^{18}O incorporation, and thereby of the process, eqn (22) is used:²⁴⁰

$$\frac{\left[\frac{I(^{18}\text{O})}{I(^{16}\text{O})} \right]_{hv} - \left[\frac{I(^{18}\text{O})}{I(^{16}\text{O})} \right]_{\text{ref}}}{\left[\frac{I(^{18}\text{O})}{I(^{16}\text{O})} \right]_{\text{ref}}} \times 100\% \quad (22)$$

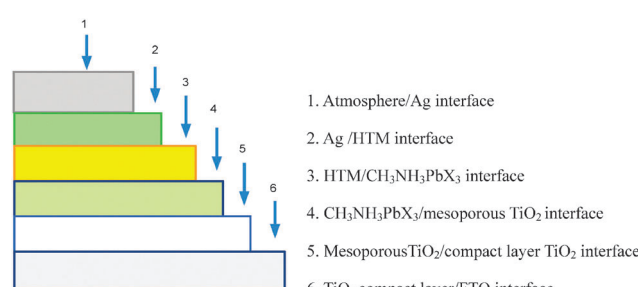


Fig. 20 Schematic drawing of an Omh-PSC cross-section with the configuration Ag/HTM/ $\text{CH}_3\text{NH}_3\text{PbX}_3$ /mp- TiO_2 /cl- TiO_2 /FTO showing all the relevant interfaces, where X is I, Br, Cl or mixed halides.

where $I(^{18}\text{O})$ is the intensity of the ^{18}O isotope of a given species and $I(^{16}\text{O})$ is the corresponding intensity of the ^{16}O isotope.

6.2 Accelerated testing conditions and protocols

Accelerated testing protocols are useful in analysing the effects of artificially rapid chemical degradation or physical changes to a solar cell device brought about by exaggerated storage conditions; these studies can be used to support long-term stability studies of solar devices. The practices for organic PV materials and devices could offer a reference point, where the most frequent accelerated testing protocols include solar-thermal cycling, solar-thermal-humidity cycling and solar-thermal-humidity-freeze, laboratory weathering and thermal cycling.²⁶⁵ Moreover, concentrated sunlight may be a novel approach to explore the degradation of Omh-perovskite materials.¹²² In addition to the accelerating protocols, accelerated testing equipment facilitates a combination of tests. For example, a temperature/humidity test (typically 85 °C/85% RH) by a pressure cooker test/highly-accelerated temperature and humidity stress test (PCT/HAST) chamber is frequently used for electronic components, semiconductors, and PV modules, while illumination/temperature is a popular test for materials. It is believed that similar environmental stress screening can be adopted to evaluate the reliability of Omh-PSC components accordingly.

6.3 H_2^{18}O and $^{18}\text{O}_2$ isotopic labeling protocols

Characterizing the performance of the solar cell under various atmospheric conditions can verify the stability of the device in a particular atmosphere, but does not in any way measure the degree of atmospheric oxidation.²⁶⁶ In addition, as each layer in the cell acts as a barrier, varying a layer may modify the overall need for encapsulation. This barrier effect could be verified by dealing with oxygen transmission inside the solar cell by an isotopically labelled dry oxygen ($^{18}\text{O}_2$) atmosphere or with an oxygen-free humid (H_2^{18}O) atmosphere.

7. Conclusion and prospects

The field of Omh-PSCs is undergoing rapid development, in which the majority of research attempts are focused on fabricating devices with better efficiencies. An evenly vital topic that has gained less concentration is the improvement of the quite deprived stability. Only promising steps have been achieved from a few minutes to thousands of hours (2000 h). Thus, there may be various causes of device failure, which need to be explored in-depth. The major causes responsible for this kind of degradation may be related to various possible external factors, such as moisture, oxygen, temperature, UV light, etc., as well as internal intrinsic factors such as ion migration, electro-migration and interfacial reactions. Knowledge of degradation mechanisms, structures and phase transformations under different operating conditions play key roles in predicting material and device behaviour. In this review, we have reviewed various causes and their associated mechanisms of degradation. These degradations could be originated mainly from the different components

of the device, the architecture of the device itself and/or from various interfaces connecting different layers of the device.

The degradation of different device components such as the Omh-perovskite material itself, hole transporting materials and counter electrodes can take place for different reasons. These component degradations will collectively lead to overall device degradation and may further restrict practical applications. Thus, identifying the contributions from each component to the device degradation would be more beneficial. For instance, Omh-perovskites are easy to degrade under different environmental conditions. Primary emphasis should be given to a comprehensive understanding of the crystal structure of these materials under varying conditions. Other families of these materials are also available and showed promising stability. In addition, the use of HTMs such as spiro-MeOTAD and PEDOT:PSS is found to be destructive to the device. It would be more useful to avoid these materials due to their obvious drawbacks, as mentioned. Additionally, HTM additives such as Li-TFSI and 4-*tert*-butylpyridine are hygroscopic, which will directly affect the Omh-perovskite and lead to device deterioration. It is more important to avoid the use of such deliquescent additives. Similarly, the use of different metal counter electrodes such as silver and aluminum can also be detrimental to the device stability. Replacing such electrodes made of these metals would be beneficial. The deposition techniques of these metal electrodes such as thermal deposition can also have a strong influence on the device stability. Carbon electrode printing is a promising deposition method compared to thermal deposition, in which hot metal diffusion into organic layers could attack the active Omh-perovskite.

The issues of device architecture remain impenetrable and this should also be considered when performing future long-term stability tests. Stability studies of such devices with various designs are insufficient; an in-depth comparative stability study for the three different device architectures (planar, inverted and mesoporous) is still highly required. Similarly, the effect interface appears to be another urgent concern and as such requires additional in-depth investigation. Destructive interfacial reactions may occur in the metal/organic interface due to the diffusion of hot metal during deposition, while ion migration can also encourage confounding hysteresis effects – all of which promote device deterioration. The other critical issue at the TiO_2 /perovskite interface is the depletion of iodine, due to the strong n-type character of the TiO_2 semiconductor. The surface of TiO_2 is thought to play a catalytic role in Omh-perovskite degradation. This depletion may be further exacerbated by high temperatures or by illumination during device operation. Omh-PSC devices have complex multilayer configurations in which each part may not succeed for various reasons and the layers can undergo an interaction chemically and physically in such a way that can give rise to instability.

In this regard, it is necessary to establish efficient solutions for improving the stability to an extent that will make Omh-PSC technology attractive and feasible from commercial perspectives. Based on the current information and future outlooks, we suggest possible stability improvement approaches from three

main perspectives: Omh-perovskite materials, device architecture and interfacial aspects. Upon various structural modifications, different alternative mixed Omh-perovskites and new layered Omh-perovskite materials with promising stability under operating conditions have been explored. There is still 'room to explore various families of Omh-perovskites,' which could be more stable and better candidates for future application and fabrication of stable Omh-PSC devices. To date, the best stability was achieved using an HTM and metal electrode free mesoporous device architecture, which used a carbon as counter electrode. Interestingly, commercial carbon paste is now a promising candidate for Omh-PSC cathodes. In our opinion, the mesoporous device architecture with further improvement has great potential for practical applications not only from a stability point of view, but also for reasons of simplicity and ease of fabrication. For better improvement of this device architecture, all possible interfacial problems should be able to be solved by careful interface engineering. A good choice of anode and cathode interlayer materials may protect the active layer by means of blocking the diffusion of oxygen and water through the metal cathode/electron transport layer, or the ITO/hole-transporting layer. Above all, efficient perovskite structure engineering, suitable counter electrodes and its deposition, suitable device architecture and careful interface engineering, which consider all the mentioned environmental and intrinsic factors, as well as all other existing challenges ought to be cautiously taken to establish an all-purpose method for the production of stable Omh-PSCs. It can be confidently summarized that there is much work to be done and the guarantee of Omh-PSCs as a future choice of solution processed energy technology is everlasting.

The degradation of different Omh-perovskites, interfaces and devices remains largely unexplored. Fundamental studies on the photochemical, chemical, physical, and mechanical properties, interfacial processes and degradation mechanisms of various device components and its architecture are still needed to advance the field. Systematic studies of the relationships between Omh-perovskite materials' properties, including chemical composition, phase and crystal structure, morphology, surface and bulk chemistry, and material crystalline quality correlated to grain size are required. The degradation of Omh-perovskites caused by extrinsic and intrinsic factors should be explored to understand the origin of instability during long term use. Furthermore, the interface properties (interface defect structure relaxation, grain boundary phase transformations, grain boundary size) among the different layers determine the final stability of the resulting device. In this regard, systematic cross-sectional cell configurations showing every interface profile can be very useful in investigating interfacial stability problems. Taking the information presented as a whole, we conclude that the understanding the multifaceted chemistry of Omh-PSCs will be key for developing new materials that will bring this nascent technology to fruition. It is also imperative to investigate all proposed degradations further and decide possible approaches for stability improvements. Accelerated testing protocols, such as temperature/RH combinations, illumination and moisture must be established and documented for stability studies under indoor and

outdoor situations, so that the inconsistency in stability reports from various research groups can be gradually harmonized under standardized conditions.

Acknowledgements

The financial support from the Ministry of Science and Technology (MoST) (104-3113-E-011-001-, 104-ET-E-001-ET, 103-2221-E-011-156-MY3, 102-2221-E-011-157-) and the Top University Projects of Ministry of Education (MoE) (100H45140), as well as the facilities of support from National Taiwan University of Science and Technology (NTUST) are acknowledged.

References

- 1 C. R. Osterwald and T. J. McMahon, *Prog. Photovoltaics*, 2009, **17**, 11–33.
- 2 OXFORD PVs – Next generation solar power, January 2015.
- 3 H.-S. Kim, C.-R. Lee, J.-H. Im, K.-B. Lee, T. Moehl, A. Marchioro, S.-J. Moon, R. Humphry-Baker, J.-H. Yum, J. E. Moser, M. Grätzel and N.-G. Park, *Sci. Rep.*, 2012, **2**, 591.
- 4 A. Mei, X. Li, L. Liu, Z. Ku, T. Liu, Y. Rong, M. Xu, M. Hu, J. Chen, Y. Yang, M. Grätzel and H. Han, *Science*, 2014, **345**, 295–298.
- 5 J. Burschka, N. Pellet, S.-J. Moon, R. Humphry-Baker, P. Gao, M. K. Nazeeruddin and M. Grätzel, *Nature*, 2013, **499**, 316–319.
- 6 T. Leijtens, G. E. Eperon, S. Pathak, A. Abate, M. M. Lee and H. J. Snaith, *Nat. Commun.*, 2013, **4**, 2885.
- 7 H. Zhou, Y. Shi, Q. Dong, H. Zhang, Y. Xing, K. Wang, Y. Du and T. Ma, *J. Phys. Chem. Lett.*, 2014, **5**, 3241–3246.
- 8 G. Hodes, *Science*, 2013, **342**, 317–318.
- 9 M. Antonietta Loi and J. C. Hummelen, *Nat. Mater.*, 2013, **12**, 1087–1089.
- 10 M. A. Green, K. Emery, Y. Hishikawa, W. Warta and E. D. Dunlop, *Prog. Photovoltaics*, 2015, **23**, 1–9.
- 11 S. Kim, J.-W. Chung, H. Lee, J. Park, Y. Heo and H.-M. Lee, *Sol. Energy Mater. Sol. Cells*, 2013, **119**, 26–35.
- 12 S. Mathew, A. Yella, P. Gao, R. Humphry-Baker, F. E. CurchodBasile, N. Ashari-Astani, I. Tavernelli, U. Rothlisberger, K. NazeeruddinMd and M. Grätzel, *Nat. Chem.*, 2014, **6**, 242–247.
- 13 <http://mms.businesswire.com/bwapps/mediaserver/ViewMedia?mgid=354751&vid=4Heliatek>, press release, 2013.
- 14 J. C. B. A. Marchioro, J. Teuscher, M. Grätzel and J.-E. Moser, *Proc. SPIE*, 2013, **8811**, 881108.
- 15 H.-S. Kim, C.-R. Lee, J.-H. Im, K.-B. Lee, T. Moehl, A. Marchioro, S.-J. Moon, R. Humphry-Baker, J.-H. Yum, J. E. Moser, M. Grätzel and N.-G. Park, *Sci. Rep.*, 2012, **2**, 591.
- 16 D. B. Mitzi, *J. Mater. Chem.*, 2004, **14**, 2355–2365.
- 17 D. B. Mitzi, K. Chondroudis and C. R. Kagan, *IBM J. Res. Dev.*, 2001, **45**, 29–45.
- 18 D. B. Mitzi, C. A. Feild, W. T. A. Harrison and A. M. Guloy, *Nature*, 1994, **369**, 467–469.

- 19 D. B. Mitzi, S. Wang, C. A. Feild, C. A. Chess and A. M. Guloy, *Science*, 1995, **267**, 1473–1476.
- 20 K. Chondroudis and D. B. Mitzi, *Chem. Mater.*, 1999, **11**, 3028–3030.
- 21 A. Kojima, K. Teshima, Y. Shirai and T. Miyasaka, *J. Am. Chem. Soc.*, 2009, **131**, 6050–6051.
- 22 L. Etgar, P. Gao, Z. Xue, Q. Peng, A. K. Chandiran, B. Liu, M. K. Nazeeruddin and M. Grätzel, *J. Am. Chem. Soc.*, 2012, **134**, 17396–17399.
- 23 D. B. Mitzi, *J. Chem. Soc., Dalton Trans.*, 2001, 1–12, DOI: 10.1039/B007070J.
- 24 C. C. Stoumpos, C. D. Malliakas and M. G. Kanatzidis, *Inorg. Chem.*, 2013, **52**, 9019–9038.
- 25 G. Xing, N. Mathews, S. Sun, S. S. Lim, Y. M. Lam, M. Grätzel, S. Mhaisalkar and T. C. Sum, *Science*, 2013, **342**, 344–347.
- 26 S. D. Stranks, G. E. Eperon, G. Grancini, C. Menelaou, M. J. P. Alcocer, T. Leijtens, L. M. Herz, A. Petrozza and H. J. Snaith, *Science*, 2013, **342**, 341–344.
- 27 J.-H. Im, C.-R. Lee, J.-W. Lee, S.-W. Park and N.-G. Park, *Nanoscale*, 2011, **3**, 4088–4093.
- 28 M. M. Lee, J. Teuscher, T. Miyasaka, T. N. Murakami and H. J. Snaith, *Science*, 2012, **338**, 643–647.
- 29 J. Salbeck, N. Yu, J. Bauer, F. Weissortel and H. Bestgen, *Synth. Met.*, 1997, **91**, 209–215.
- 30 U. Bach, D. Lupo, P. Comte, J. E. Moser, F. Weissortel, J. Salbeck, H. Spreitzer and M. Grätzel, *Nature*, 1998, **395**, 583–585.
- 31 G. Giorgi, J.-I. Fujisawa, H. Segawa and K. Yamashita, *J. Phys. Chem. Lett.*, 2013, **4**, 4213–4216.
- 32 J. H. Heo, S. H. Im, J. H. Noh, T. N. Mandal, C.-S. Lim, J. A. Chang, Y. H. Lee, H.-J. Kim, A. Sarkar, K. Nazeeruddin, M. Grätzel and S. I. Seok, *Nat. Photonics*, 2013, **7**, 486–491.
- 33 J. H. Noh, S. H. Im, J. H. Heo, T. N. Mandal and S. I. Seok, *Nano Lett.*, 2013, **13**, 1764–1769.
- 34 M. Liu, M. B. Johnston and H. J. Snaith, *Nature*, 2013, **501**, 395–398.
- 35 M. A. Green, A. Ho-Baillie and H. J. Snaith, *Nat. Photonics*, 2014, **8**, 506–514.
- 36 H. Zhou, Q. Chen, G. Li, S. Luo, T.-B. Song, H.-S. Duan, Z. Hong, J. You, Y. Liu and Y. Yang, *Science*, 2014, **345**, 542–546.
- 37 J. A. Christians, J. S. Manser and P. V. Kamat, *J. Phys. Chem. Lett.*, 2015, **6**, 852–857.
- 38 N. J. Jeon, J. H. Noh, W. S. Yang, Y. C. Kim, S. Ryu, J. Seo and S. I. Seok, *Nature*, 2015, **517**, 476–480.
- 39 G. Hodes and D. Cahen, *Nat. Photonics*, 2014, **8**, 87–88.
- 40 O. Malinkiewicz, A. Yella, Y. H. Lee, G. M. Espallargas, M. Graetzel, M. K. Nazeeruddin and H. J. Bolink, *Nat. Photonics*, 2014, **8**, 128–132.
- 41 N. K. Noel, S. D. Stranks, A. Abate, C. Wehrenfennig, S. Guarnera, A.-A. Haghghirad, A. Sadhanala, G. E. Eperon, S. K. Pathak, M. B. Johnston, A. Petrozza, L. M. Herz and H. J. Snaith, *Energy Environ. Sci.*, 2014, **7**, 3061–3068.
- 42 F. Hao, C. C. Stoumpos, D. H. Cao, R. P. H. Chang and M. G. Kanatzidis, *Nat. Photonics*, 2014, **8**, 489–494.
- 43 J. Burschka, A. Dualeh, F. Kessler, E. Baranoff, N.-L. Cevey-Ha, C. Yi, M. K. Nazeeruddin and M. Grätzel, *J. Am. Chem. Soc.*, 2011, **133**, 18042–18045.
- 44 Y. S. Kwon, J. Lim, H.-J. Yun, Y.-H. Kim and T. Park, *Energy Environ. Sci.*, 2014, **7**, 1454–1460.
- 45 B. Suarez, V. Gonzalez-Pedro, T. S. Ripolles, R. S. Sanchez, L. Otero and I. Mora-Sero, *J. Phys. Chem. Lett.*, 2014, **5**, 1628–1635.
- 46 J. J. Choi, X. Yang, Z. M. Norman, S. J. L. Billinge and J. S. Owen, *Nano Lett.*, 2013, **14**, 127–133.
- 47 V. Roiati, S. Colella, G. Lerario, L. De Marco, A. Rizzo, A. Listorti and G. Gigli, *Energy Environ. Sci.*, 2014, **7**, 1889–1894.
- 48 V. Roiati, E. Mosconi, A. Listorti, S. Colella, G. Gigli and F. De Angelis, *Nano Lett.*, 2014, **14**, 2168–2174.
- 49 H. Yu, F. Wang, F. Xie, W. Li, J. Chen and N. Zhao, *Adv. Funct. Mater.*, 2014, **24**, 7102–7108.
- 50 T. Supasai, N. Rujisamphan, K. Ullrich, A. Chemseddine and T. Dittrich, *Appl. Phys. Lett.*, 2013, **103**, 183906.
- 51 A. Dualeh, N. Tétreault, T. Moehl, P. Gao, M. K. Nazeeruddin and M. Grätzel, *Adv. Funct. Mater.*, 2014, **24**, 3250–3258.
- 52 A. Dualeh, P. Gao, S. I. Seok, M. K. Nazeeruddin and M. Grätzel, *Chem. Mater.*, 2014, **26**, 6160–6164.
- 53 A. Seemann, H. J. Egelhaaf, C. J. Brabec and J. A. Hauch, *Org. Electron.*, 2009, **10**, 1424–1428.
- 54 M. O. Reese, A. M. Nardes, B. L. Rupert, R. E. Larsen, D. C. Olson, M. T. Lloyd, S. E. Shaheen, D. S. Ginley, G. Rumbles and N. Kopidakis, *Adv. Funct. Mater.*, 2010, **20**, 3476–3483.
- 55 M. Manceau, S. Chambon, A. Rivaton, J.-L. Gardette, S. Guillerez and N. Lemaitre, *Sol. Energy Mater. Sol. Cells*, 2010, **94**, 1572–1577.
- 56 F. C. Krebs and K. Norrman, *Prog. Photovoltaics*, 2007, **15**, 697–712.
- 57 E. Carter, A. F. Carley and D. M. Murphy, *J. Phys. Chem. C*, 2007, **111**, 10630–10638.
- 58 D. C. Hurum, A. G. Agrios, K. A. Gray, T. Rajh and M. C. Thurnauer, *J. Phys. Chem. B*, 2003, **107**, 4545–4549.
- 59 H. Al-Dmour and D. M. Taylor, *Appl. Phys. Lett.*, 2009, **94**, 223309.
- 60 M. Iwamoto, Y. Yoda, M. Egashira and T. Seiyama, *J. Phys. Chem.*, 1976, **80**, 1989–1994.
- 61 U. B. Cappel, T. Daeneke and U. Bach, *Nano Lett.*, 2012, **12**, 4925–4931.
- 62 A. Stevanovic, M. Büttner, Z. Zhang and J. T. Yates, *J. Am. Chem. Soc.*, 2011, **134**, 324–332.
- 63 Z. Zhang and J. T. Yates, *Chem. Rev.*, 2012, **112**, 5520–5551.
- 64 S. K. Pathak, A. Abate, P. Ruckdeschel, B. Roose, K. C. Gödel, Y. Vaynzof, A. Santhala, S.-I. Watanabe, D. J. Hollman, N. Noel, A. Sepe, U. Wiesner, R. Friend, H. J. Snaith and U. Steiner, *Adv. Funct. Mater.*, 2014, **24**, 6046–6055.
- 65 S. K. Pathak, A. Abate, T. Leijtens, D. J. Hollman, J. Teuscher, L. Pazos, P. Docampo, U. Steiner and H. J. Snaith, *Adv. Energy Mater.*, 2014, **4**, 1301667.

- 66 K. Schwanitz, U. Weiler, R. Hunger, T. Mayer and W. Jaegermann, *J. Phys. Chem. C*, 2006, **111**, 849–854.
- 67 K. Schwanitz, E. Mankel, R. Hunger, T. Mayer and W. Jaegermann, *Chimia*, 2007, **61**, 796–800.
- 68 I. Nakamura, N. Negishi, S. Kutsuna, T. Ihara, S. Sugihara and K. Takeuchi, *J. Mol. Catal. A: Chem.*, 2000, **161**, 205–212.
- 69 D. C. Cronemeyer, *Phys. Rev.*, 1959, **113**, 1222–1226.
- 70 J. Bisquert, F. Fabregat-Santiago, I. Mora-Seró, G. Garcia-Belmonte, E. M. Barea and E. Palomares, *Inorg. Chim. Acta*, 2008, **361**, 684–698.
- 71 M. A. Henderson, W. S. Epling, C. L. Perkins, C. H. F. Peden and U. Diebold, *J. Phys. Chem. B*, 1999, **103**, 5328–5337.
- 72 G. Lu, A. Linsebigler and J. T. Yates, *J. Chem. Phys.*, 1995, **102**, 4657–4662.
- 73 G. Munuera, V. Rives-Arnau and A. Saucedo, *J. Chem. Soc., Faraday Trans. 1*, 1979, **75**, 736–747.
- 74 A. Abate, T. Leijtens, S. Pathak, J. Teuscher, R. Avolio, M. E. Errico, J. Kirkpatrick, J. M. Ball, P. Docampo, I. McPherson and H. J. Snaith, *Phys. Chem. Chem. Phys.*, 2013, **15**, 2572–2579.
- 75 T. Leijtens, J. Lim, J. Teuscher, T. Park and H. J. Snaith, *Adv. Mater.*, 2013, **25**, 3227–3233.
- 76 J. Bisquert, A. Zaban and P. Salvador, *J. Phys. Chem. B*, 2002, **106**, 8774–8782.
- 77 Y. Yu, K. Wu and D. Wang, *Appl. Phys. Lett.*, 2011, **99**, 192104.
- 78 J. Weidmann, T. Dittrich, E. Konstantinova, I. Lauermann, I. Uhendorf and F. Koch, *Sol. Energy Mater. Sol. Cells*, 1999, **56**, 153–165.
- 79 S. N. Habisreutinger, T. Leijtens, G. E. Eperon, S. D. Stranks, R. J. Nicholas and H. J. Snaith, *Nano Lett.*, 2014, **14**, 5561–5568.
- 80 I. C. Smith, E. T. Hoke, D. Solis-Ibarra, M. D. McGehee and H. I. Karunadasa, *Angew. Chem., Int. Ed.*, 2014, **53**, 11232–11235.
- 81 J. You, Y. Yang, Z. Hong, T.-B. Song, L. Meng, Y. Liu, C. Jiang, H. Zhou, W.-H. Chang, G. Li and Y. Yang, *Appl. Phys. Lett.*, 2014, **105**, 183902.
- 82 G. E. Eperon, V. M. Burlakov, P. Docampo, A. Goriely and H. J. Snaith, *Adv. Funct. Mater.*, 2014, **24**, 151–157.
- 83 G. Niu, W. Li, F. Meng, L. Wang, H. Dong and Y. Qiu, *J. Mater. Chem. A*, 2014, **2**, 705–710.
- 84 J. A. Christians, P. A. Miranda Herrera and P. V. Kamat, *J. Am. Chem. Soc.*, 2015, **137**, 1530–1538.
- 85 B. R. Vincent, K. N. Robertson, T. S. Cameron and O. Knop, *Can. J. Chem.*, 1987, **65**, 1042–1046.
- 86 J. Yang, B. D. Siempelkamp, D. Liu and T. L. Kelly, *ACS Nano*, 2015, **9**, 1955–1963.
- 87 X. Dong, X. Fang, M. Lv, B. Lin, S. Zhang, J. Ding and N. Yuan, *J. Mater. Chem. A*, 2015, **3**, 5360–5367.
- 88 A. M. A. Leguy, Y. Hu, M. Campoy-Quiles, M. I. Alonso, O. J. Weber, P. Azarhoosh, M. van Schilfgaarde, M. T. Weller, T. Bein, J. Nelson, P. Docampo and P. R. F. Barnes, *Chem. Mater.*, 2015, **27**, 3397–3407.
- 89 B. Hailegnaw, S. Kirmayer, E. Edri, G. Hodes and D. Cahen, *J. Phys. Chem. Lett.*, 2015, **6**, 1543–1547.
- 90 M. Jørgensen, K. Norrman, S. A. Gevorgyan, T. Tromholt, B. Andreasen and F. C. Krebs, *Adv. Mater.*, 2012, **24**, 580–612.
- 91 T. Baikie, Y. Fang, J. M. Kadro, M. Schreyer, F. Wei, S. G. Mhaisalkar, M. Graetzel and T. J. White, *J. Mater. Chem. A*, 2013, **1**, 5628–5641.
- 92 S. Aharon, A. Dymshits, A. Rotem and L. Etgar, *J. Mater. Chem. A*, 2015, **3**, 9171–9178.
- 93 C. Herring, *J. Appl. Phys.*, 1950, **21**, 437–445.
- 94 E. L. Unger, E. T. Hoke, C. D. Bailie, W. H. Nguyen, A. R. Bowring, T. Heumuller, M. G. Christoforo and M. D. McGehee, *Energy Environ. Sci.*, 2014, **7**, 3690–3698.
- 95 S. Ito, S. Tanaka, K. Manabe and H. Nishino, *J. Phys. Chem. C*, 2014, **118**, 16995–17000.
- 96 H.-S. Kim, S. H. Im and N.-G. Park, *J. Phys. Chem. C*, 2014, **118**, 5615–5625.
- 97 E. Mosconi, A. Amat, M. K. Nazeeruddin, M. Grätzel and F. De Angelis, *J. Phys. Chem. C*, 2013, **117**, 13902–13913.
- 98 R. E. Wasylisen, O. Knop and J. B. Macdonald, *Solid State Commun.*, 1985, **56**, 581–582.
- 99 A. Poglitsch and D. Weber, *J. Chem. Phys.*, 1987, **87**, 6373–6378.
- 100 M. L. Agiorgousis, Y.-Y. Sun, H. Zeng and S. Zhang, *J. Am. Chem. Soc.*, 2014, **136**, 14570–14575.
- 101 A. Buin, P. Pietsch, J. Xu, O. Voznyy, A. H. Ip, R. Comin and E. H. Sargent, *Nano Lett.*, 2014, **14**, 6281–6286.
- 102 W.-J. Yin, T. Shi and Y. Yan, *Appl. Phys. Lett.*, 2014, **104**, 063903.
- 103 A. Walsh, D. O. Scanlon, S. Chen, X. G. Gong and S.-H. Wei, *Angew. Chem., Int. Ed.*, 2015, **54**, 1791–1794.
- 104 M. H. Du, *J. Mater. Chem. A*, 2014, **2**, 9091–9098.
- 105 J. M. Azpiroz, E. Mosconi, J. Bisquert and F. De Angelis, *Energy Environ. Sci.*, 2015, **8**, 2118–2127.
- 106 M.-H. Du, *J. Phys. Chem. Lett.*, 2015, **6**, 1461–1466.
- 107 Y. Zhao and K. Zhu, *Chem. Commun.*, 2014, **50**, 1605–1607.
- 108 A. Pisoni, J. Jaćimović, O. S. Barišić, M. Spina, R. Gaál, L. Forró and E. Horváth, *J. Phys. Chem. Lett.*, 2014, **5**, 2488–2492.
- 109 R. Gottesman, E. Haltzi, L. Gouda, S. Tirosh, Y. Bouhadana, A. Zaban, E. Mosconi and F. De Angelis, *J. Phys. Chem. Lett.*, 2014, **5**, 2662–2669.
- 110 T. Oku, M. Zushi, Y. Imanishi, A. Suzuki and K. Suzuki, *Appl. Phys. Express*, 2014, **7**, 121601.
- 111 Z. Song, S. C. Watthage, A. B. Phillips, B. L. Tompkins, R. J. Ellingson and M. J. Heben, *Chem. Mater.*, 2015, **27**, 4612–4619.
- 112 E. Edri, S. Kirmayer, A. Henning, S. Mukhopadhyay, K. Gartsman, Y. Rosenwaks, G. Hodes and D. Cahen, *Nano Lett.*, 2014, **14**, 1000–1004.
- 113 W.-J. Yin, T. Shi and Y. Yan, *Adv. Mater.*, 2014, **26**, 4653–4658.
- 114 J. S. Yun, A. Ho-Baillie, S. Huang, S. H. Woo, Y. Heo, J. Seidel, F. Huang, Y.-B. Cheng and M. A. Green, *J. Phys. Chem. Lett.*, 2015, **6**, 875–880.
- 115 Q. Dong, Y. Fang, Y. Shao, P. Mulligan, J. Qiu, L. Cao and J. Huang, *Science*, 2015, **347**, 967–970.

- 116 W. Nie, H. Tsai, R. Asadpour, J.-C. Blancon, A. J. Neukirch, G. Gupta, J. J. Crochet, M. Chhowalla, S. Tretiak, M. A. Alam, H.-L. Wang and A. D. Mohite, *Science*, 2015, **347**, 522–525.
- 117 D. Shi, V. Adinolfi, R. Comin, M. Yuan, E. Alarousu, A. Buin, Y. Chen, S. Hoogland, A. Rothenberger, K. Katsiev, Y. Losovyj, X. Zhang, P. A. Dowben, O. F. Mohammed, E. H. Sargent and O. M. Bakr, *Science*, 2015, **347**, 519–522.
- 118 N. K. Noel, A. Abate, S. D. Stranks, E. S. Parrott, V. M. Burlakov, A. Goriely and H. J. Snaith, *ACS Nano*, 2014, **8**, 9815–9821.
- 119 A. Abate, M. Saliba, D. J. Hollman, S. D. Stranks, K. Wojciechowski, R. Avolio, G. Grancini, A. Petrozza and H. J. Snaith, *Nano Lett.*, 2014, **14**, 3247–3254.
- 120 D. W. de Quilettes, S. M. Vorpahl, S. D. Stranks, H. Nagaoka, G. E. Eperon, M. E. Ziffer, H. J. Snaith and D. S. Ginger, *Science*, 2015, **348**, 683–686.
- 121 M. Zhang, H. Yu, M. Lyu, Q. Wang, J.-H. Yun and L. Wang, *Chem. Commun.*, 2014, **50**, 11727–11730.
- 122 R. K. Misra, S. Aharon, B. Li, D. Mogilyansky, I. Visoly-Fisher, L. Etgar and E. A. Katz, *J. Phys. Chem. Lett.*, 2015, **6**, 326–330.
- 123 I. P. Swainson, M. G. Tucker, D. J. Wilson, B. Winkler and V. Milman, *Chem. Mater.*, 2007, **19**, 2401–2405.
- 124 N. Onoda-Yamamuro, O. Yamamuro, T. Matsuo and H. Suga, *J. Phys. Chem. Solids*, 1992, **53**, 277–281.
- 125 J. Kim, S. Choi, A. Jun, H. Y. Jeong, J. Shin and G. Kim, *ChemSusChem*, 2014, **7**, 1669–1675.
- 126 G. Niu, X. Guo and L. Wang, *J. Mater. Chem. A*, 2015, **3**, 8970–8980.
- 127 A. S. Bhalla, R. Guo and R. Roy, *Mater. Res. Innovations*, 2000, **4**, 3–26.
- 128 H. J. Snaith, A. Abate, J. M. Ball, G. E. Eperon, T. Leijtens, N. K. Noel, S. D. Stranks, J. T.-W. Wang, K. Wojciechowski and W. Zhang, *J. Phys. Chem. Lett.*, 2014, **5**, 1511–1515.
- 129 J. Even, L. Pedesseau, J.-M. Jancu and C. Katan, *J. Phys. Chem. Lett.*, 2013, **4**, 2999–3005.
- 130 P. E. Shaw, A. Ruseckas and I. D. W. Samuel, *Adv. Mater.*, 2008, **20**, 3516–3520.
- 131 C. Li, X. Lu, W. Ding, L. Feng, Y. Gao and Z. Guo, *Acta Crystallogr., Sect. B: Struct. Sci.*, 2008, **64**, 702–707.
- 132 C. A. Randall, A. S. Bhalla, T. R. Shroud and L. E. Cross, *J. Mater. Res.*, 1990, **5**, 829–834.
- 133 F. S. Galasso, *Structure, properties, and preparation of perovskite-type compounds*, Pergamon Press, Oxford, New York, 1969.
- 134 C. Motta, F. El-Mellouhi, S. Kais, N. Tabet, F. Alharbi and S. Sanvito, *Nat. Commun.*, 2015, **6**, 7026.
- 135 D. B. Mitzi, *Prog. Inorg. Chem.*, John Wiley & Sons, Inc., 2007, pp. 1–121, DOI: 10.1002/9780470166499.
- 136 I. Borriello, G. Cantele and D. Ninno, *Phys. Rev. B: Condens. Matter Mater. Phys.*, 2008, **77**, 235214.
- 137 G. E. Eperon, S. D. Stranks, C. Menelaou, M. B. Johnston, L. M. Herz and H. J. Snaith, *Energy Environ. Sci.*, 2014, **7**, 982–988.
- 138 N. Pellet, P. Gao, G. Gregori, T.-Y. Yang, M. K. Nazeeruddin, J. Maier and M. Grätzel, *Angew. Chem., Int. Ed.*, 2014, **53**, 3151–3157.
- 139 M. M. Lee, J. Teuscher, T. Miyasaka, T. N. Murakami and H. J. Snaith, *Science*, 2012, **338**, 643–647.
- 140 S. Aharon, S. Gamliel, B. E. Cohen and L. Etgar, *Phys. Chem. Chem. Phys.*, 2014, **16**, 10512–10518.
- 141 S. Aharon, B. E. Cohen and L. Etgar, *J. Phys. Chem. C*, 2014, **118**, 17160–17165.
- 142 J. M. Ball, M. M. Lee, A. Hey and H. J. Snaith, *Energy Environ. Sci.*, 2013, **6**, 1739–1743.
- 143 E. Edri, S. Kirmayer, D. Cahen and G. Hodes, *J. Phys. Chem. Lett.*, 2013, **4**, 897–902.
- 144 E. Edri, S. Kirmayer, M. Kulbak, G. Hodes and D. Cahen, *J. Phys. Chem. Lett.*, 2014, **5**, 429–433.
- 145 J. M. Frost, K. T. Butler, F. Brivio, C. H. Hendon, M. van Schilfgaarde and A. Walsh, *Nano Lett.*, 2014, **14**, 2584–2590.
- 146 Y. Tidhar, E. Edri, H. Weissman, D. Zohar, G. Hodes, D. Cahen, B. Rybtchinski and S. Kirmayer, *J. Am. Chem. Soc.*, 2014, **136**, 13249–13256.
- 147 O. Yamamuro, M. Oguni, T. Matsuo and H. Suga, *Thermochim. Acta*, 1986, **98**, 327–338.
- 148 S. T. Williams, F. Zuo, C.-C. Chueh, C.-Y. Liao, P.-W. Liang and A. K. Y. Jen, *ACS Nano*, 2014, **8**, 10640–10654.
- 149 M. Antoniadou, E. Siranidi, N. Vaenas, A. G. Kontos, E. Stathatos and P. Falaras, *Journal of Surfaces and Interfaces of Materials*, 2014, **2**, 323–327.
- 150 Q. Chen, H. Zhou, Y. Fang, A. Z. Stieg, T.-B. Song, H.-H. Wang, X. Xu, Y. Liu, S. Lu, J. You, P. Sun, J. McKay, M. S. Goorsky and Y. Yang, *Nat. Commun.*, 2015, **6**, 7269.
- 151 S. Colella, E. Mosconi, P. Fedeli, A. Listorti, F. Gazza, F. Orlandi, P. Ferro, T. Besagni, A. Rizzo, G. Calestani, G. Gigli, F. De Angelis and R. Mosca, *Chem. Mater.*, 2013, **25**, 4613–4618.
- 152 Z. Hawash, L. K. Ono, S. R. Raga, M. V. Lee and Y. Qi, *Chem. Mater.*, 2015, **27**, 562–569.
- 153 L. K. Ono, P. Schulz, J. J. Endres, G. O. Nikiforov, Y. Kato, A. Kahn and Y. Qi, *J. Phys. Chem. Lett.*, 2014, **5**, 1374–1379.
- 154 M.-C. Jung, S. R. Raga, L. K. Ono and Y. Qi, *Sci. Rep.*, 2015, **5**, 9863.
- 155 F. C. Krebs, S. A. Gevorgyan and J. Alstrup, *J. Mater. Chem.*, 2009, **19**, 5442–5451.
- 156 W. Chen, Y. Wu, J. Liu, C. Qin, X. Yang, A. Islam, Y.-B. Cheng and L. Han, *Energy Environ. Sci.*, 2015, **8**, 629–640.
- 157 C.-H. Chiang, Z.-L. Tseng and C.-G. Wu, *J. Mater. Chem. A*, 2014, **2**, 15897–15903.
- 158 Y.-J. Jeon, S. Lee, R. Kang, J.-E. Kim, J.-S. Yeo, S.-H. Lee, S.-S. Kim, J.-M. Yun and D.-Y. Kim, *Sci. Rep.*, 2014, **4**, 6953.
- 159 M. Jørgensen, K. Norrman and F. C. Krebs, *Sol. Energy Mater. Sol. Cells*, 2008, **92**, 686–714.
- 160 M. P. de Jong, L. J. van IJzenoord and M. J. A. de Voigt, *Appl. Phys. Lett.*, 2000, **77**, 2255–2257.
- 161 S. R. Dupont, M. Oliver, F. C. Krebs and R. H. Dauskardt, *Sol. Energy Mater. Sol. Cells*, 2012, **97**, 171–175.

- 162 T. C. Sum and N. Mathews, *Energy Environ. Sci.*, 2014, **7**, 2518–2534.
- 163 S. P. Singh and P. Nagarjuna, *Dalton Trans.*, 2014, **43**, 5247–5251.
- 164 H. J. Snaith, *J. Phys. Chem. Lett.*, 2013, **4**, 3623–3630.
- 165 P. Gao, M. Grätzel and M. K. Nazeeruddin, *Energy Environ. Sci.*, 2014, **7**, 2448–2463.
- 166 Y. Shao, Z. Xiao, C. Bi, Y. Yuan and J. Huang, *Nat. Commun.*, 2014, **5**, 5784.
- 167 J.-Y. Jeng, Y.-F. Chiang, M.-H. Lee, S.-R. Peng, T.-F. Guo, P. Chen and T.-C. Wen, *Adv. Mater.*, 2013, **25**, 3727–3732.
- 168 G. Li, R. Zhu and Y. Yang, *Nat. Photonics*, 2012, **6**, 153–161.
- 169 Y. Zhou, C. Fuentes-Hernandez, J. Shim, J. Meyer, A. J. Giordano, H. Li, P. Winget, T. Papadopoulos, H. Cheun, J. Kim, M. Fenoll, A. Dindar, W. Haske, E. Najafabadi, T. M. Khan, H. Sojoudi, S. Barlow, S. Graham, J.-L. Brédas, S. R. Marder, A. Kahn and B. Kippelen, *Science*, 2012, **336**, 327–332.
- 170 W. Zhang, B. Zhao, Z. He, X. Zhao, H. Wang, S. Yang, H. Wu and Y. Cao, *Energy Environ. Sci.*, 2013, **6**, 1956–1964.
- 171 D. A. Mengistie, M. A. Ibrahem, P.-C. Wang and C.-W. Chu, *ACS Appl. Mater. Interfaces*, 2014, **6**, 2292–2299.
- 172 O. Malinkiewicz, C. Roldán-Carmona, A. Soriano, E. Bandiello, L. Camacho, M. K. Nazeeruddin and H. J. Bolink, *Adv. Energy Mater.*, 2014, **4**, 1400345.
- 173 J. Seo, S. Park, Y. Chan Kim, N. J. Jeon, J. H. Noh, S. C. Yoon and S. I. Seok, *Energy Environ. Sci.*, 2014, **7**, 2642–2646.
- 174 P. Docampo, J. M. Ball, M. Darwich, G. E. Eperon and H. J. Snaith, *Nat. Commun.*, 2013, **4**, 2761.
- 175 J. Bisquert, *J. Phys. Chem. B*, 2004, **108**, 2323–2332.
- 176 H. J. Snaith and M. Grätzel, *Adv. Mater.*, 2007, **19**, 3643–3647.
- 177 K. Zhu, N. R. Neale, A. F. Halverson, J. Y. Kim and A. J. Frank, *J. Phys. Chem. C*, 2010, **114**, 13433–13441.
- 178 L. Wang, C. McCleese, A. Kovalsky, Y. Zhao and C. Burda, *J. Am. Chem. Soc.*, 2014, **136**, 12205–12208.
- 179 Y. Zhao, A. M. Nardes and K. Zhu, *Faraday Discuss.*, 2014, **176**, 301–312.
- 180 T. Salim, S. Sun, Y. Abe, A. Krishna, A. C. Grimsdale and Y. M. Lam, *J. Mater. Chem. A*, 2015, **3**, 8943–8969.
- 181 P. Qin, S. Tanaka, S. Ito, N. Tetreault, K. Manabe, H. Nishino, M. K. Nazeeruddin and M. Grätzel, *Nat. Commun.*, 2014, **5**, 3834.
- 182 K.-C. Wang, P.-S. Shen, M.-H. Li, S. Chen, M.-W. Lin, P. Chen and T.-F. Guo, *ACS Appl. Mater. Interfaces*, 2014, **6**, 11851–11858.
- 183 J. A. Christians, R. C. M. Fung and P. V. Kamat, *J. Am. Chem. Soc.*, 2014, **136**, 758–764.
- 184 W. Wang, J. Yuan, G. Shi, X. Zhu, S. Shi, Z. Liu, L. Han, H.-Q. Wang and W. Ma, *ACS Appl. Mater. Interfaces*, 2015, **7**, 3994–3999.
- 185 J. Liu, Y. Wu, C. Qin, X. Yang, T. Yasuda, A. Islam, K. Zhang, W. Peng, W. Chen and L. Han, *Energy Environ. Sci.*, 2014, **7**, 2963–2967.
- 186 H. Greijer, J. Lindgren and A. Hagfeldt, *J. Phys. Chem. B*, 2001, **105**, 6314–6320.
- 187 J. Shi, J. Dong, S. Lv, Y. Xu, L. Zhu, J. Xiao, X. Xu, H. Wu, D. Li, Y. Luo and Q. Meng, *Appl. Phys. Lett.*, 2014, **104**, 063901.
- 188 R. Zuo, L. Li and Z. Gui, *Ceram. Int.*, 2000, **26**, 673–676.
- 189 R. Shannon, *Acta Crystallogr.*, 1976, **32**, 751–767.
- 190 J. F. Verwey, *J. Phys. Chem. Solids*, 1970, **31**, 163–168.
- 191 P. Docampo and H. J. Snaith, *Nanotechnology*, 2011, **22**, 225403.
- 192 S. Guarnera, A. Abate, W. Zhang, J. M. Foster, G. Richardson, A. Petrozza and H. J. Snaith, *J. Phys. Chem. Lett.*, 2015, **6**, 432–437.
- 193 A. Dutta, C.-T. Huang, T.-C. Chen, C.-Y. Lin, C.-H. Chiu, Y.-C. Lin, C.-S. Chang and Y.-C. He, *Nat. Commun.*, 2015, **6**, 6374.
- 194 H. L. Clever and F. J. Johnston, *J. Phys. Chem. Ref. Data*, 1980, **9**, 751–784.
- 195 L. Zheng, Y.-H. Chung, Y. Ma, L. Zhang, L. Xiao, Z. Chen, S. Wang, B. Qu and Q. Gong, *Chem. Commun.*, 2014, **50**, 11196–11199.
- 196 F. Zhang, X. Yang, H. Wang, M. Cheng, J. Zhao and L. Sun, *ACS Appl. Mater. Interfaces*, 2014, **6**, 16140–16146.
- 197 Z. Wei, H. Chen, K. Yan and S. Yang, *Angew. Chem.*, 2014, **126**, 13455–13459.
- 198 M.-C. Hsiao, S.-H. Liao, M.-Y. Yen, P.-I. Liu, N.-W. Pu, C.-A. Wang and C.-C. M. Ma, *ACS Appl. Mater. Interfaces*, 2010, **2**, 3092–3099.
- 199 D. Liu and T. L. Kelly, *Nat. Photonics*, 2014, **8**, 133–138.
- 200 Z. Ku, Y. Rong, M. Xu, T. Liu and H. Han, *Sci. Rep.*, 2013, **3**, 3132.
- 201 Z. Li, S. A. Kulkarni, P. P. Boix, E. Shi, A. Cao, K. Fu, S. K. Batabyal, J. Zhang, Q. Xiong, L. H. Wong, N. Mathews and S. G. Mhaisalkar, *ACS Nano*, 2014, **8**, 6797–6804.
- 202 E. Edri, S. Kirmayer, S. Mukhopadhyay, K. Gartsman, G. Hodes and D. Cahen, *Nat. Commun.*, 2014, **5**, 3461.
- 203 M. K. I. Senevirathna, P. K. D. D. P. Pitigala, E. V. A. Premalal, K. Tennakone, G. R. A. Kumara and A. Konno, *Sol. Energy Mater. Sol. Cells*, 2007, **91**, 544–547.
- 204 D. Kuang, P. Wang, S. Ito, S. M. Zakeeruddin and M. Grätzel, *J. Am. Chem. Soc.*, 2006, **128**, 7732–7733.
- 205 M. Lira-Cantu, K. Norrman, J. W. Andreasen, N. Casan-Pastor and F. C. Krebs, *J. Electrochem. Soc.*, 2007, **154**, B508–B513.
- 206 A. Kay and M. Grätzel, *Chem. Mater.*, 2002, **14**, 2930–2935.
- 207 E. Palomares, J. N. Clifford, S. A. Haque, T. Lutz and J. R. Durrant, *J. Am. Chem. Soc.*, 2002, **125**, 475–482.
- 208 Z. Liu, K. Pan, M. Liu, M. Wang, Q. Lü, J. Li, Y. Bai and T. Li, *Electrochim. Acta*, 2005, **50**, 2583–2589.
- 209 X.-T. Zhang, I. Sutanto, T. Taguchi, K. Tokuhiro, Q.-B. Meng, T. N. Rao, A. Fujishima, H. Watanabe, T. Nakamori and M. Uragami, *Sol. Energy Mater. Sol. Cells*, 2003, **80**, 315–326.
- 210 E. Palomares, J. N. Clifford, S. A. Haque, T. Lutz and J. R. Durrant, *J. Am. Chem. Soc.*, 2003, **125**, 475–482.
- 211 H.-S. Kim, J.-W. Lee, N. Yantara, P. P. Boix, S. A. Kulkarni, S. Mhaisalkar, M. Grätzel and N.-G. Park, *Nano Lett.*, 2013, **13**, 2412–2417.

- 212 M. K. Nazeeruddin, A. Kay, I. Rodicio, R. Humphry-Baker, E. Mueller, P. Liska, N. Vlachopoulos and M. Graetzel, *J. Am. Chem. Soc.*, 1993, **115**, 6382–6390.
- 213 L. W. R. Gao, B. Ma, C. Zhan and Y. Qiu, *Langmuir*, 2010, **26**, 2460–2465.
- 214 R. Gao, L. Wang, Y. Geng, B. Ma, Y. Zhu, H. Dong and Y. Qiu, *J. Phys. Chem. C*, 2011, **115**, 17986–17992.
- 215 E. Palomares, J. N. Clifford, S. A. Haque, T. Lutz and J. R. Durrant, *Chem. Commun.*, 2002, 1464–1465, DOI: 10.1039/B202515A.
- 216 F. Luo, L. Wang, B. Ma and Y. Qiu, *J. Photochem. Photobiol. A*, 2008, **197**, 375–381.
- 217 T. Zewdu, J. N. Clifford and E. Palomares, *Phys. Chem. Chem. Phys.*, 2012, **14**, 13076–13080.
- 218 J. Tian, R. Gao, Q. Zhang, S. Zhang, Y. Li, J. Lan, X. Qu and G. Cao, *J. Phys. Chem. C*, 2012, **116**, 18655–18662.
- 219 G. Niu, L. Wang, R. Gao, B. Ma, H. Dong and Y. Qiu, *J. Mater. Chem.*, 2012, **22**, 16914–16919.
- 220 Y. Ogomi, K. Kukihara, S. Qing, T. Toyoda, K. Yoshino, S. Pandey, H. Momose and S. Hayase, *ChemPhysChem*, 2014, **15**, 1062–1069.
- 221 B. G. Frost, N. F. van Hulst, E. Lunedei, G. Matteucci and E. Rikkers, *Appl. Phys. Lett.*, 1996, **68**, 1865–1867.
- 222 H. Oji, E. Ito, M. Furuta, K. Kajikawa, H. Ishii, Y. Ouchi and K. Seki, *J. Electron Spectrosc. Relat. Phenom.*, 1999, **101–103**, 517–521.
- 223 M. Löglund and J. L. Brédas, *J. Chem. Phys.*, 1994, **101**, 4357–4364.
- 224 H. Antoniadis, B. R. Hsieh, M. A. Abkowitz, S. A. Jenekhe and M. Stolka, *Synth. Met.*, 1994, **62**, 265–271.
- 225 V. I. Annenkov, S. G. Garanin, V. A. Eroshenko, N. V. Zhidkov, A. V. Zubkov, S. V. Kalipanov, N. A. Kalmykov, V. P. Kovalenko, V. A. Krotov, S. G. Lapin, S. P. Martynenko, V. I. Pankratov, V. S. Faizullin, V. A. Khrustalev, N. M. Khudikov and V. S. Chebotar, *Quantum Electron.*, 2009, **39**, 719.
- 226 J.-Y. Lee, S. T. Connor, Y. Cui and P. Peumans, *Nano Lett.*, 2008, **8**, 689–692.
- 227 J. H. Kim, S. T. Williams, N. Cho, C.-C. Chueh and A. K. Y. Jen, *Adv. Energy Mater.*, 2015, **5**, 1401229.
- 228 F. C. Krebs, *Sol. Energy Mater. Sol. Cells*, 2006, **90**, 3633–3643.
- 229 C. J. Brabec, N. S. Sariciftci and J. C. Hummelen, *Adv. Funct. Mater.*, 2001, **11**, 15–26.
- 230 K. Tennakone, G. R. R. A. Kumara, I. R. M. Kottekoda, K. G. U. Wijayantha and V. P. S. Perera, *J. Phys. D: Appl. Phys.*, 1998, **31**, 1492.
- 231 P. Wang, S. M. Zakeeruddin, P. Comte, R. Charvet, R. Humphry-Baker and M. Grätzel, *J. Phys. Chem. B*, 2003, **107**, 14336–14341.
- 232 P. Wang, S. M. Zakeeruddin, R. Humphry-Baker and M. Grätzel, *Chem. Mater.*, 2004, **16**, 2694–2696.
- 233 T. W. Matthew Carnie and D. Worsley, *Int. J. Photoenergy*, 2012, **2012**, 9.
- 234 A. Abate, J. Martí-Rujas, P. Metrangolo, T. Pilati, G. Resnati and G. Terraneo, *Cryst. Growth Des.*, 2011, **11**, 4220–4226.
- 235 A. Hinsch, J. M. Kroon, R. Kern, I. Uhendorf, J. Holzbock, A. Meyer and J. Ferber, *Prog. Photovoltaics*, 2001, **9**, 425–438.
- 236 H. Pettersson and T. Gruszecki, *Sol. Energy Mater. Sol. Cells*, 2001, **70**, 203–212.
- 237 P. M. Sommeling, M. Späth, H. J. P. Smit, N. J. Bakker and J. M. Kroon, *J. Photochem. Photobiol. A*, 2004, **164**, 137–144.
- 238 M. Grätzel, *J. Photochem. Photobiol. C*, 2003, **4**, 145–153.
- 239 S. Gevorgyan, M. V. Madsen, H. F. Dam, M. Jørgensen, C. J. Fell, K. F. Anderson, B. C. Duck, A. Mescheloff, E. A. Katz, A. Elschner, R. Roesch, H. Hoppe, M. Hermenau, M. Riede and F. C. Krebs, *Sol. Energy Mater. Sol. Cells*, 2013, **116**, 187–196.
- 240 K. Norrman and F. C. Krebs, *Surf. Interface Anal.*, 2004, **36**, 1542–1549.
- 241 J. A. Hauch, P. Schilinsky, S. A. Choulis, R. Childers, M. Biele and C. J. Brabec, *Sol. Energy Mater. Sol. Cells*, 2008, **92**, 727–731.
- 242 J. Wu, J. Wang, J. Lin, Y. Xiao, G. Yue, M. Huang, Z. Lan, Y. Huang, L. Fan, S. Yin and T. Sato, *Sci. Rep.*, 2013, **3**, 2058.
- 243 J. Wu, J. Wang, J. Lin, Z. Lan, Q. Tang, M. Huang, Y. Huang, L. Fan, Q. Li and Z. Tang, *Adv. Energy Mater.*, 2012, **2**, 78–81.
- 244 Y. Chen, T. Chen and L. Dai, *Adv. Mater.*, 2015, **27**, 1053–1059.
- 245 J. You, Z. Hong, Y. Yang, Q. Chen, M. Cai, T.-B. Song, C.-C. Chen, S. Lu, Y. Liu, H. Zhou and Y. Yang, *ACS Nano*, 2014, **8**, 1674–1680.
- 246 B. Conings, L. Baeten, C. De Dobbelaere, J. D'Haen, J. Manca and H.-G. Boyen, *Adv. Mater.*, 2014, **26**, 2041–2046.
- 247 F. Lang, A. Juma, V. Somsongkul, T. Dittrich and M. Arunchaiya, *Hybrid Mater.*, 2014, **1**, DOI: 10.2478/hyma-2014-0002.
- 248 N. Onoda-Yamamoto, T. Matsuo and H. Suga, *J. Phys. Chem. Solids*, 1990, **51**, 1383–1395.
- 249 E. Mosconi, C. Quarti, T. Ivanovska, G. Ruani and F. De Angelis, *Phys. Chem. Chem. Phys.*, 2014, **16**, 16137–16144.
- 250 C. Quarti, G. Grancini, E. Mosconi, P. Bruno, J. M. Ball, M. M. Lee, H. J. Snaith, A. Petrozza and F. D. Angelis, *J. Phys. Chem. Lett.*, 2014, **5**, 279–284.
- 251 A. Maalej, Y. Abid, A. Kallel, A. Daoud, A. Lautié and F. Romain, *Solid State Commun.*, 1997, **103**, 279–284.
- 252 M. Ledinský, P. Löper, B. Niesen, J. Holovsky, S.-J. Moon, J.-H. Yum, S. De Wolf, A. Fejfar and C. Ballif, *J. Phys. Chem. Lett.*, 2015, **6**, 401–406.
- 253 E. T. Hoke, D. J. Slotcavage, E. R. Dohner, A. R. Bowring, H. I. Karunadasa and M. D. McGehee, *Chem. Sci.*, 2015, **6**, 613–617.
- 254 J. Feng, *APL Mater.*, 2014, **2**, 081801.
- 255 V. Brand, C. Bruner and R. H. Dauskardt, *Sol. Energy Mater. Sol. Cells*, 2012, **99**, 182–189.
- 256 S. Savagatrup, A. D. Printz, T. F. O'Connor, A. V. Zaretski and D. J. Lipomi, *Chem. Mater.*, 2014, **26**, 3028–3041.
- 257 Y. Zhao, A. M. Nardes and K. Zhu, *Faraday Discuss.*, 2014, **176**, 301–312.

- 258 A. J. Frank, N. Kopidakis and J. v. d. Lagemaat, *Coord. Chem. Rev.*, 2004, **248**, 1165–1179.
- 259 Q. Wang, S. Ito, M. Grätzel, F. Fabregat-Santiago, I. Mora-Seró, J. Bisquert, T. Bessho and H. Imai, *J. Phys. Chem. B*, 2006, **110**, 25210–25221.
- 260 N. Kopidakis, E. A. Schiff, N. G. Park, J. van de Lagemaat and A. J. Frank, *J. Phys. Chem. B*, 2000, **104**, 3930–3936.
- 261 A. Zaban, M. Greenshtein and J. Bisquert, *ChemPhysChem*, 2003, **4**, 859–864.
- 262 G. Pellegrino, A. Alberti, G. G. Condorelli, F. Giannazzo, A. La Magna, A. M. Paoletti, G. Pennesi, G. Rossi and G. Zanotti, *J. Phys. Chem. C*, 2013, **117**, 11176–11185.
- 263 P. Docampo, F. C. Hanusch, S. D. Stranks, M. Döblinger, J. M. Feckl, M. Ehrenspurger, N. K. Minar, M. B. Johnston, H. J. Snaith and T. Bein, *Adv. Energy Mater.*, 2014, **4**.
- 264 S. A. Gevorgyan, M. Jørgensen and F. C. Krebs, *Sol. Energy Mater. Sol. Cells*, 2008, **92**, 736–745.
- 265 M. O. Reese, S. A. Gevorgyan, M. Jørgensen, E. Bundgaard, S. R. Kurtz, D. S. Ginley, D. C. Olson, M. T. Lloyd, P. Morville, E. A. Katz, A. Elschner, O. Haillant, T. R. Currier, V. Shrotriya, M. Hermenau, M. Riede, K. R. Kirov, G. Trimmel, T. Rath, O. Inganäs, F. Zhang, M. Andersson, K. Tvingstedt, M. Lira-Cantu, D. Laird, C. McGuiness, S. Gowrisanker, M. Pannone, M. Xiao, J. Hauch, R. Steim, D. M. DeLongchamp, R. Rösch, H. Hoppe, N. Espinosa, A. Urbina, G. Yaman-Uzunoglu, J.-B. Bonekamp, A. M. van Breemen, C. Girotto, E. Voroshazi and F. C. Krebs, *Sol. Energy Mater. Sol. Cells*, 2011, **95**, 1253–1267.
- 266 H. Neugebauer, C. Brabec, J. C. Hummelen and N. S. Sariciftci, *Sol. Energy Mater. Sol. Cells*, 2000, **61**, 35–42.